Wavelength Conversion By Four Wave Mixing In Passive InGaAsP/InP Waveguides

by

Ali M. Darwish

B.S., University of Maryland (1990)
S.M., University of Maryland (1992)

Submitted to the Department of Electrical Engineering and Computer Science
in partial fulfillment of the requirements for the degree of

Doctor of Philosophy

at the

MASSACHUSETTS INSTITUTE OF TECHNOLOGY

September, 1996

Author .....
Department of Electrical Engineering and Computer Science
August 8, 1996

Certified by .....
E. P. Ippen
Elihu Thomson Professor of Electrical Engineering
Thesis Supervisor

Accepted by ....
Frederic R. Morgenthaler
Chairman, Departmental Committee on Graduate Students

Wavelength Conversion By Four Wave Mixing In Passive InGaAsP/InP Waveguides

by

Ali M. Darwish

Submitted to the Department of Electrical Engineering and Computer Science
on August 8, 1996, in partial fulfillment of the
requirements for the degree of
Doctor of Philosophy

Abstract

High-speed long distance transmission networks are at the focus of research today. Wavelength Division Multiplexing (WDM) is a prime candidate for increasing the capacity of communication systems. Four-Wave Mixing (FWM) is an attractive all-optical technique for the wavelength switching and multiplexing that is needed in such systems. This thesis examines wavelength conversion by FWM in passive waveguides as an alternative to current methods. We have demonstrated wavelength conversion in the 1.5 μm regime using the near bandgap nonlinearity of semiconductor quantum wells. Issues like nonlinearity characterization, enhancement and speed are studied. In addition, relevant issues such as group delay, effects of nonlinear loss and index changes on FWM, and short-pulse distortion are addressed. In a 7.5 mm long passive InGaAsP/InP single quantum well waveguide, a wavelength shift of 20 nm has been obtained with -11 dB conversion efficiency using picosecond pulses. We confirmed the ultrafast nature of the nonlinearity by measuring the conversion efficiency as a function of the frequency shift. An order of magnitude increase in the value of n_2 close to the bandgap is observed compared with the off-resonance value. Nonlinear loss and index changes are shown to place fundamental limitations on four wave mixing (FWM) conversion efficiency. We investigate the effect of nonlinear loss analytically with a system of coupled first-order differential equations. The result indicates the presence of a maximum conversion efficiency that is geometry-independent. The analysis allows us to find the optimum device length and operating conditions and understand important issues in short pulse FWM. We verify the theoretical results with a picosecond pulse FWM experiment. This thesis combines experimental and analytical efforts.

Thesis Supervisor: E. P. Ippen

To my parents

Acknowledgments

First and foremost I thank my creator and sustainer for his countless gifts, unconditional love, and for introducing me to his source of inspiration – the Qur'an. I thank to him for blessing me with such a great advisor – Professor Erich Ippen. I am deeply grateful to Professor Ippen for his support and encouragement, and his brilliant experimental insights. My appreciation to him as a person and a scientist can not be expressed in words. I would like also to thank Professor Haus for many inspiring ideas. A special word of thanks for Dr. Joe Donnelly for serving on my thesis committee, for his willingness to help, and for making my research as smooth as possible. I appreciate the time and effort Dr. Han Le spent with me in the first two years of my research. I learned a great deal from him. None of the experiments would have been possible without the diligent work of both Dr. J. Donnelly and Dr. H. Le. I thank Prof. Jim Fujimoto, for teaching me Nonlinear Optics. Marilyn Pierce's compassionate administration of graduate student concerns is most appreciated.

I am thankful to Donna Gale, Cindy Koph, and Mary Aldridge for keeping our group running smoothly. I am sure I will forgive them for not letting me use their PCs – they had a good reason.

A very special word of thanks goes to my first and last lab mentor, Dr. Katie Hall. Her early support was invaluable and her sense of humor was enjoyable. I am also thankful to Gadi Lenz for helping with LabView and the stepper motor programming. He provided the salt and pepper for my experimental work. Charlie Hultgren and Dave Dougherty provided the late night jolt of fun and were both very helpful and willing to discuss lab problems. Siegfried Fleischer provided me with company during odd hours of the night and gave me many weird ideas to think about. To other students and visiting scientists who have helped me and became my friends, Gunter Steinmeyer, Erik Thoen, Jerry Chen, Frazana Khatri, Steve Cheng, Jay Damask, John Moores, Lynn Nelson, Chris Doerr, Kohichi Tamura, William Wong, Keren Bergman, Brett Bouma, Pat Chou, and my officemates Stephan Boppart, Boris Golubovic, and Charles Yu, thank you. It has been a pleasure to interact with you. My sincere apologies to anyone whom I overlooked or misspelled their name.

I am grateful for the support of the National Science Foundation (NSF) Fellowship.

I can not begin to describe how indebted I am to my great parents, Dr. Mohamed A. Darwish, and Dr. Hanaa El-Kadri. What pleases me most about

finishing my PhD is that it shall please you. And that's my highest goal. Whatever I achieve is owed to you alone. I cherish the friendship of my brothers and sisters – Ahmed, Kareem, Mariam and Amina.

To my lovely wife Eman, thank you for your patience and continuing moral support. Without you the trip would have been very harsh. Finally, I am appreciative to my three months old son Abraham. You have given me much more than you will ever realize.

Contents

List of Figures

Chapter 1

Introduction

Fiber-optic systems have revolutionized the field of communications and led to the advent of the so-called information age. Optical fibers with their low loss and wide bandwidth provide an attractive medium for long-distance information transmission. The first fiber-optic trans-oceanic link used a hybrid electro-optic design which employed electronic repeaters for signal amplification and restoration. Such systems were limited by low-speed electronic bottle-necks. To overcome these limitations and extend the capacity and flexibility of communication networks, a variety of all-optical communication systems have been proposed. In an all-optical system, one may transmit a large number of communication channels simultaneously through multiplexing techniques. There are mainly two ways to accomplish this: time-division multiplexing (TDM) [1] and wavelength division multiplexing (WDM). In the case of TDM, bits associated with different channels are interleaved (all of the pulses have the same carrier frequency) to form a composite bit stream. TDM is well suited for digital signals. In WDM systems, several channels, each with different carrier frequency, are spaced

in the frequency domain. The carrier frequency spacing should be large enough to avoid inter-channel spectra overlap and cross-talk. WDM systems offer many advantages including the ease of accessing fiber bandwidth and the ability to accept varying modulation speeds and formats. An essential component in WDM systems is an all-optical wavelength shifter. Nondegenerate Four Wave Mixing (FWM) is an important parametric process for wavelength conversion in WDM systems.

The subject of this thesis will be wavelength shifting using FWM in passive low-loss InGaAsP/InP single quantum well (QW) waveguides. Chapter 2 is a review of FWM theory and applications. Chapter 3 introduces research directions in wavelength conversion at $\lambda = 1.5\ \mu m$ and presents the motives for using passive InGaAsP/InP QW waveguides. In chapter 4, an evaluation of InGaAsP/InP waveguides' fundamental parameters such as the third order nonlinearity (real and imaginary parts), linear loss, and GVD are presented. In addition, experimental demonstration of efficient CW and pulsed FWM wavelength conversion is reported. In Chapter 5, the effect of nonlinear absorption and index changes on FWM is examined theoretically and experimentally. In chapter 6, the issue of intense ultrashort pulse wavelength conversion by FWM is discussed. Finally, future research directions and thesis summary are given in Chapter 7.

Chapter 2

FWM Theory and Applications

2.1 FWM Basic Equations

Four wave mixing is an important third-order parametric[1] process in nonlinear optics. It involves, in general, the interaction of *four* optical fields, hence the name. The four optical fields at frequencies ω_1, ω_2, ω_3 and ω_4 interact such that

$$\omega_1 + \omega_2 = \omega_3 + \omega_4$$

FWM is a parametric process in which the total photon energy is conserved ($\hbar\omega_1 + \hbar\omega_2 + \hbar\omega_3 + \hbar\omega_4 = 0$)–see Figure 2-1. An intense optical field propagating through a material will generate linear and nonlinear polarizations whose magnitudes are

[1] A parametric process is one in which the nonlinear medium, such as optical fiber, plays a passive role except for mediating the interaction among several optical fields through its nonlinear response. The name comes from the fact the light modulates the parameters of the nonlinear medium. Four wave mixing, parametric amplification, harmonic generation, and refractive index changes are examples of parametric processes.

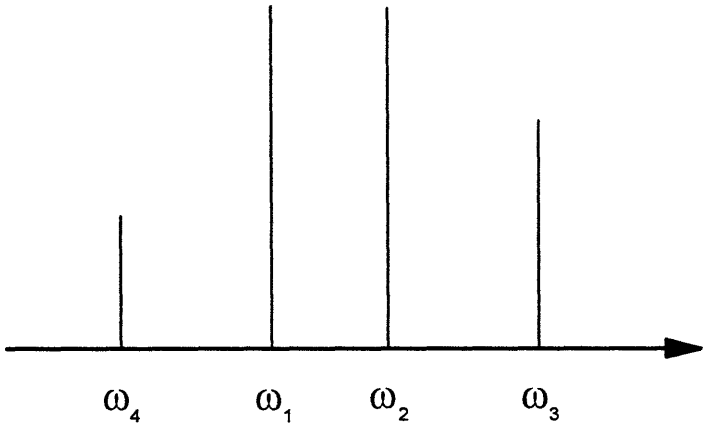

Figure 2-1: In FWM four optical fields interact such that $\omega_1 + \omega_2 = \omega_3 + \omega_4$. Typically, the intense beams, ω_1, and ω_2 are refered to as the pump fields.

governed by optical susceptibilities such as $\chi^{(1)}$, $\chi^{(2)}$, $\chi^{(3)}$, etc. [2]-[6]. Since FWM is a third order process only $\chi^{(3)}$ shall be of concern. Specifically, only nonlinear polarizations of the form

$$P^{NL} \sim \frac{3}{4} \epsilon_0 \chi^{(3)} \cdot \tilde{E}^2 \tilde{E}^* \tag{2.1}$$

shall be of interest (the * denotes conjugation). Consider the electric field of four interacting waves with different frequencies, each field given by

$$\tilde{E}_i(z,t) = E_i(z,t)\, e^{i(k_i z - \omega_i t)} \tag{2.2}$$

where $E_i(z,t)$ is the slowly varying envelope, ω_i is the optical carrier frequency, k_i is the propagation wave vector, and $i = 1, 2, 3$ or 4. The total field is given by

$$\tilde{E} = \tilde{E}_1 + \tilde{E}_2 + \tilde{E}_3 + \tilde{E}_4 \tag{2.3}$$

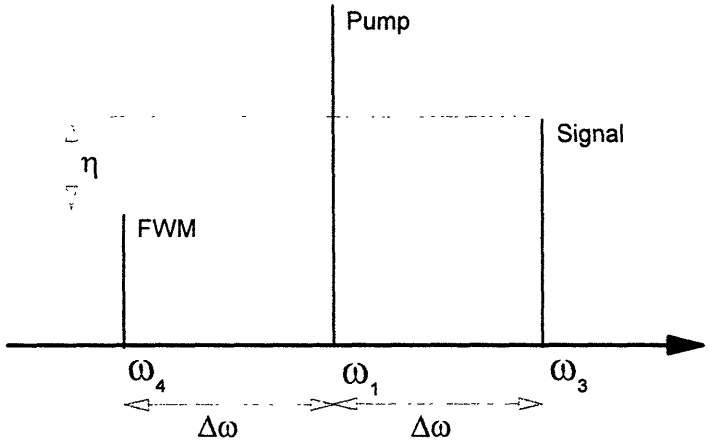

Figure 2-2: In FWM, the pump ω_1 and signal ω_3 interact to produce the FWM signal ω_4 such that $\omega_4 = 2\omega_1 - \omega_3$. The difference in frequency between the pump and singal fields is denoted by $\Delta\omega$ and the ratio of the FWM to signal fields is defined as the conversion efficiency η.

Each of the interacting fields obeys the wave equation in the form [3], in MKS units,

$$\left(\frac{\partial^2}{\partial z^2} - \mu_0\epsilon\frac{\partial^2}{\partial t^2}\right)\tilde{E} = \mu_0\frac{\partial^2}{\partial t^2}P^{NL} \tag{2.4}$$

If the envelope $E_i(z,t)$ varies much slower than the spatial frequency of the mode, then the wave equation (2.4) may be simplified further. In the *slowly varying amplitude approximation*, equation (2.4) may be writen as

$$\frac{\partial}{\partial z}E_i(z) = -i\frac{\mu_0\omega c}{2n}P^{NL}e^{-ikz} \tag{2.5}$$

where c is the speed of light, and n is the index of refraction.

We are interested in the case where there is a single pump field so that $\tilde{E}_1$ and $\tilde{E}_2$ are actually one field. In FWM experiments, a pump and a signal mix to produce

a FWM signal at $\omega_4 = 2\omega_1 - \omega_3$ where ω_1, ω_3 and ω_4 are the frequencies of the pump, signal and FWM beams respectively (see Figure 2-2). Also, in our case, we can assume that the *signal* field $\widetilde{E}_3$ and the FWM *generated* field $\widetilde{E}_4$ are much weaker than the pump field $\widetilde{E}_1$. Substituting equation (2.3) in equation (2.5), assuming a linear loss coefficient equal to α, and making use of Eq. (2.2) and (2.1) we obtain the following set of coupled nonlinear equations,

$$\frac{\partial E_1}{\partial z} = -\frac{\alpha_1}{2}E_1 + i\kappa |E_1|^2 E_1 \tag{2.6}$$

$$\frac{\partial E_3}{\partial z} = -\frac{\alpha_3}{2}E_3 + 2i\kappa |E_1|^2 E_3 \tag{2.7}$$

$$\frac{\partial E_4}{\partial z} = -\frac{\alpha_4}{2}E_4 + 2i\kappa |E_1|^2 E_4 + i\gamma\chi^{(3)}E_1^2 E_3^* e^{i\triangle kz} \tag{2.8}$$

where we define

$$\gamma \equiv \frac{3\pi}{4}\frac{1}{n\lambda}$$

$$\triangle k \equiv k_3 + k_4 - 2k_1$$

where λ is the field's wavelength, E_3^* denotes the complex conjugate of E_3, and we use κ to denote the self and cross modulation terms of $\chi^{(3)}$ that are not involved in the FWM process. Strictly speaking, we should use different κ's in the above equations. In the first equation we should use κ_{11}, proportional to $\chi^{(3)}(\omega_1;\omega_1,-\omega_1,\omega_1)$. In the second, κ_{31} is proportional to $\chi^{(3)}(\omega_3;\omega_1,-\omega_1,\omega_3)$ and in the third κ_{41} is proportional to $\chi^{(3)}(\omega_4;\omega_1,-\omega_1,\omega_4)$. For simplicity, we assumed $\kappa_{11} = \kappa_{31} = \kappa_{41} = \kappa$. In addition,

$\chi^{(3)}$ in the last term of the third equation denotes $\chi^{(3)}(\omega_4;\omega_1,\omega_1,-\omega_3)$. Henceforth, when we refer to $\chi^{(3)}$, we are referring to the one in the last term of equation (2.8). If, in addition to the loss, we have gain, then $-\alpha$ should be replaced with $g-\alpha$ where g is the gain coefficient. Equation (2.6) indicates that the pump field gets modified with propagation in two aspects. First, the linear loss term $-(\alpha_1/2)E_1$ attenuates the pump field while the nonlinear term $i\kappa\left|E_1\right|^2 E_1$ $(= i\left|E_1\right|^2 E_1 \cdot (Re\{\kappa\} + i\, Im\{\kappa\}))$ affects both the amplitude and the phase of the pump field. The purely imaginary part of the nonlinear term, $i\left|E_1\right|^2 E_1 \cdot Re\{\kappa\}$, modulates the phase of the pump field and is commonly referred to as the self-phase modulation (SPM) term. SPM leads to an intensity dependent refractive index as will be shown. This leads to spectral broadening of optical pulses. On the other hand the purely real part of the nonlinear term, $-\left|E_1\right|^2 E_1 \cdot Im\{\kappa\}$, leads to self-attenuation through two-photon absorption (TPA). Equation (2.7) governs the propagation of the signal field and has two ingredients. The first is the linear loss term $-(\alpha_3/2)E_3$, and the second is the nonlinear term $i2\kappa\left|E_1\right|^2 E_3$ $(= i2\left|E_1\right|^2 E_3 \cdot (Re\{\kappa\} + i\, Im\{\kappa\}))$. Again, the purely imaginary part of the nonlinear term, $i2\left|E_1\right|^2 E_3 \cdot Re\{\kappa\}$, modulates the phase of the signal field and is commonly referred to as the cross-phase modulation (XPM) term. Note the factor of 2 in the XPM term. The XPM term accounts for the pump-induced refractive index changes experienced by the signal field. And the purely real part of the nonlinear term $-2\left|E_1\right|^2 E_3 \cdot Im\{\kappa\}$ accounts for the pump-induced attenuation experienced by the signal field. Equation (2.8) is the most significant since it describes the generation of the FWM field E_4. The first two terms $-(\alpha_4/2)E_4$ and $i2\kappa\left|E_1\right|^2 E_4$ play the same role they played in Eq. (2.7). The last term $i\gamma\chi^{(3)}E_1^2 E_3^* e^{i\triangle kz}$ is the

FWM term. It is the source term that describes the generation of the FWM field E_4.

The nonlinear loss coefficient, $\mathrm{Im}\{\kappa\}$, may be related to the commonly used TPA coefficient β by multiplying equation (2.6) by E_1^*, equation (2.6)* by E_1, adding, and using the fact that β is defined through the relation $\partial I_1/\partial z = -\alpha I_1 - \beta I_1^2$, and that I_1 is related to $|E_1|^2$ by

$$I_1 = \frac{1}{2}\frac{n}{120\pi}|E_1|^2, \tag{2.9}$$

to obtain

$$\beta = \frac{480\pi}{n} Im\{\kappa\}. \tag{2.10}$$

Similarly, assuming the nonlinearity is ultrafast, $\mathrm{Re}\{\kappa\}$ may be related to n_2 by multiplying equation (2.6) by E_1^*, equation (2.6)* by E_1, subtracting, and using the fact that n_2 is defined through the relation $n = n_0 + n_2 I$, to obtain

$$n_2 = \frac{120\lambda}{n} Re\{\kappa\}. \tag{2.11}$$

It is helpful to examine the simplest form of the FWM equations (2.6)-(2.8). In the small signal regime (small $|E_1|^2$) the nonlinear terms containing κ may be neglected in the equations (2.6)-(2.8) and equation (2.8) simplifies to

$$\frac{\partial E_4}{\partial z} = -\frac{\alpha_4}{2}E_4 + i\gamma\chi^{(3)}E_1^2E_3^*e^{i\triangle kz} \tag{2.12}$$

Note that the driving term, second term, in equation (2.12) above is proportional

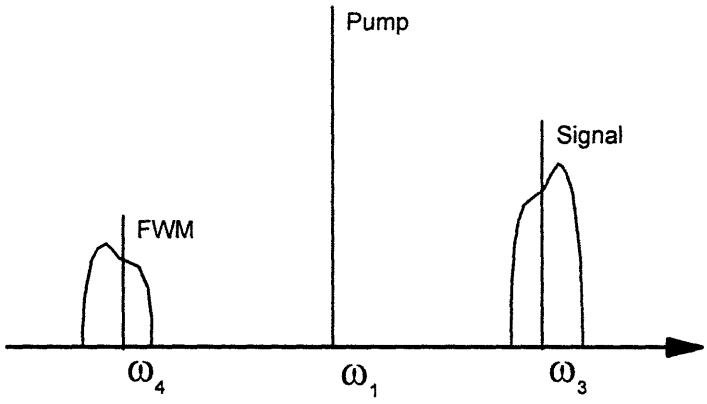

Figure 2-3: In FWM the generated field is not a frquency translated replica of the signal field but, rather, it is a spectrally inverted replica of the signal.

to E_3^* rather than E_3. As a result, in FWM the generated field E_4 is the complex conjugate of the signal field. That leads to spectral inversion of the signal field (see Figures 2-3 and 2-4). Equation (2.12) may be readily integrated yielding, the well known *small signal* expression, assuming $\triangle k = 0$ and $\alpha_1 \backsimeq \alpha_3 \backsimeq \alpha_4 = \alpha$,

$$\eta_{ss} \equiv \left|\frac{E_4(L)}{E_{30}}\right|^2 = e^{-\alpha L}\left(\gamma\left|\chi^{(3)}\right| \cdot L_{eff} \cdot |E_{10}|^2\right)^2, \tag{2.13}$$

where E_{10} and E_{30} are the *input* pump and signal amplitudes respectively, L_{eff} is the effective interaction length defined as $L_{eff} \equiv (1 - e^{-\alpha L})/\alpha$, and L is the physical interaction length. Using relation (2.9), we may express η_{ss} as

$$\eta_{ss} = \frac{I_4}{I_{30}} = e^{-\alpha L}\left(\gamma' \left|\chi^{(3)}\right| \cdot L_{eff} \cdot I_{10}\right)^2 \tag{2.14}$$

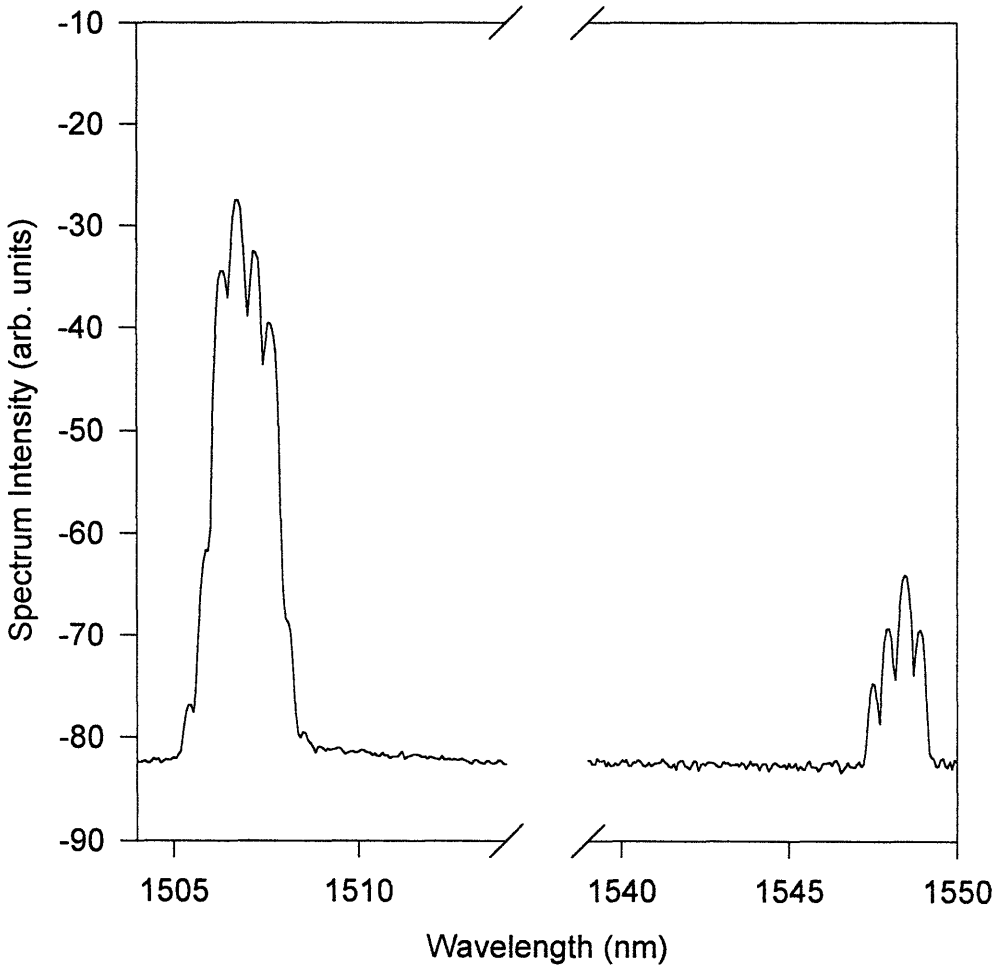

Figure 2-4: An experimental demonstration (performed in our lab.) of the optical phase conjugation nature of the FMW process. Note the $x - axis$ scale has been expanded to show the detailed structure of the signal and FWM fields. The pump field is not shown.

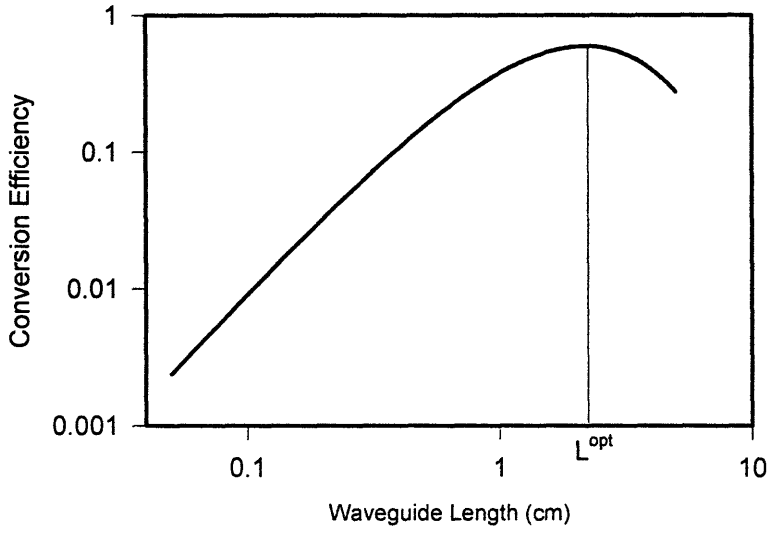

Figure 2-5: Normalized conversion efficiency as a function of waveguide length L, assuming a linear loss coefficient $\alpha = 0.5\,\mathrm{cm}^{-1}$. The optimum length is $L_{ss}^{opt} = \ln(3)/\alpha$ which equals 2.2 cm in this case.

where I_{30} is the signal input intensity, I_{10} is the pump's input intensity and

$$\gamma' \equiv \frac{180\pi^2}{n^2\lambda}$$

In order to express η in terms of power P we have to do a proper overlap integral over the propagation mode. If we assume $E_i(x,y,z) = \psi(x,y)\,E_i(z)$, where the spatial amplitude profile $\psi(x,y)$ is the same for all fields, then we should replace I_{10} in the equation (2.14) and in all the following conversion efficiency equations by P_{10}/A'_{eff}

so that

$$\eta_{ss} = e^{-\alpha L}\left(\gamma' \left|\chi^{(3)}\right| \cdot L_{eff} \cdot \frac{P_{10}}{A'_{eff}}\right)^2$$

where

$$A'_{eff} \equiv \frac{\left[\int_{-\infty}^{\infty}\int \psi^2(x,y)\,dxdy\right]^2}{\int_{-\infty}^{\infty}\int \psi^4(x,y)\,dxdy}$$

Note that I_{10} $(= P_{10}/A'_{eff})$ is *not* the *peak intensity* usually given by

$$\begin{aligned} P_{10} &= \int_{-\infty}^{\infty}\int I_{10}^{peak}\psi^2(x,y)\,dxdy \\ &= I_{10}^{peak}A_{eff} \end{aligned}$$

where

$$A_{eff} \equiv \int_{-\infty}^{\infty}\int \psi^2(x,y)\,dxdy$$

If we assume a gaussian mode profile $\psi(x,y) = \exp(-(x^2+y^2)/w_0)$, then we find

$$\frac{A'_{eff}}{A_{eff}} = 2$$

Equations (2.13) and (2.14) show clearly the fundamental dependencies of the FWM conversion efficiency. First, it depends quadratically on the pump's input intensity I_{10}, the effective length L_{eff}, and the third order nonlinearity $\left|\chi^{(3)}\right|$. Typical plots of η_{ss} as a function of L and I_{10} are shown in Figures 2-5 and 2-6, respectively. The conversion efficiency's dependence on L is given by $e^{-\alpha L}(1-e^{-\alpha L})^2/\alpha^2$. Hence, η_{ss} is proportional to L^2 for small values (compared to $1/\alpha$) of L, exponential for

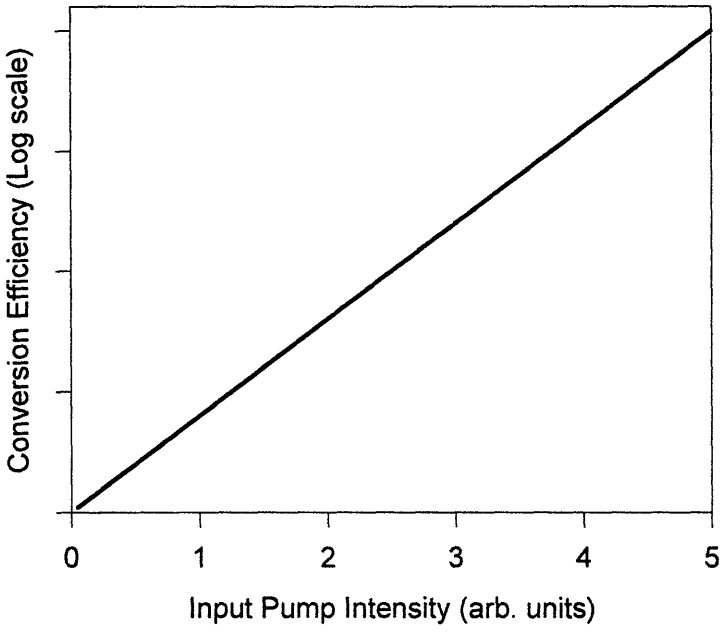

Figure 2-6: Normalized conversion efficiency as a function of pump intensity.

large values of L, and has a peak in between. In the *small signal* case, the optimum length is $L_{ss}^{opt} = \ln(3)/\alpha$, as may be verified by direct differentiation.

In deriving equation (2.14) we assumed that the wavelengths of the pump, signal, and FWM fields are close enough such that $\alpha_1 \backsimeq \alpha_3 \backsimeq \alpha_4 = \alpha$. If that is not valid, then equations (2.6)-(2.8) must be solved again. Assuming $\alpha_1 \neq \alpha_3 \neq \alpha_4$ we obtain

$$\eta_{ss} = \frac{I_4}{I_{30}} = e^{-\alpha_3 L} \left(\gamma' \left|\chi^{(3)}\right| \cdot L'_{eff} \cdot I_{10}\right)^2 \tag{2.15}$$

where

$$\begin{aligned} L'_{eff} &= \left(\frac{1 - e^{-\alpha_{eff} L}}{\alpha_{eff}}\right) \\ \alpha_{eff} &= (2\alpha_1 + \alpha_3 - \alpha_4)/2 \end{aligned}$$

The conversion efficiency's length dependence is now slightly more complicated. It has two linear loss coefficients, α_3 and α_{eff}, instead of one α.

2.2 FWM Phase Matching

The effect of group velocity dispersion (GVD) on FWM has been ignored, so far, in the preceding analysis by setting $\triangle k = 0$ in equations (2.6)-(2.8). The bit rate in a communication system is limited inherently by the GVD, which is responsible for the broadening of optical pulses during their propagation inside the waveguide. The GVD in waveguides may arise due to various reasons. In practice there are mainly two sources of GVD (1) material dispersion and (2) waveguide dispersion. The material

dispersion is due to the variation of the refractive index of the waveguide material. The waveguide dispersion is due to the dependence of the propagation constant of each mode with wavelength. Typically, the material dispersion and waveguide dispersion are measured together.

To study the effect of GVD on FWM, $\triangle k$ should be retained in equations (2.6)-(2.8). The simplest and most fundamental effect of GVD may be understood by "turning-off" all other effects. Assume that $\alpha_1 = \alpha_3 = \alpha_4 = 0$, and that $\kappa = 0$ so that we are left with

$$\frac{\partial E_4}{\partial z} = i\gamma\chi^{(3)} E_1^2 E_3^* e^{i\triangle kz} \tag{2.16}$$

which may be easily integrated yielding

$$\eta_{ss} = \left(\gamma \left|\chi^{(3)}\right| |E_{10}|^2 \frac{\sin(\triangle k\, L/2)}{(\triangle k/2)}\right)^2 \tag{2.17}$$

Using relation (2.9), we may express η_{ss} as

$$\eta_{ss} = \left(\gamma' \left|\chi^{(3)}\right| I_{10} \frac{\sin(\triangle k\, L/2)}{(\triangle k/2)}\right)^2 \tag{2.18}$$

where

$$\triangle k \equiv \frac{\omega_3 n(\omega_3) + \omega_4 n(\omega_4) - 2\omega_1 n(\omega_1)}{c}$$

where γ and γ' are the same as before, $n(\omega_i)$ is the effective index at frequency ω_i and c is the speed of light. The phase matching parameter $\triangle k$ can be simplified

by using a linear approximation for $n(\omega)$: $n(\omega) = n(\omega_1) + (dn/d\omega)(\omega - \omega_1)$. In the linear approximation, we may express, assuming all fields have the same polarization so that birefringence can be ignored,

$$\triangle k \equiv 2\frac{dn}{d\omega}(\triangle\omega)^2/c$$

Alternatively, if we express $k(\omega)$ as

$$k(\omega) = k(\omega_1) + \frac{dk}{d\omega}\triangle\omega + \frac{1}{2}\frac{d^2k}{d\omega^2}(\triangle\omega)^2,$$

then we have

$$\begin{aligned} \triangle k &\equiv \frac{d^2k}{d\omega^2}(\triangle\omega)^2 \\ \text{GVD} &\equiv \frac{d^2k}{d\omega^2} \end{aligned}$$

The group velocity dispersion (GVD) coefficient is defined as the second derivative of the wave vector with frequency. Typical plots of η_{ss} as a function of L and $\triangle\omega$ are shown in Figures 2-7 and 2-8, respectively, assuming GVD $= 3000\,ps^2/km$. The conversion efficiency's dependence on L is given by $(\sin(\Delta kL/2)/(\Delta kL/2))^2$. Hence, η_{ss} is proportional to L^2 for small values (compared to $\pi/\Delta k$) of L, sinusoidal for large values of L, and has nulls at $L = m\,\pi/\Delta k$, $m = 0, 2, 4, ..$ etc. The conversion efficiency's dependence on $\Delta\omega$ has $\sin(x)/x$ form with nulls at $\Delta\omega = (2\pi/(L \cdot GVD))^{1/2}$.

The GVD may be measured in one of several ways including observation of short

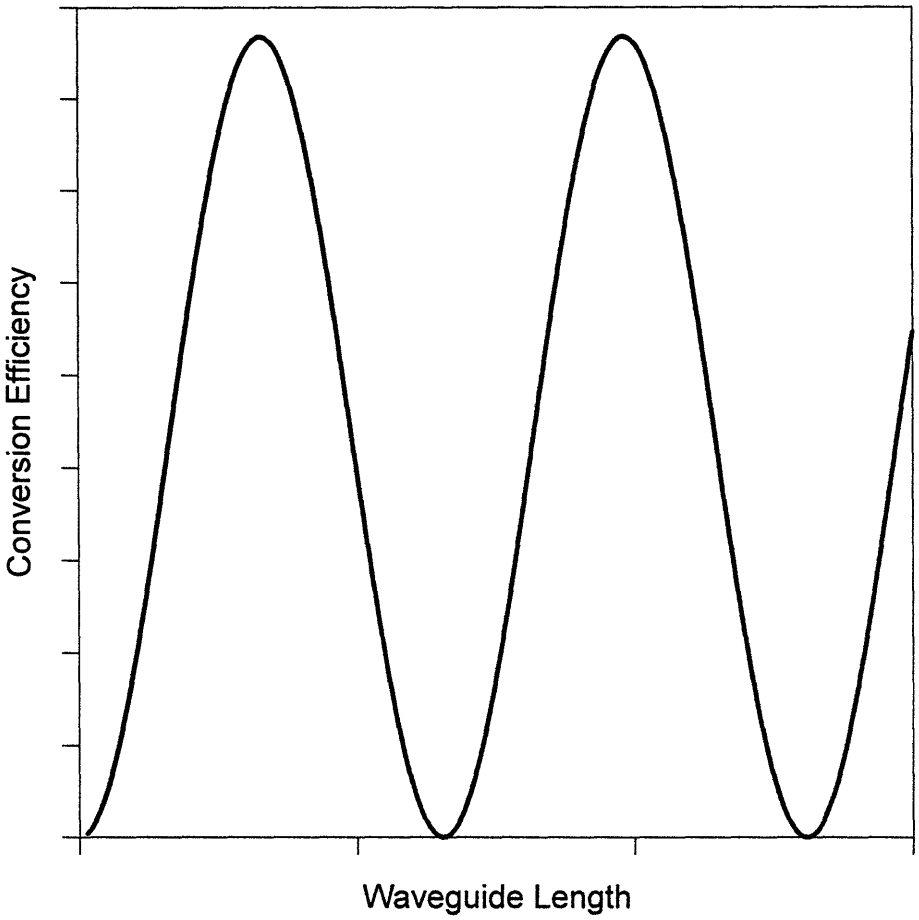

Figure 2-7: Normalized conversion efficiency as a function of waveguide length, assuming GVD $= 3000\, ps^2/km$. The conversion efficiency goes in- and out-of-phase as a function of length. The nulls appear when the length is a multiple of $\pi/\Delta k$.

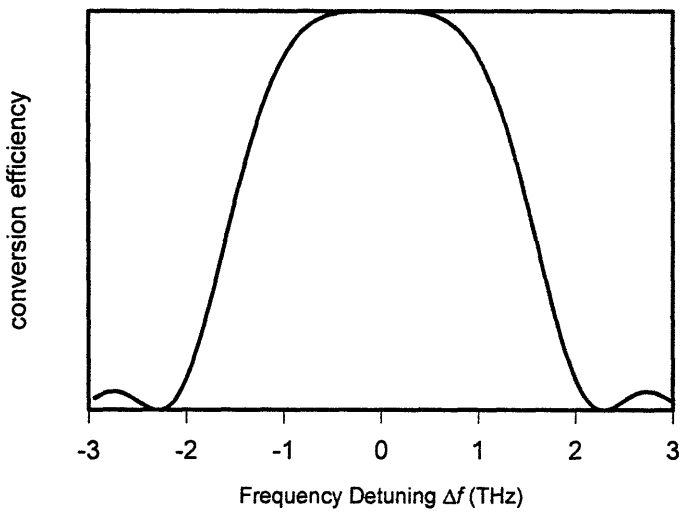

Figure 2-8: Normalized conversion efficiency as a function of frequency detuning, assuming $L = 1\,cm$, GVD $= 3000\,ps^2/km$. Note that η's dependence on Δf has the form $\sin(x)/x$. The phase matching nulls appear at $\Delta\omega = \sqrt{2\pi/(L \cdot \text{GVD})}$.

pulse broadening, short pulse round-trip time delay, and other frequency domain techniques. The FWM phase matching requirement may be used as a measurement technique for the GVD. The GVD coefficient may be measured by studying the tuning characteristic of the FWM signal. By tuning the input signal away from the pump wavelength in small steps and recording $\eta(\Delta\lambda)$, we should observe a $|sin(\Delta kL/2)/(\Delta kL/2)|^2$ behavior as predicted by the conversion efficiency formula (2.18). Given Δk, we may directly extract the GVD coefficient.

So far, we have assumed that either $\alpha = 0$ or that $\Delta k = 0$. Now consider the general case where $\Delta k \neq 0$, $\alpha_1 \neq \alpha_3 \neq \alpha_4 \neq 0$. This case is similar to the one where $\alpha_1 \neq \alpha_3 \neq \alpha_4 \neq 0$, in the previous section, except that now $\Delta k \neq 0$. By inspection we see that the solution in this case is the same as equation (2.15) except that $\alpha_{eff} = (2\alpha_1 + \alpha_3 - \alpha_4)/2$ is replaced with $\alpha''_{eff} = (2\alpha_1 + \alpha_3 - \alpha_4)/2 + i\,\Delta k$. Another way of writing equation (2.15) is

$$\eta_{ss} = e^{-\alpha_3 L} \left(\gamma \left| \chi^{(3)} \right| |E_{10}|^2 \, \frac{e^{-\alpha''_{eff} L/2}}{\alpha''_{eff}/2} \sinh(\alpha''_{eff} L/2) \right)^2 \tag{2.19}$$

However, now α''_{eff} is a complex number. Equation (2.19) may be simplified further by using that fact that $\sinh(a+b) = \sinh(a) \cdot \cosh(b) + \cosh(a) \cdot \sinh(b)$ and the fact that $\cosh(i\,x) = \cos(x)$, $\sinh(i\,x) = i\,\sin(x)$ to obtain the final result,

$$\eta_{ss} = e^{-\alpha_3 L} \left(\gamma \left| \chi^{(3)} \right| |E_{10}|^2 \right)^2 \frac{4\, e^{-\alpha_{eff} L}}{\alpha_{eff}^2 + \Delta k^2} \left(\cosh^2(\alpha_{eff} L/2) - \cos^2(\Delta kL/2) \right) \tag{2.20}$$

where α_{eff} is defined as before ($\alpha_{eff} = (2\alpha_1 + \alpha_3 - \alpha_4)/2$). Equation (2.20), as

expected, reduces to equation (2.15) when $\Delta k = 0$, and to equation (2.17) when $\alpha_1 = \alpha_3 = \alpha_4 = 0$. Also equation (2.20) may be expressed in terms of I_{10} by replacing γ by γ' and $|E_{10}|^2$ by I_{10}. Figure 2-9 shows a plot of the normalized conversion efficiency as a function of Δf for several values of α. The effect of loss is to (1) reduce the conversion efficiency, (2) reduce the contrast between the peaks and valleys, and (3) "wash-out" the sharp phase matching nulls characteristic of the phase matching process. In Figure 2-9 $\Delta k_\pi = 2\pi / L$. The dependence of the conversion efficiency on L is shown in Figure 2-10, assuming $\alpha_{eff} = 1$ cm^{-1} and $\alpha_3 = 1$ cm^{-1}, and different values of Δk_π. When $\alpha_{eff}/\Delta k_\pi$ is large, η's dependence on length resembles that of Figure 2-5. On the other hand, when $\alpha_{eff}/\Delta k_\pi$ is small, η's dependence resembles the other limit – pronounced phase matching oscillations (see Figure 2-7). Phase mismatching minimas (when $\Delta kL/2 = \pi$) are clearly evident in the last two graphs where $\alpha_{eff}/\Delta k_\pi \ll 1$.

2.3 Third-Order Nonlinearity

The third-order nonlinear optical susceptibility $\chi^{(3)}$ has been considered a constant, so far (see equation (2.1)). However, in general, $\chi^{(3)}$ is a function of frequency such that

$$P^{(3)}(\omega_4) = \frac{3\epsilon_0}{4} \int \chi^{(3)}(\omega_4;\, \omega_1,\, \omega_2,\, \omega_3)\, E_1(\omega_1)\, E_2(\omega_2)\, E_3^*(\omega_3)$$
$$\delta(\omega_4 - \omega_1 - \omega_2 + \omega_3)\, d\omega_1\, d\omega_2\, d\omega_3$$

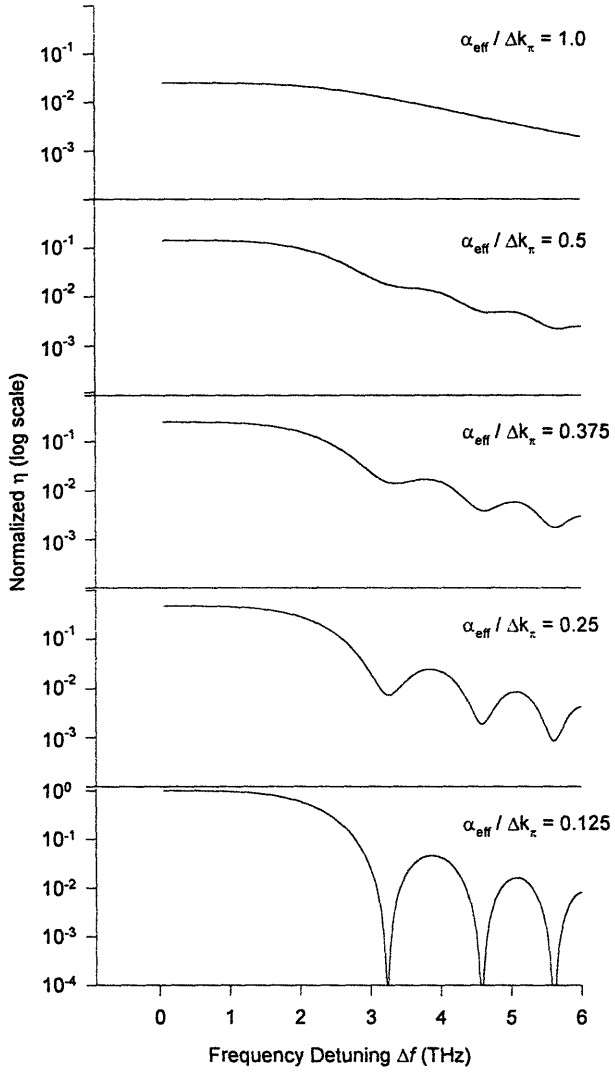

Figure 2-9: Normalized conversion efficiency as a function of Δf, assuming GVD equals 3000 ps^2/km, $L = 1$ cm, and $\Delta k_\pi = 2\pi / L$, plotted for different values of α. Note that as the ratio of $\alpha/\Delta k_\pi$ increases, the phase matching nulls "wash-out" and the contrast between peaks and minimums is reduced.

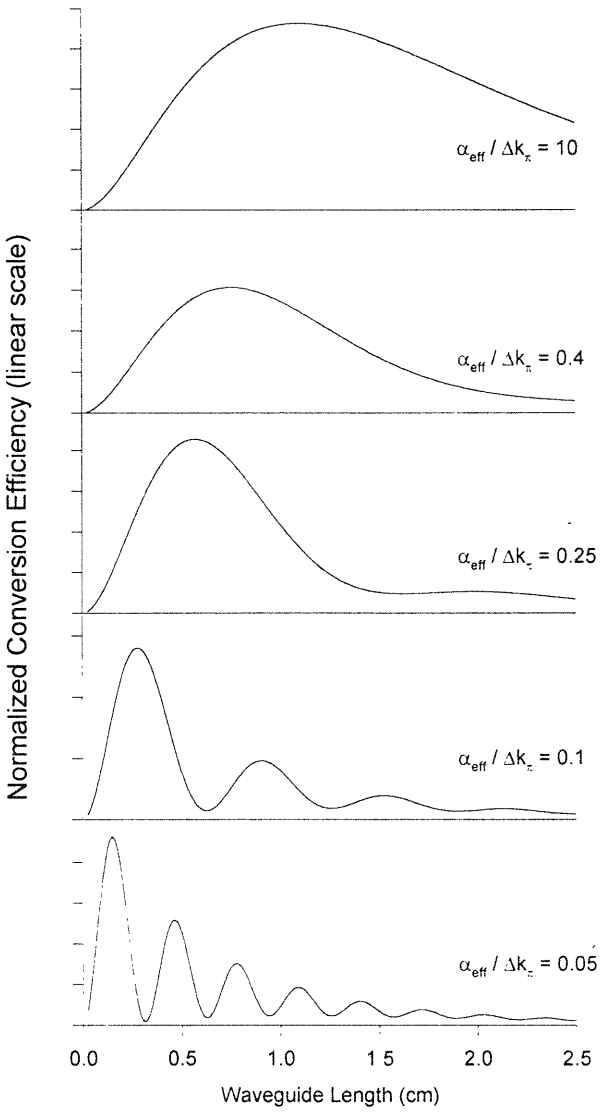

Figure 2-10: Normalized conversion efficiency as a function of L, assuming $\alpha_{eff} = 1$ cm^{-1} and $\alpha_3 = 1$ cm^{-1}. In the above graphs, α_3 and α_{eff} were kept fixed while Δk_π $(= 2\,\pi\,/\,L)$ was changed. When $\alpha_{eff}/\Delta k_\pi$ is large, η's dependence on length resembles that where GVD $= 0$. On the other hand, when $\alpha_{eff}/\Delta k_\pi$ is small, η's dependence resembles the other limit – pronounced phase matching oscillations. Phase matching minimas (when $\Delta kL/2 = n\pi$) are clearly evident when $\alpha_{eff}/\Delta k_\pi \ll 1$.

In the present case, $\omega_1 = \omega_2$, $E_1(\omega_1) = E_2(\omega_2)$, a monochromatic frequency field, and $\omega_3 = \omega_1 + \Delta\omega$. Hence, $\omega_4 = \omega_1 - \Delta\omega$. Typically, $\omega_1 \gg \Delta\omega$ and given $\omega_1, \chi^{(3)}$ is a function of $\Delta\omega$ only. The FWM process will produce the nonlinear polarization in the following manner. Through the nonlinear interaction of $E_1(\omega_1)$ and $E_3(\omega_3)$, the medium is modulated (in phase and amplitude) at the beat frequency $\Delta\omega$. The amplitude and phase gratings formed by modulation of the medium, in turn, scatter the pump field creating the FWM field $E_4(\omega_4)$. The FWM conversion efficiency is proportional to the modulation grating strength squared which, in turn, is proportional to $\left|\chi^{(3)}(\Delta\omega)\right|^2$. The time domain $\chi^{(3)}(t)$ is the related to $\chi^{(3)}(\Delta\omega)$ by the Fourier transform relation

$$\chi^{(3)}(\Delta\omega) \sim \int_{-\infty}^{\infty} \chi^{(3)}(t)\, e^{i\,\Delta\omega\, t}\, dt. \tag{2.21}$$

Through the FWM process $\left|\chi^{(3)}(\Delta\omega)\right|^2$ can be measured directly. In the time domain, pump-probe techniques can be applied to measure $\chi^{(3)}(t)$ directly [7]. Although measurements obtained by time or frequency domain techniques are directly related in theory (see equation (2.21)), in practice it is difficult to relate the two if there are many nonlinearities involved. As an example, consider a material with three nonlinear mechanisms such that

$$\chi^{(3)}(t) = A_1\, e^{-t/\tau_1} + A_2\, e^{-t/\tau_2} + A_3\, e^{-t/\tau_3} \tag{2.22}$$

where A_i and τ_i represent the complex magnitude and lifetime of each nonlinear mechanism. The transform of (2.22) equals

$$\chi^{(3)}(\Delta\omega) \sim \frac{A_1\,\tau_1}{1+i\,\Delta\omega\,\tau_1} + \frac{A_2\,\tau_2}{1+i\,\Delta\omega\,\tau_2} + \frac{A_3\,\tau_3}{1+i\,\Delta\omega\,\tau_3}. \tag{2.23}$$

The magnitude of (2.23) is a complicated function and determining the poles and zeroes accurately is difficult. A slow nonlinear mechanism will limit the usefulness of the FWM process as a wavelength shifting mechanism to signals with low modulation speeds. On the other hand, a material with an instantaneous nonlinearity, $\chi^{(3)}(t) = \delta(t)$, will have a simple $\chi^{(3)}(\Delta\omega) = constant$ – which is what was assumed in the proceeding sections. In particular, if the conversion efficiency's dependence on frequency detuning follows a $(sin(\Delta\omega)/\Delta\omega)^2$, then that will confirm that the nonlinearity is, indeed, ultrafast.

2.4 FWM Applications

Understanding the fundamentals of the FWM process in passive waveguides will open the door to many other operations beyond wavelength conversion. The reason is that FWM is a very versatile process with numerous applications. These applications include all-optical data demultiplexing [8], data multiplexing [9] and clock recovery, all of which are essential operations in TDM systems. FWM usage for Optical Phase Conjugation (OPC) [10] for image distortion correction is another important area of research. A closely related application to OPC is dispersion compensation in

fiber optic communication networks by midway signal conjugation [11]. FWM and Group Velocity Dispersion (GVD) are directly related through the phase matching condition. Hence, FWM may be used to measure the GVD coefficient of the medium. In addition, FWM may be employed for pulse shaping and compression [12]. It may also be used for measuring the magnitude of the third order nonlinearity tensor [13] of various nonlinear materials since the FWM conversion efficiency is directly related to $|\chi^{(3)}|^2$. Moreover, it may be used as a spectroscopic tool for studying ultrafast carrier dynamics [14]-[15] since $\chi^{(3)}$ is a sensitive function of the magnitude and phase of various nonlinear processes (see equation (2.23)). Other applications of FWM include ultrafast switching and spectrum manipulation. Beside its useful applications, the presence of FWM in many communication systems may lead to undesirable effects such as inter-channel cross-talk.

FWM is closely related to many other methods of all-optical switching since it makes use of $\chi^{(3)}$ of the interaction medium. A large $\chi^{(3)}$ is generally desirable, but there are important differences between methods. In FWM the quantity of interest is $|\chi^{(3)}|$, while in all-optical switching based on index changes alone, the ratio $\mathrm{Re}\{\chi^{(3)}\}/\mathrm{Im}\{\chi^{(3)}\}$ determines the material's figure of merit [18]. For example, nonlinear index changes in passive semiconductor waveguides are limited by nonlinear absorption [19]-[20]. Nonetheless, FWM in passive waveguides may remain attractive since $\mathrm{Im}\{\chi^{(3)}\}$ contributes directly to $|\chi^{(3)}|$, the quantity of interest in FWM.

Chapter 3

Wavelength Conversion by FWM

This thesis focuses on FWM as a wavelength conversion mechanism at $\lambda = 1.5$ μm. There are many possible means to accomplish wavelength conversion. The least sophisticated of these is signal detection and subsequent modulation of a laser at the new desired wavelength. However, this method has a built-in electronic speed bottle-neck and is not readily scalable. More sophisticated demonstrations to date include using one of several available nonlinearities in semiconductor amplifiers and laser structures or in fiber optics. These techniques employ cross-gain [21]-[22] or cross-phase saturation [23]-[24]. The cross-gain saturation technique involves the transmission of two colors through a semiconductor amplifier; an input signal and a weak CW signal (of the desired wavelength). When the input signal is in the high-state (or logic "1"), it saturates the amplifier and the CW signal is in the low-state (or logic "0") and vice versa. Hence, an inverted replica of the input signal is produced at a different wavelength. In the phase saturation technique, a semiconductor amplifier is put into one arm of an interferometer and the phase modulation associated with gain saturation

is used to impose modulation on a new wave. An advantage of this technique is the spatial separation of the input signal and the wavelength converted signal. All cross-gain or cross-phase modulation techniques for wavelength conversion are restricted to Amplitude Shift Keying (ASK) modulation formats and single channel operation. In addition, modulation rates are limited by the stimulated recombination time constant. In contrast, FWM-based wavelength conversion is transparent to both bit rate and modulation format. Hence, it is well suited for multi-channel wavelength conversion. The disadvantages of FWM conversion include the need for powerful pump, the need for post-mixing filtering of the pump and input signals, and the potential degradation of signal-to-noise-ratio (SNR) and inter-channel cross-talk levels.

3.1 FWM Medium

Most optical materials have $\chi^{(3)} \neq 0$ and may potentially be used for FWM. However, in most cases the conversion efficiency will be very small since the third order nonlinearity is usually minute. In spite of the small value of the third order nonlinearity, a relatively large conversion efficiency can be achieved. This is possible because in waveguide structures the spotsize is small and the interaction length is large (for low loss waveguides). A figure of merit for the conversion efficiency in waveguide structures is $(\chi^{(3)} L_{eff} / A_{eff})^2$ – see equation (2.14). There are three main choices of materials for wavelength conversion using FWM at $\lambda = 1.5$ μm, optical fiber, semiconductor amplifiers, and passive semiconductor waveguides. Comparing the figure of merit for optical fiber and semiconductor waveguides (for rough estimates assume

$A_{eff} = 35\,\mu m^2$ for fiber and $A_{eff} = 3\,\mu m^2$ for a semiconductor waveguide and the same peak power) we find

$$\frac{(\chi^{(3)} L_{eff}/A'_{eff})^2{}_{\text{fiber}}}{(\chi^{(3)} L_{eff}/A'_{eff})^2{}_{\text{semi.}}} \simeq 4.6 \cdot 10^{-12} \frac{L^2_{eff\ \text{fiber}}}{L^2_{eff\ \text{semi.}}}$$

where we assumed $\chi^{(3)}_{\text{fiber}} = 2.5 \cdot 10^{-18}\ cm^2/V^2$ (equivalent to $n_2 = 3.2 \cdot 10^{-16}\, cm^2/W$– see reference [28]) and $\chi^{(3)}_{\text{semi.}} = 1 \cdot 10^{-13}\ cm^2/V^2$ (more on this later). Clearly, L^2_{eff} for fiber needs to be much bigger than L^2_{eff} for semiconductors in order to have comparable figures of merit. In the case above, for the figures of merit to be equal, we need $L_{eff\ \text{fiber}} \simeq (4.7 \cdot 10^5)\, L_{eff\ \text{semi}}$. This illustrates the fact that for the conversion efficiency to be significant in fiber, kilometers of fibers may be needed. A long interaction length will lead to increased latency; a kilometer of fiber will result in a time delay of approximately 5 microseconds. The advantage of FWM in optical fiber is that the nonlinearity is ultrafast and well understood. Few FWM experiments have been performed in optical fiber [25]-[26].

3.2 FWM in Semiconductor Waveguides

The medium of choice for most FWM experiments has been semiconductor amplifiers [27]. Semiconductors, in contrast with optical fiber, have large third order nonlinearities, low latency, are compact and can be monolithically integrated. Low-loss passive waveguides, beside sharing most of the advantages of semiconductor amplifiers, should offer high saturation powers, simplicity and longer interaction lengths.

In semiconductor amplifiers, several mechanisms participate in the FWM process [7]. Carrier population modulation participates with a characteristic time constant $\tau \sim$ 300 ps, carrier cooling with $\tau \sim 600$ fs, carrier heating delay and spectral hole burning with $\tau \sim 100$ fs. Finally, an instantaneous two-photon absorption and a Kerr effect take part in the FWM process. Each nonlinearity contributes to the FWM process through its real (index) part as well as its imaginary (loss/gain) part. The resulting $|\chi^{(3)}|^2$ is an asymmetric bias-dependent function of $\Delta\omega$, the frequency detuning between the pump and input signal. $|\chi^{(3)}\ (\Delta\omega \sim \text{GHz})|^2$ is larger than $|\chi^{(3)}(\Delta\omega \sim \text{THz})|^2$ by several orders of magnitude, typically 40-50 dB, due to carrier population modulation [14]. In contrast, in passive waveguides, the nonlinearity relies only on the instantaneous effects and does not suffer from speed limitations imposed by the carrier modulation time constant or the carrier heating time constant. This leads to a symmetric, frequency-difference-independent (flat) conversion efficiency, η, assuming phase matching, and simpler conversion of multi-channel, broadband, signals that avoids the need for gain equalization. The absence of amplified spontaneous emission in passive waveguides should provide a reduced wavelength-independent signal-to-noise-ratio (SNR) degradation and noise floor. Finally, for multi-channel signals, passive waveguides should provide considerably lower cross-talk, between closely spaced channels, than active waveguides due to the absence of carrier population modulation.

In general, the pump power required to achieve a certain conversion efficiency is expected to be higher in passive waveguides than in semiconductor amplifiers due to the lack of gain. This is the main disadvantage of FWM in passive waveguides. However, an important consideration is that passive waveguides have higher satu-

ration powers than semiconductor amplifiers; two-photon absorption is the principle fundamental saturation mechanism in passive waveguides. With low-loss and high saturation power, longer interaction lengths and higher pump powers are accepted in passive waveguides. Consequently in multi-channel situations, the allowed power per channel is higher. This fact along with the flatness of $\eta(\Delta\omega)$ and the low cross-talk among channels makes passive waveguides an attractive medium for frequency translating multi-channel signals.

3.3 Third Order Nonlinearity Resonant Enhancement

In semiconductor amplifiers the nonlinear gain modulation contributes significantly to the magnitude of third order nonlinearity [30]. In passive semiconductor waveguides the absence of gain will result in a reduced third order nonlinearity. However, close to the bandgap a resonant enhancement in the third order nonlinearity should be present. A general expression for the n^{th} order nonlinearity, close to resonance, is [31]

$$\chi^{(n)}(-\omega_\sigma : \omega_1, \ldots \omega_n) \propto \sum_{g,b_1 \ldots b_n} \frac{(\varepsilon_\sigma^* \cdot \mu_{gb_1}^*)(\varepsilon_1 \cdot \mu_{b_1 b_2}) \cdots (\varepsilon_n \cdot \mu_{b_n g})}{(\Omega_{b_1 g} - \omega_1 - \ldots - \omega_n) \cdots (\Omega_{b_n g} - \omega_n)}$$

where ε_i is the polarization unit vector, μ_{ij} is the dipole matrix element vector, $\Omega_{ij} = (E_i - E_j)/\hbar$, and the summation $\sum_{g,b_1 \ldots b_n}$ is over all atomic states. If a quantum well (QW) is incorporated in the waveguide then the sharp excitonic resonance will enhance the third order nonlinearity [16]-[17]. In that case, the QW $\chi^{(3)}$ is the sum

of the heavy-hole and light-hole exciton resonances and $\chi^{(3)}$ may be written as [16]

$$\chi^{(3)}(\omega_4 = 2\omega_1 - \omega_3) \propto \quad D_h \frac{(\varepsilon_4^* \cdot \mu_h^*)(\varepsilon_1 \cdot \mu_h)^2 (\varepsilon_3^* \cdot \mu_h^*)}{[(\omega_h - \omega_1)^2 + \Delta\omega^2](\omega_h - \omega_1)} + D_l \frac{(\varepsilon_4^* \cdot \mu_l^*)(\varepsilon_1 \cdot \mu_l)^2 (\varepsilon_3^* \cdot \mu_l^*)}{[(\omega_l - \omega_1)^2 + \Delta\omega^2](\omega_l - \omega_1)} \tag{3.1}$$

where D is the relative density of states and h and l denote the heavy- and light-hole bands, respectively. The relative magnitudes of the dipole matrix elements are $\varepsilon_{TE} \cdot \mu_h = 1$, $\varepsilon_{TE} \cdot \mu_l = 1/\sqrt{3}$, $\varepsilon_{TM} \cdot \mu_h = 0$, and $\varepsilon_{TM} \cdot \mu_l = -\sqrt{4/3}$. For TE excitation, the heavy-hole exciton resonance contributes to $\chi^{(3)}_{1111}$ with a relative magnitude of 1, and the second term contributes to $\chi^{(3)}_{1111}$ with a relative magnitude of 1/9. For TM excitation, the second term is nonzero and contributes to $\chi^{(3)}_{1212}$, $\chi^{(3)}_{2121}$, and $\chi^{(3)}_{2222}$ with relative magnitudes of 4/9, 4/9, and 16/9, respectively. In our experiments a low loss passive InGaAsP/InP Quantum Well waveguide was used. In our case, the heavy-hole bandgap was smaller than the light-hole one due to the nondegeneracy of the heavy-hole/light-hole bands. Although some TM measurements we performed, the majority of the experimental work was performed with TE modes for all the fields. The waveguide anisotropy is a direct consequence of having a QW and should not exist in cubic symmetry bulk materials. It may be possible to remove waveguide anisotropy by clever band structure engineering (e.g. the use of stress or strain) [40]. Having an isotropic waveguide will lead to polarization insensitive wavelength conversion, a desirable property in optical communication systems.

Chapter 4

FWM in InGaAsP/InP Waveguides

4.1 InGaAsP/InP Waveguides

The waveguide samples used in our experiments are passive InGaAsP/InP single and multiple Quantum Well (QW) waveguides with bandgaps at $\lambda = 1.5$ μm. The waveguides were fabricated at Lincoln Labs using an organometallic vapor-phase epitaxy (OMVPE) process. By operating close to the bandgap, we take advantage of the resonance enhancement of $\chi^{(3)}$. Having a sharp exciton edge and high spatial uniformity in these waveguides is essential for the resonance enhancement of $\chi^{(3)}$. The ridge width was chosen so that the waveguide supports a single mode at $\lambda = 1.5$ μm, the erbium-doped fiber amplifier (EDFA) wavelength. The QW width (100 Å) and InP barriers were engineered to provide a sharp exciton edge. Low-temperature ($T = 4.5\,K$) photoluminescence spectra of quaternary InGaAsP quantum wells with

InP barriers was used to assess the sharpness of the exciton edge [35].

4.2 Waveguide Linear Loss

Since we are using a passive waveguide *and* operating close to the bandgap, the linear loss coefficient, α, is important. A lossy waveguide will result in a small conversion efficiency by producing a small L_{eff} and $e^{-\alpha L}$ factors. A considerable theoretical and experimental effort was devoted by our collaborators at Lincoln Labs in order to produce low loss waveguides. It is important to characterize the loss coefficient as a function of wavelength because as $|\chi^{(3)}|$ increases, close to the bandgap, so does α. What is important is the rate of increase of $|\chi^{(3)}|$ and α. The linear loss coefficient is expected to increase as $1/(\omega_1 - \omega_{ex})^2$ [40] while $|\chi^{(3)}|$ is expected to increase as $1/(\omega_1 - \omega_{ex})^3$ according to equation (3.1), where ω_1 is the pump frequency and ω_{ex} is the exciton resonance frequency. Hence, $\eta_{ss}(\omega)$ should increase as $1/(\omega_1 - \omega_{ex})^2$ roughly, assuming $L_{ss}^{opt} = \ln(3)/\alpha$. To begin with, we measured the linear absorption coefficient at $\lambda = 1555$ nm using Fabry-Perot fringes [41] in an uncoated sample. The measured waveguide loss was 2 dB/cm leading to $\alpha(1555) = 0.46$ cm^{-1}. Then, the waveguide's transmission at different wavelengths was measured using a weak CW beam. Given $\alpha(1555)$, we normalized the waveguide transmission data to obtain $\alpha(\lambda)$ in the proximity of the bandgap (see Figure 4-1).

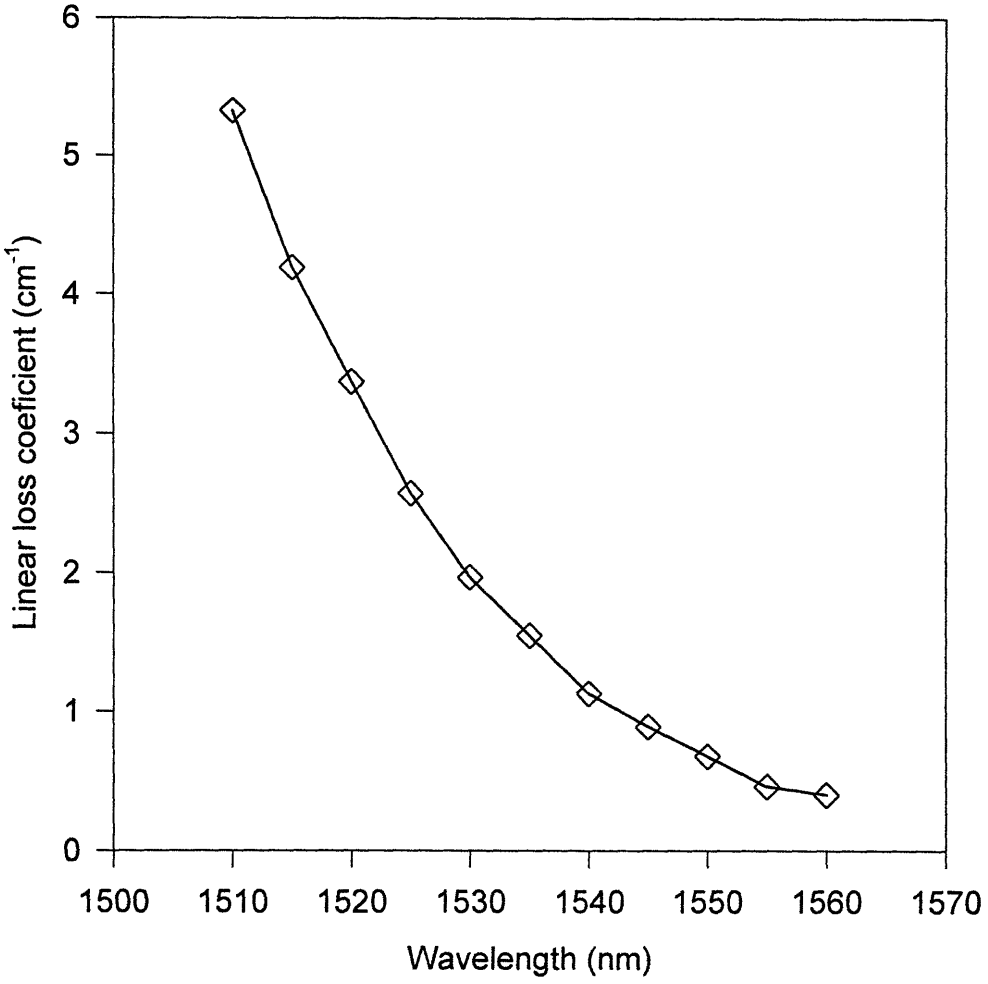

Figure 4-1: The linear loss coeficient α as a function of wavelength. The linear loss increases quickly as the bandgap is approached.

4.3 Two Photon Absorption Coefficient Measurement

We measured the TPA coefficient using standard nonlinear transmission techniques [48]. Nonlinear transmission techniques rely on the intensity propagation equation,

$$\frac{\partial I(z)}{\partial z} = -\alpha I(z) - \beta I^2(z)$$

where α is the linear loss coefficient and β is the TPA coefficient. The solution of this equation is

$$I(z) = \frac{I_{10} \cdot e^{-\alpha z}}{1 + \beta I_{10} L_{eff}} \tag{4.1}$$

It is seen that as the input intensity I_{10} is increased to a regime where $\beta I_{10} L_{eff} \gg 1$, the output intensity $I(z)$ becomes independent of the input intensity. This is known as optical limiting [45], [46]. To measure β experimentally, equation (4.1) is rewritten as

$$\frac{1}{T} = e^{\alpha z} + \beta I_{10} L_{eff} e^{\alpha z}$$

where $T \equiv I(L)/I_{10}$ is the waveguide transmission. By measuring and plotting $1/T$ for different input intensities, we should obtain a straight line with a slope directly proportional to β. Figures 4-2 and 4-3 show the experimentally measured output I and $1/T$ as a function of I_{10}, respectively, at $\lambda = 1560$ nm. From the data, we infer a $\beta(\lambda) \simeq 46$ cm/GW (equivalent to $\mathrm{Im}\{\chi^{(3)}\} = 5.4 \cdot 10^{-14}$ cm^2/V^2) after correcting for a $sech^2(t)$ pulse shape. This process was repeated at various wavelengths and we

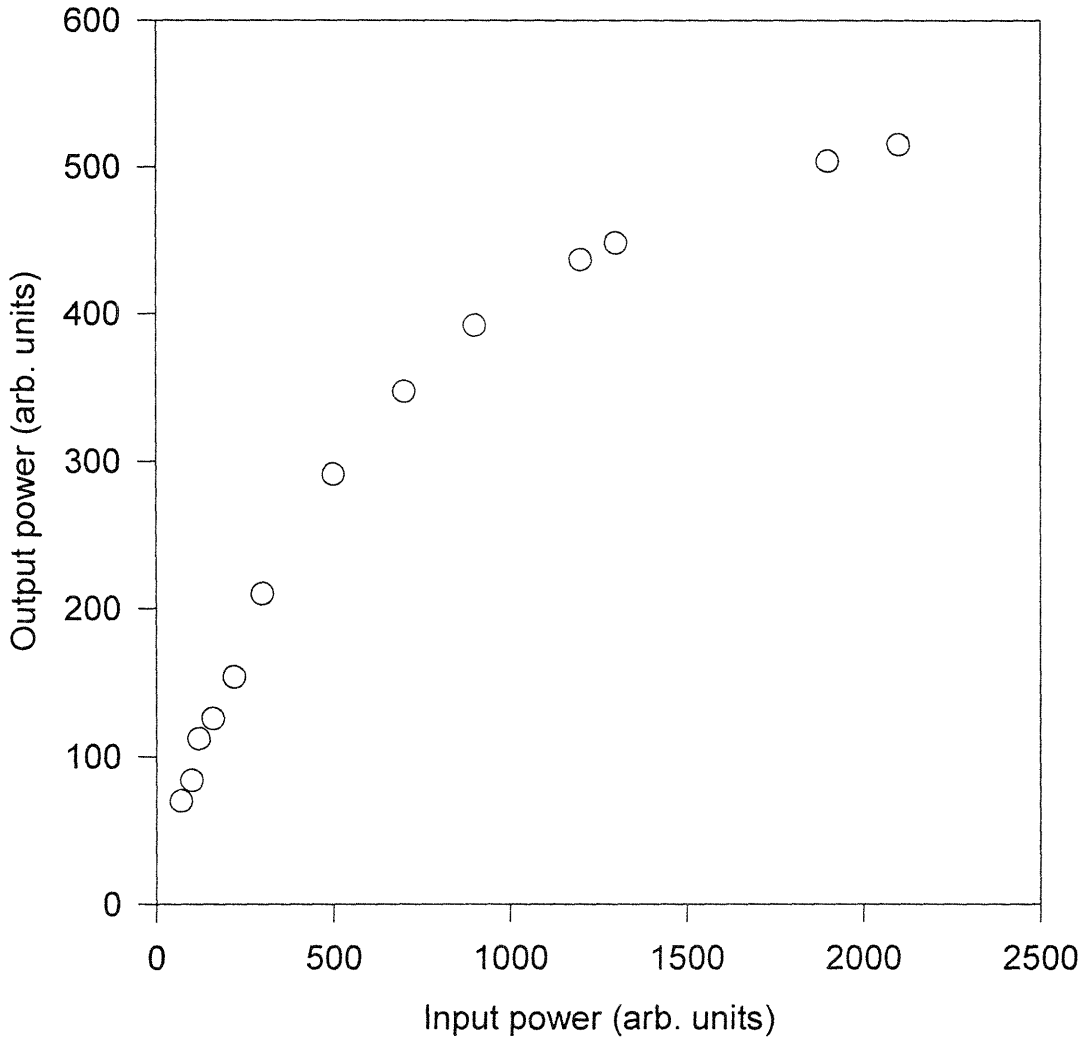

Figure 4-2: Output power (or intensity) versus input power (or intensity). The deviation from the straight line (corresponding to linear transmission) is due to two photon absorption.

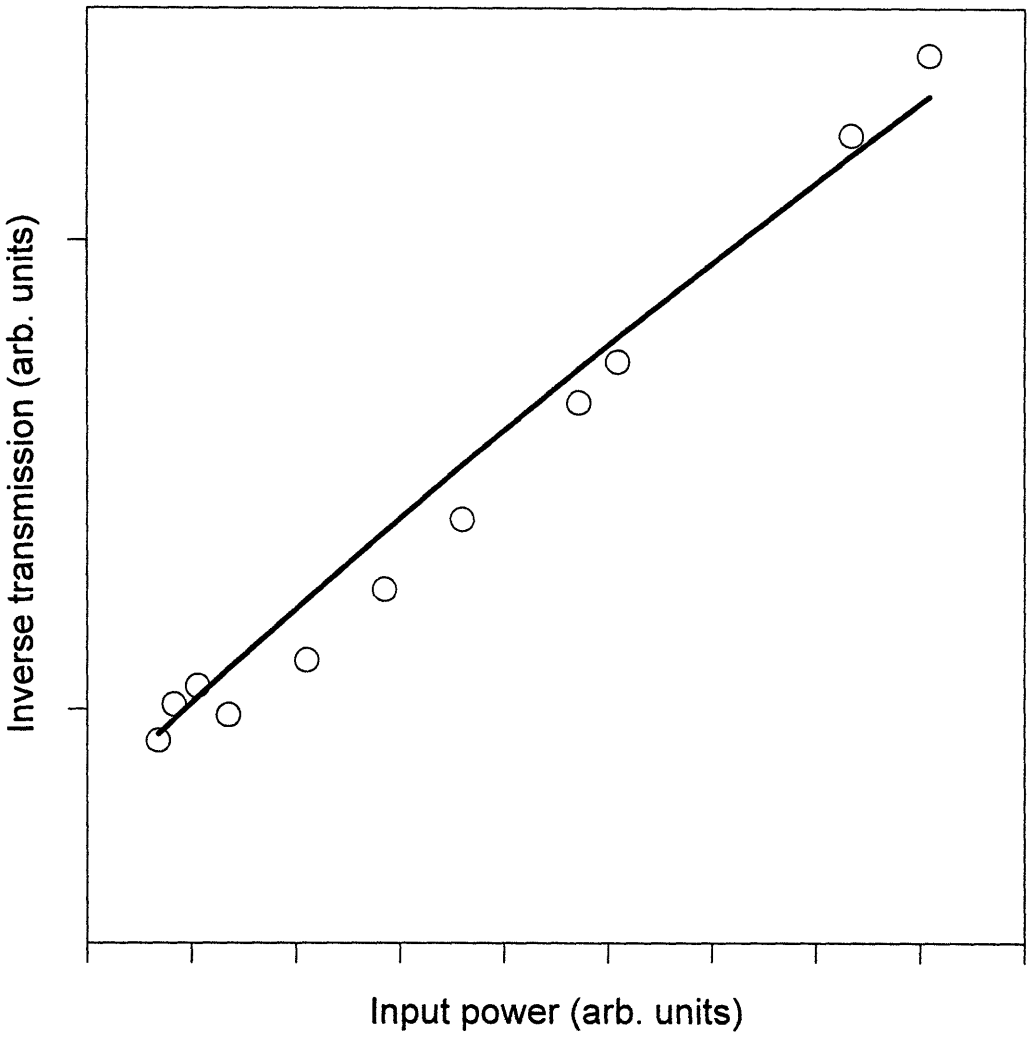

Figure 4-3: Measured inverse transmission (circles) and best fit (solid line) as a function of input power (or intensity). The slope of the line is proportional to the TPA coefficient.

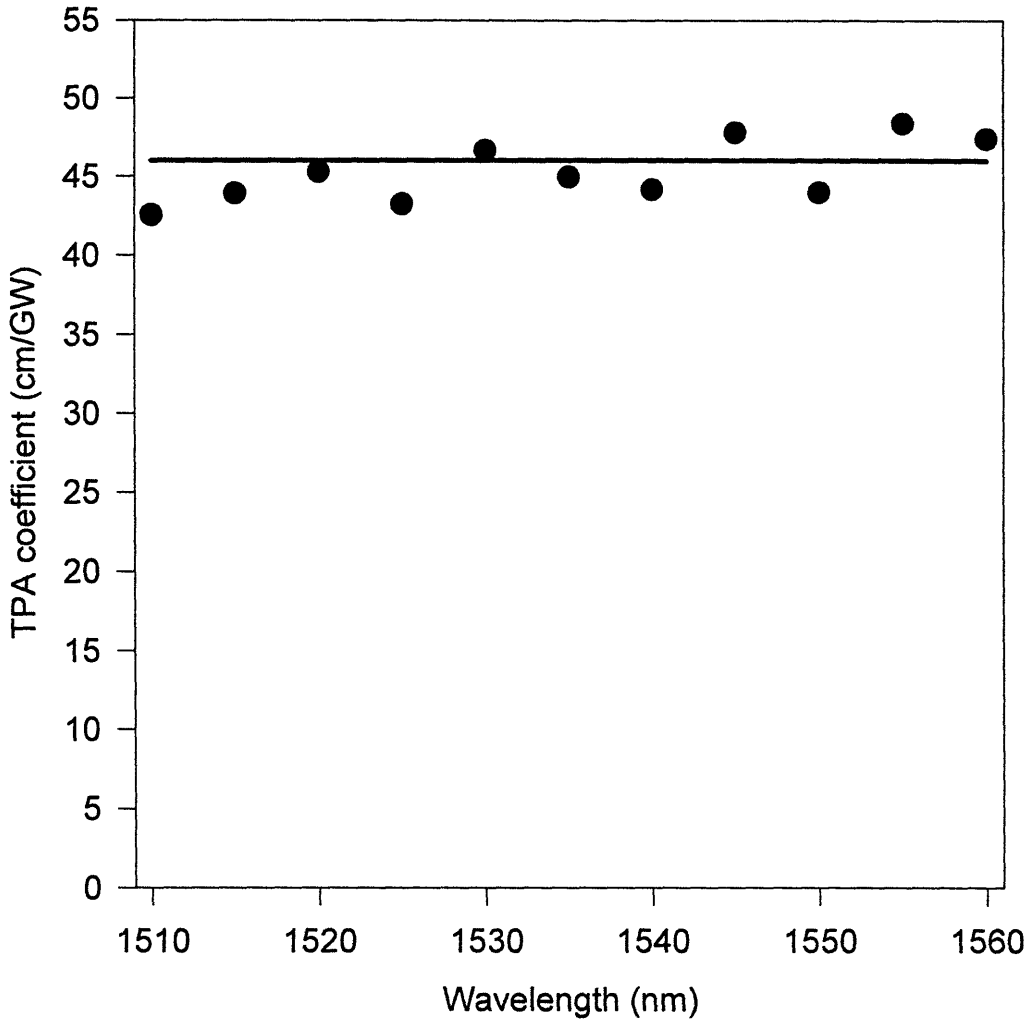

Figure 4-4: Two photon absorption coefficient as a function of wavelength. As expected, β values are essentially wavelength independent.

measured $\beta(\lambda)$ (see Figure 4-4). The experimentally measured TPA coefficient is flat close to the bandgap as predicted by theoretical calculations [47].

In the above theoretical analysis and measurements, we assumed that TPA was the only nonlinear loss mechanism. This assumption is justified below bandgap if second harmonic generation (SHG) (proportional to $\left|\chi^{(2)}\right|$) is negligible. The reason is that SHG can deplete an input signal as predicted by [4],

$$\frac{\partial E_1}{\partial z} = -\frac{\alpha_1}{2}E_1 - \frac{i}{2}\xi E_1^* E_3^{2\omega}\, e^{-i\,\Delta k\, z} \tag{4.2}$$

$$\frac{\partial E_3^{2\omega}}{\partial z} = -\frac{\alpha_3}{2}E_3^{2\omega} - \frac{i}{2}\xi E_1^2\, e^{-i\,\Delta k\, z} \tag{4.3}$$

where

$$\xi = \frac{2\omega_1 d}{nc}$$

where d is the nonlinear optical coefficient directly proportional to $\chi^{(2)}$, $E_3^{2\omega}$ is the field of the SHG generated signal, and E_1 is the pump field. To find the maximum SHG depletion loss, assume for now that $\Delta k = 0$. To estimate the SHG depletion term $-(i/2)\,\xi E_1^* E_3^{2\omega}$ we have to know $E_3^{2\omega}$. Since we are interested in the maximum value of $E_3^{2\omega}$ we can replace $E_1(z)$ in equation (4.3) by E_{10}. Equation (4.3) is of the form, $\partial f/\partial z = c_1 f + c_2$ which has the solution, $f = (c_2/c_1)\,\left(e^{c_1 z} - 1\right)$. Thus,

$$E_3^{2\omega}(z) = \frac{i\xi E_{10}^2}{\alpha_3}\left(e^{-\alpha_3 z/2} - 1\right).$$

In our case, the SHG field is well above band and will be quickly absorbed. The maximum value of $E_3^{2\omega}(z)$ is $-i\xi E_{10}^2/\alpha_3$. Substituting back into equation (4.2) we

find,

$$\frac{\partial E_1}{\partial z} = -\frac{\alpha_1}{2} E_1 - \frac{1}{2\alpha_3} \xi^2 |E_1|^2 E_1$$

The nonlinear loss term in should be compared with the TPA loss term $-\kappa''\ |E_1|^2 E_1$ (equation (5.1)). The ratio of the SHG to TPA nonlinear loss terms is

$$\begin{aligned} Ratio &= \frac{\xi^2}{2\alpha_3} \frac{1}{\kappa''} \\ &= 960\pi \left(\frac{2\pi}{\lambda_1}\right)^2 \frac{d^2}{n^3 \alpha_3 \beta} \end{aligned}$$

Although the value of d for InGaAsP is not readily available in the literature, we can get an order of magnitude estimate of the d by using that of GaAs. Comparing the d values of several zinc blende semiconductors [4] we see that their d values are of the same order of magnitude. For GaAs, $d \simeq 9 \cdot 10^{-11}\ m/V$ [32]. As a rough estimate, assume $n = 3.5, \beta = 46\, cm/GW$ and $\alpha_3 = 10^3\ \mathrm{cm}^{-1}$ (recall that SHG wavelength 750 nm is well above bandgap and hence quickly absorbed), hence we have $Ratio \simeq 0.2$. So far we ignored phase matching although the SHG process is *not* phase matched. The value of Δn is at least 0.2 (see reference [33]). Thus, $\Delta k = (2\pi/\lambda)\, \Delta n$, and the coherence length (defined by $\Delta k L_{coh} \equiv \pi$) $L_{coh} \simeq 3.7\, \mu m$. Hence, we should multiply *Ratio* by the factor $(\exp(-\alpha_3 L_{coh}/2) - 1) \simeq 0.17$ and we have

$$Ratio \simeq 0.03$$

The ratio of SHG to TPA *power* is actually $Ratio^2$ which equals $9 \cdot 10^{-4}$. In calculating the *Ratio*, we made many assumptions, however, as long as $Ratio^2 \ll 1$, we can

neglect pump depletion due to SHG generation and assume that it did not interfere with measurements of the TPA coefficient above. Experimental uncertainties in the waveguide coupling efficiency and pulse width and shape are probably the largest sources of error in the measurement.

4.4 FWM experiment

The waveguide sample used in the following experiments is an AR-coated, 7.5 mm long, passive InGaAsP/InP single Quantum Well (QW) waveguide, with a QW bandgap of $\simeq$1490 nm (TE mode). Details of the device design and fabrication are given in reference [34]-[35]. By operating close to the bandgap, we take advantage of the resonant enhancement of $\chi^{(3)}$, and the conversion efficiency is significantly increased. Two color-center lasers, KCl:Tl and NaCl:OH, are used to provide pump and signal beams. Both lasers are synchronously pumped by an actively mode-locked Nd:YAG laser that produces 100 ps pulses at 100 MHz repetition rate. The KCl:Tl laser, tunable from 1460 nm to 1560 nm, produces 10 ps pulses; the NaCl:OH laser, tunable from 1530 nm to 1660 nm, produces 3-10 ps pulses. Both color-center lasers can be operated CW.

4.4.1 Light Coupling

Light is coupled in (and out of) the ridge waveguide using AR-coated aspheric lenses (purchased from Thor Labs.). After many trials, with different lenses and microscope objectives, these lenses were found to work best because of their low loss and low

numerical aperture (NA). The coupling loss was estimated by comparing the input power with the output power (assuming the output coupler collects most of output light) in an essentially lossless short waveguide sample ($\lambda_g = 1.3$ μm) with identical dimensions to the 1.5 μm sample. The coupling loss was estimated to be $\sim$ 6 dB. In the FWM experiment we need to couple two beams, pump and signal, into the waveguide using one focusing lens. To achieve that both beams should have roughly equal spotsize, assuming a flat phase front. This is partially satisfied by inserting a long focal length lens in the path of one of the beams in order to match the spotsizes at the focusing lens. Aside from the spotsize matching problem, the problem of beam overlap must be solved. To overlap the two beams we must have independent lateral and vertical control of each beam. The XYZ coupling stage of the input lens provides control for one beam only. The experimental setup should provide an independent control for the other beam.

Perhaps the biggest difficulty pertaining to coupling in (and out of) the waveguide is the fact that the waveguide is passive. The procedure for aligning the input and output coupling lenses is simple in the case of an active waveguide (i.e. an amplifier). One simply turns on the amplifier so that it emits an amplified spontaneous emission (ASE) signal then tweaks the input and output lenses to obtain maximum ASE signal. By overlapping the input beams with the ASE spot, one can couple into the waveguide. In passive waveguides the situation is not as simple. The following procedure was used successfully to couple in (and out of) the passive waveguide (see Figure 4-5):

(1) Remove the waveguide out of the optical path. Advance lenses L_1 and L_2

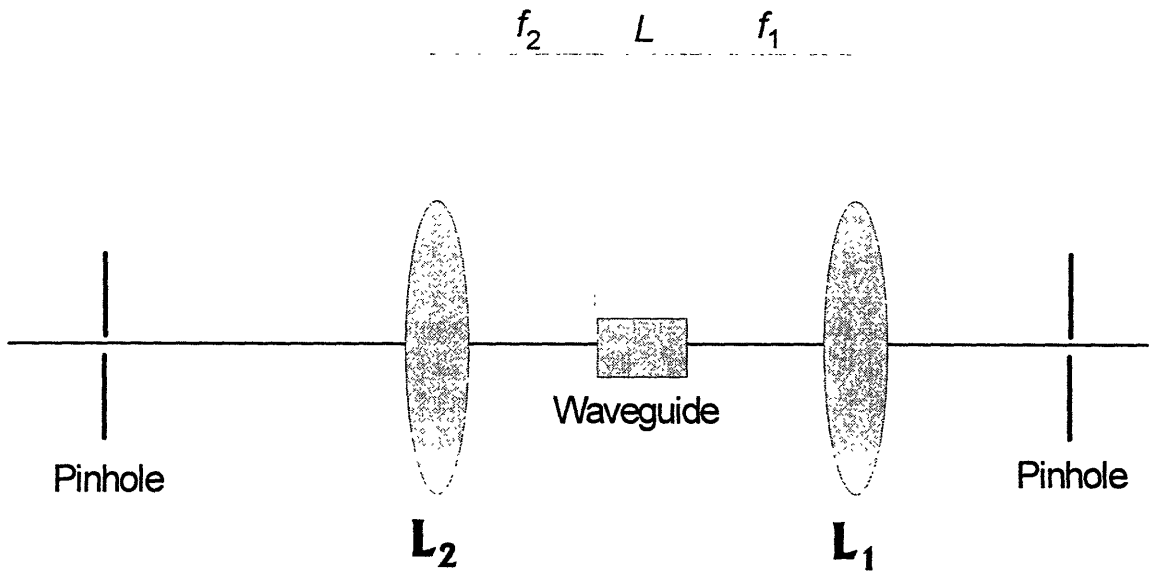

Figure 4-5: Waveguide and lens alignment. Both lenses, L_1 and L_2 are on XYZ stages as well as the waveguide.

towards each other such that the distance between them equals $f_1 + f_2$. Align the optical beams through the two pinholes located before and after the coupling lenses.

(2) Retract lenses L_1 and L_2 away from each other by a distance greater than L (the waveguide physical length). Insert the waveguide in the optical path such that the distance between lens L_1 and the waveguide input facet equals $\sim 1.5\, f_1$ and the distance between lens L_2 and the waveguide output facet equals, roughly, f_2. Now the output coupling lens is close to its correct positions and the input coupling lens illuminates the entire input facet.

(3) Move the output lens vertically and laterally to collect light exiting from the output facet. Adjust the distance between the output lens and the waveguide (along z-direction) in order to image the waveguide output facet on the IR card or on a IR

camera. The output facet's guiding layer[1] is illuminated by the light from the input facet. This imaging step is perhaps the most difficult part because the output facet is typically very faint and it is easy to mistake it for a diffraction fringe.

(4) Once the distance between the output lens and the waveguide is properly set and the output facet is imaged, attention is turned to the input lens. Adjust the input lens's vertical position to maximize the light collected from the guiding layer. The Z-position of the input lens may now be adjusted to maximize again the guiding layer light.

(5) Move the output lens laterally. Waveguides will appear brighter than the rest of the guiding layer. Once a waveguide is identified, the output pinhole should be closed so that it passes light from the waveguide only. Place a photodetector to measure the waveguide light. Now the input lens may be adjusted laterally and vertically to increase light through the waveguide. Tweak the Z-position and readjust the lateral and vertical positions iteratively until the maximum amount of light is guided through the waveguide. If the input lens is perfectly aligned with the waveguide, there should be essentially little or no leaked light into the rest of the guiding layer. To check that, open the output diaphragm (pinhole). Only the waveguide should be bright and the rest of the output facet should be completely dark.

[1]The guiding layer is the horizontal InGaAsP slab in the waveguide structure. It is responsible for guiding the light in the vertical direction. The ridge is responsible for the lateral guiding.

4.4.2 FWM Spectrum

With the input and output lenses properly aligned and the two beams coupled into the waveguide, the rest of the FWM becomes straightforward. The output light is then directed to an optical spectrum analyzer. The FWM signal should be visible. Figure 4-6 shows a typical power spectrum. Another example of a FWM power spectrum is shown in Figure (4-7). In this case, the pump and signal fields are of equal magnitude and each plays a double role. The FWM signal at 1540 nm is produced by the field at 1550 nm acting as a pump and the field at 1560 nm acting as signal field. Similarly, the FWM signal at 1570 nm is produced by the field at 1560 nm acting as a pump and the field at 1550 nm acting as signal field.

4.4.3 Third Order Nonlinearity Measurement

Now we turn our attention to measuring $|\chi^{(3)}|$ as a function of wavelength in order to evaluate the enhancement in $|\chi^{(3)}|$ in the vicinity of the bandgap. First, we tuned the KCl:Tl and NaCl:OH lasers from 1560 nm to 1510 nm in steps of 5 nm while maintaining a small fixed wavelength separation between them. At each step the conversion efficiency and peak powers were recorded and we obtained $|\chi^{(3)}(\lambda)|$, see Figure 4-8, using the small signal conversion efficiency formula, equation (2.14),

$$\eta_{ss} = e^{-\alpha_3 \cdot L} \cdot \left[\frac{180 \cdot \pi^2}{n^2 \cdot \lambda} \cdot \frac{P_{\text{peak}} \cdot L_{\text{eff}} \cdot |\chi^{(3)}|}{A'_{eff}} \right]^2$$

where P_{peak} is the pump peak power. In our case, $L = 7.5$ mm, $A'_{eff} = 2 \cdot A_{\text{eff}} = 6 \cdot 10^{-8}$ cm^2, $n = 3.25$ and $\alpha(\lambda)$ is given by Figure 4-1. We observe that $|\chi^{(3)}|$ increases

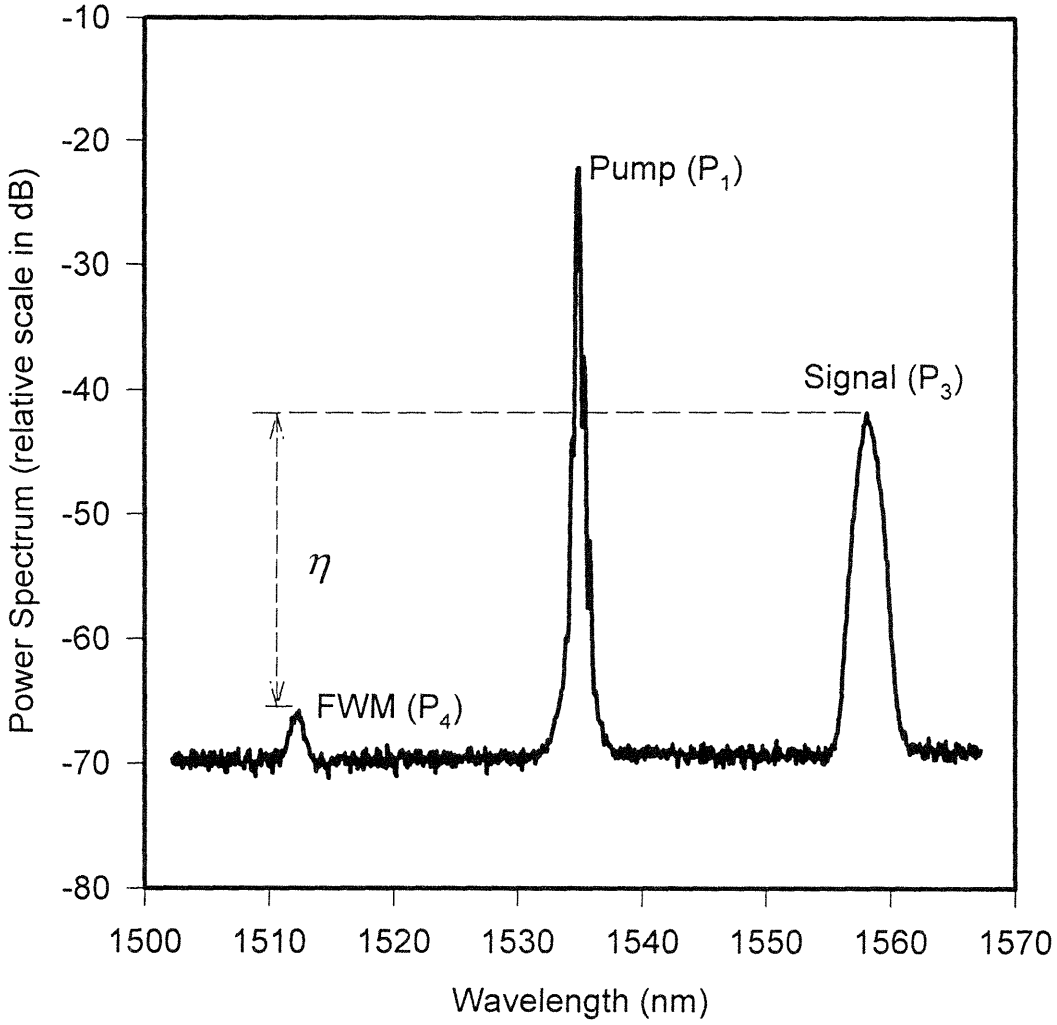

Figure 4-6: Typical FWM experiment output spectrum.

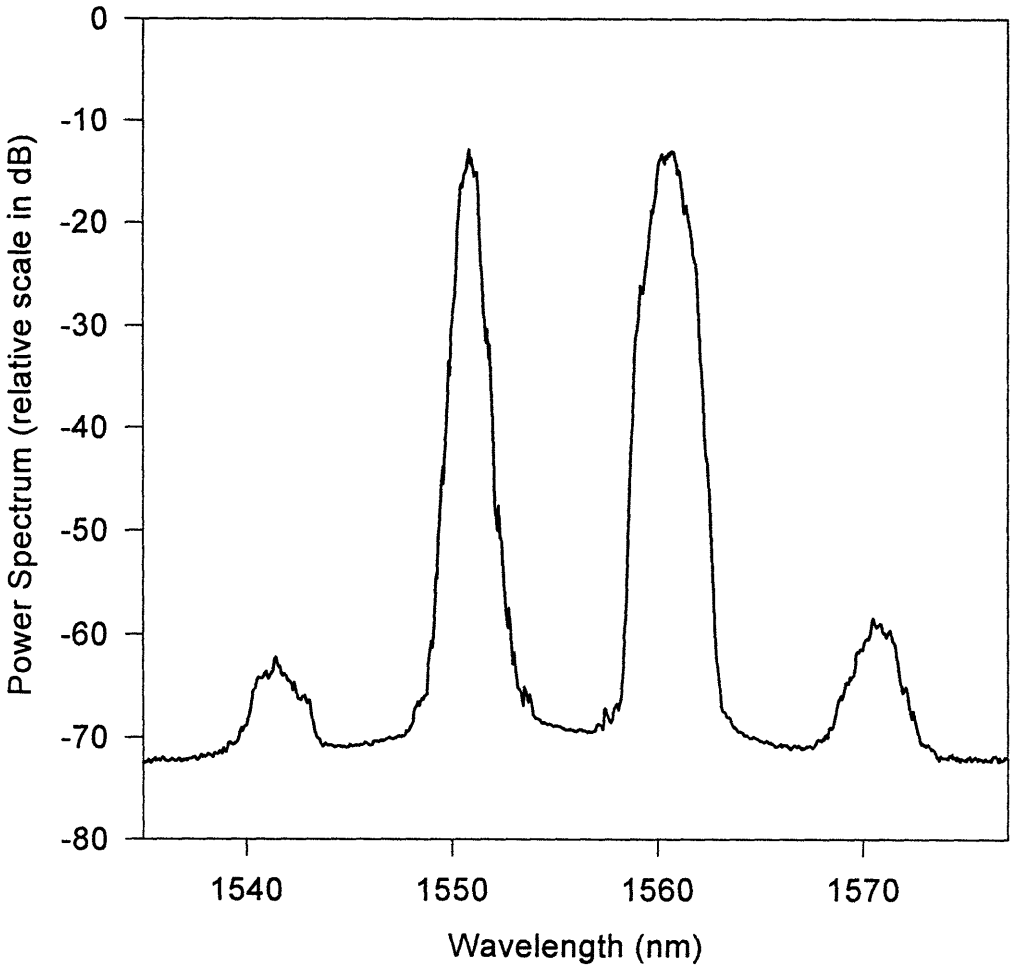

Figure 4-7: Typical power spectrum of FWM experiment. The pump and signal beams produce a FWM signal. In this spectrum the pump and signal are of equal power and each plays the role of 'pump' and 'signal' field at the same time producing two FWM signals.

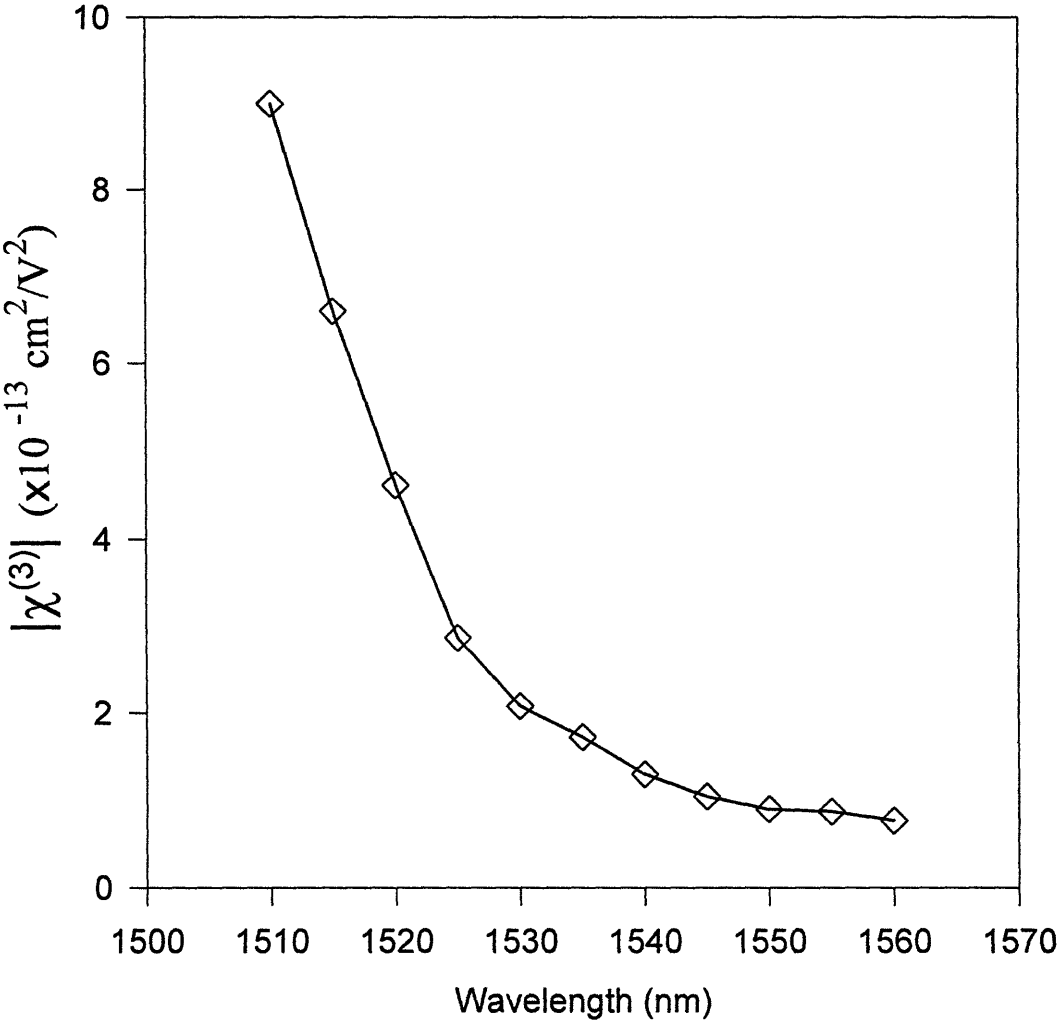

Figure 4-8: The third order nonlinearity as a function of wavelength. The resonant enhancement is clear. An order of magnitude improvement in $\left|\chi^{(3)}\right|$ is observed.

by an order of magnitude close to the bandgap compared with the off-resonance $|\chi^{(3)}|$. However, as $|\chi^{(3)}(\lambda)|$ is enhanced, $\alpha(\lambda)$ increases quickly. The quantity of interest is $\eta(\lambda)$ which we plot on a relative scale in Figure 4-9. The conversion efficiency peaks close to the bandgap; then it starts decreasing due to excessive linear absorption. In our case, the conversion efficiency quadruples (assuming fixed device length of 7.5 mm) at the peak wavelength of 1515 nm (~1.5 % below the bandgap energy) compared with its off-resonance value. Note that the conversion efficiency can be enhanced further by optimization of device length; especially close to the bandgap where the linear loss increases and the optimum length formula calls for a L shorter than 7.5 mm.

To verify the nature (reactive vs. resistive) of the enhancement of $|\chi^{(3)}|$ in the proximity of the bandgap, we measured the two photon absorption coefficient, $\beta(\lambda)$, which is directly proportional to $\mathrm{Im}\{\chi^{(3)}\}$. With high peak-power, short pulses, the values of $\beta(\lambda)$ were measured using a power saturation technique [42]. The measured data is shown in Figure 4-10. As expected, the values of $\beta(\lambda)$ remain constant as the bandgap is approached. Hence, the enhancement in $|\chi^{(3)}|$ is purely in the reactive part, $\mathrm{Re}\{\chi^{(3)}\}$; and close to the bandgap $\mathrm{Re}\{\chi^{(3)}\} \approx |\chi^{(3)}|$ since $\mathrm{Re}\{\chi^{(3)}\} >> \mathrm{Im}\{\chi^{(3)}\}$. The measured average value of $\beta(\lambda) = 46$ cm/GW is of similar magnitude although somewhat smaller than the previously reported value of 60 cm/GW for a multi-quantum-well passive InGaAsP/InP waveguide at 200 nm away from the bandgap [36]. Since the nonlinearity is ultrafast, $\mathrm{Re}\{\chi^{(3)}\}$ may be represented as n_2 (where $n = n_0 + n_2 I$). The values of n_2, as a function of wavelength are plotted in Figure 4-10. These n_2 values compare favorably with previous measurements in active waveguides

Figure 4-9: Normalized conversion efficiency as a function of wavelength. A four-fold increase is observed in the value of η, compared with the off-resonance value. Further enhancement is possible through the optimization of waveguide length.

InGaAsP [30]. Note that in Figure 4-10 only the magnitude of n_2 is plotted. From our measurements we can not determine the sign of n_2. However, n_2 is expected to be negative [36], [37], [38],.

4.5 Waveguide GVD

To study the tuning characteristic of the FWM signal, we tuned the input signal away from the pump wavelength in small steps. With a CW pump centered at 1546 nm, the input was tuned from 1515 nm to 1543 nm in steps of 0.5 nm. The resulting conversion efficiency along with a simple $|sin(\Delta kL/2)/(\Delta kL/2)|^2$ theoretical fit is shown in Figure 4-11. The close agreement between the theory and experiment confirms that the nonlinearity is, indeed, ultrafast. The fact that the nonlinearity is ultrafast, hence does not lag the driving fields, leads to a symmetric (with respect to frequency detuning) conversion efficiency since we have $\chi^{(3)}(\Delta\omega) = \chi^{(3)}(-\Delta\omega)$. This Phase matching nulls, due to group velocity dispersion (GVD), are clearly evident and provide a general measurement technique for GVD. For the case here, a GVD of 3200 ps^2/km is deduced, in agreement with values reported in the literature [29] based on time domain techniques. For the 7.5 mm waveguides used here, the 3-dB wavelength conversion bandwidth is $\sim$ 26 nm. If we double the pump power and reduce the length by half, we can wavelength shift a signal by 52 nm (7 THz) without phase mismatch.

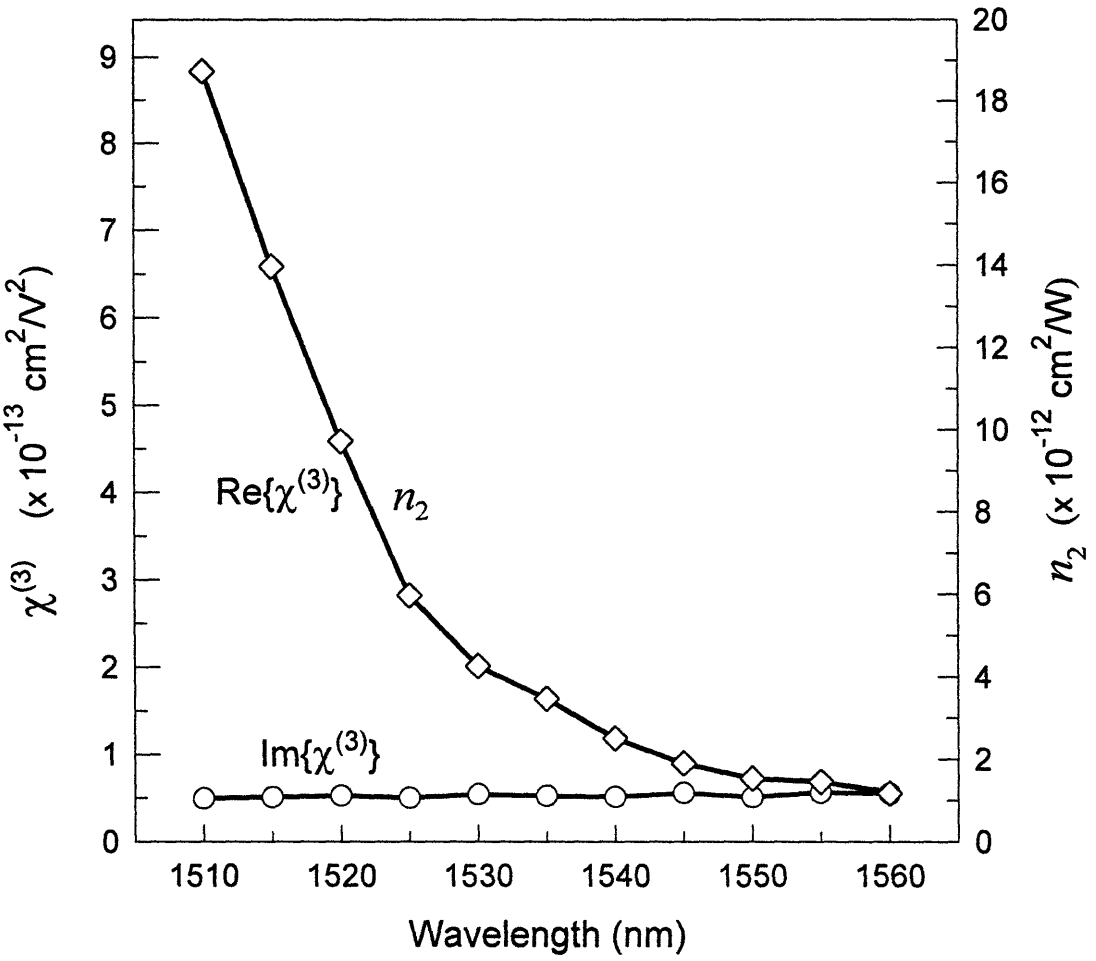

Figure 4-10: Measurement of the real and imaginary parts of the third order nonlinearity. The left $y-$axis gives the measured $\chi^{(3)}$ value while the right $y-$axis gives the corresponding n_2 value.

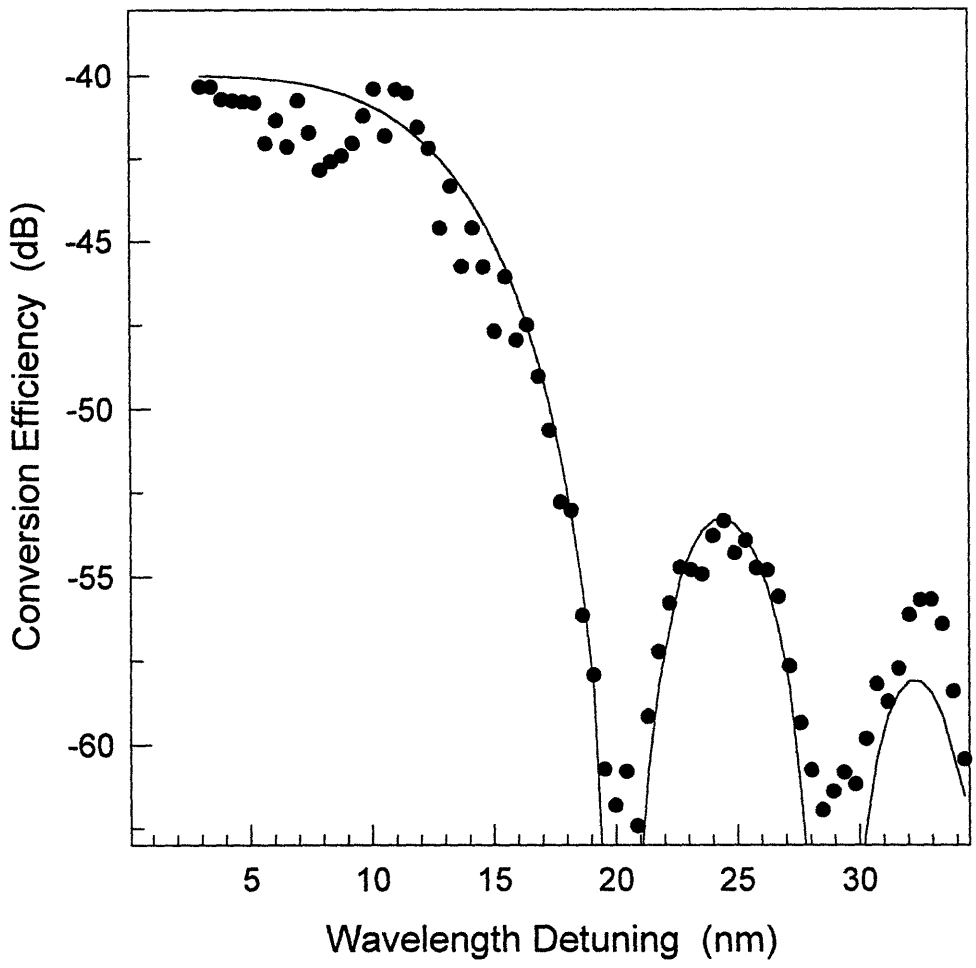

Figure 4-11: Conversion efficiency as a function of wavelength detuning along with a simple $sin(x)/x$ curve fit. The close agreement between theory and experiment suggests that the nonlinearity is ultrafast as assumed in theory.

4.6 Short Pulse Wavelength Shifting

To demonstrate high conversion efficiency, we operated the color-center lasers in a pulsed mode to obtain high peak powers. With the KCl:Tl laser producing 10 ps pulses at 1535 nm, as pump, and the NaCl:OH laser producing 3 ps pulses at 1545 nm, as signal, we demonstrate a conversion efficiency of -11 dB, as shown in Figure 4-12. The peak power of the pump pulses is ~ 0.50 W inside the waveguide.

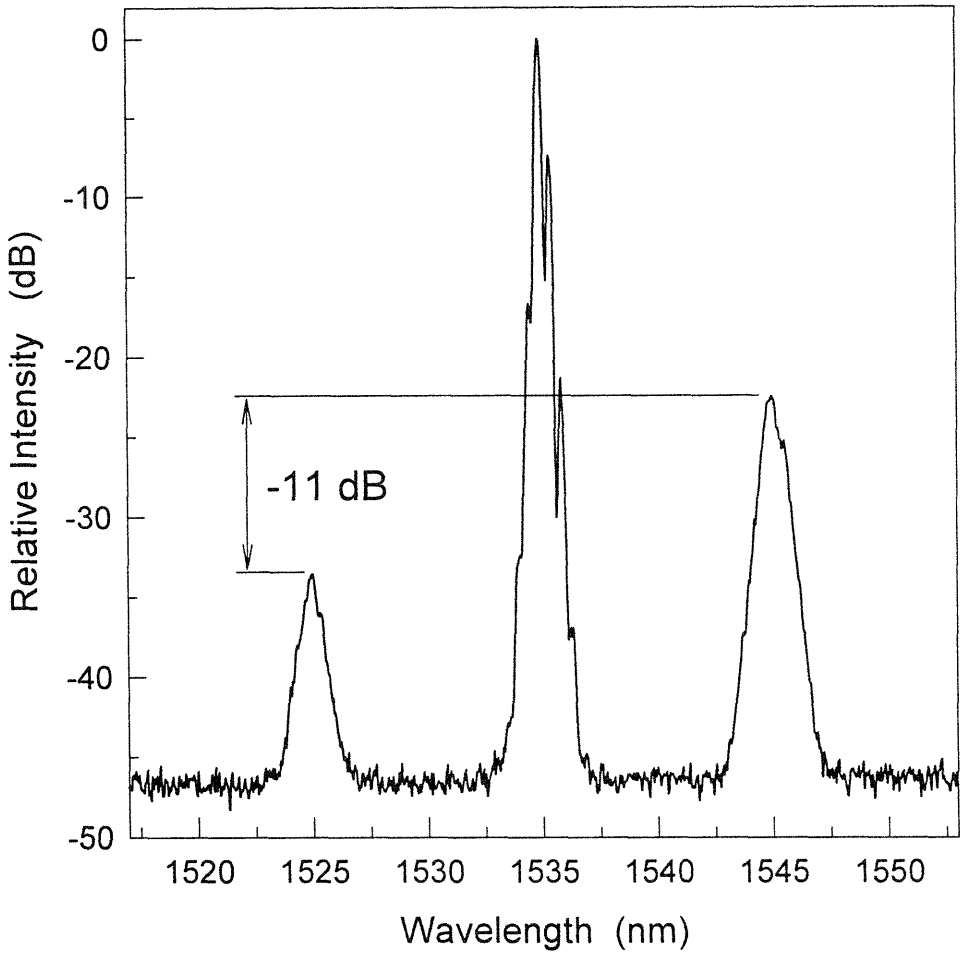

Figure 4-12: A conversion efficiency of -11 dB was achieved with a 10 ps pump (KCL:Tl laser) and a 3 ps signal (NaCl:OH laser). The wavelength translation is 20 nm ($\sim$ 3 THz).

Chapter 5

FWM and Nonlinear Effects

5.1 Nonlinear Effects

Achieving high conversion efficiency through utilizing high pump powers will inevitably introduce significant nonlinear effects. Among the simplest and most important are the nonlinear refractive-index changes (proportional to $\mathrm{Re}\{\chi^{(3)}\}$) and the nonlinear absorption (proportional to $\mathrm{Im}\{\chi^{(3)}\}$). Both are expected to affect the FWM process as the pump power increases. The role of nonlinear loss will be to attenuate the input pump and signal fields, and the nonlinear index changes will spectrally distort the pump and signal fields by self-phase-modulation (SPM) effects and cross-phase-modulation (XPM) effects, respectively and change the phase matching condition. The relative importance of nonlinear loss and index changes depends on the material's switching figure of merit [20] (proportional to $\mathrm{Re}\{\chi^{(3)}\}/\mathrm{Im}\{\chi^{(3)}\}$). While nonlinear loss effects on all-optical switching by index nonlinearities have been extensively studied [18], [43], less attention has been given to their effects on FWM

[44], [51]. Understanding the effects of nonlinear loss on the FWM process will help us define appropriate figures of merit, optimize device design, and attain the highest conversion efficiency allowed. We shall derive simple expressions for the optimum input pump intensity and the associated maximum conversion efficiency, calculate the optimum waveguide length, define a material's figure-of-merit similar to that for all-optical switching based on nonlinear index changes, and apply that to short pulse frequency conversion. Experimentally, we test the validity of the theoretical results by performing a FWM experiment with high peak power picosecond pulses in a passive InGaAsP/InP single quantum well waveguide. In the following we examine the effect of nonlinear loss alone on FWM as a limiting case, the effect of nonlinear index changes alone on FWM as another limiting case, and the general case where both nonlinear loss and index changes affect the FWM.

5.2 Effect of Nonlinear Loss on FWM

To examine the influence of nonlinear effects on FWM, we must retain the nonlinear terms in FWM equations (2.6)-(2.8). In this section, we shall focus our attention on the case where the nonlinear loss dominates. Short pulse FWM experiments utilizing high intensities in passive waveguides reveal that two-photon-absorption (TPA) reduces the conversion efficiency appreciably [17]. At high pump intensities, the nonlinear loss attenuates both the input pump and signal fields. Generally, semiconductor materials, for energies above $E_g/2$, exhibit unfavorable figures of merit [20], which further implies that nonlinear loss mechanisms, such as TPA and free-carrier-absorption

(FCA), significantly attenuate an input signal even before it acquires enough phase shift to cause spectral distortions or phase mismatch [30], [17]. In addition, nonlinear loss and index changes typically limit the conversion efficiency before signal depletion is significant.

The goal of this section is to investigate theoretically and experimentally the nonlinear loss effects, concentrating on mechanisms that behave like TPA. Theoretically, we show that nonlinear loss places a fundamental upper limit on the conversion efficiency. We derive simple expressions for the optimum input pump intensity and the associated maximum conversion efficiency, calculate the optimum waveguide length, define a material's figure-of-merit similar to that for all-optical switching based on nonlinear index changes. Experimentally, we test the validity of the theoretical results by performing a FWM experiment with high peak power picosecond pulses. Good agreement is observed between theory and experiment.

We begin our analysis by rewriting equations (2.6)-(2.8), assuming phase matching,

$$\frac{\partial E_1}{\partial z} = -\frac{\alpha_1}{2}E_1 - \kappa''\,|E_1|^2\,E_1 \tag{5.1}$$

$$\frac{\partial E_3}{\partial z} = -\frac{\alpha_3}{2}E_3 - 2\,\kappa''\,|E_1|^2\,E_3 \tag{5.2}$$

$$\frac{\partial E_4}{\partial z} = -\frac{\alpha_4}{2}E_4 - 2\,\kappa''\,|E_1|^2\,E_4 + i\gamma\chi^{(3)}E_1^2E_3^* \tag{5.3}$$

where we define

$$\kappa \equiv \kappa' + i\,\kappa'' \tag{5.4}$$

$$\kappa'' \equiv Im\{\kappa\} \tag{5.5}$$

where we have replaced $i\kappa$ by $-\kappa''$. Note that κ'' equals $Im\{\kappa\}$ which in turn is proportional to the TPA coefficient (see equation (2.10)). To solve for $E_4(z)$, we start by solving equations (5.1) and (5.2) for $E_1(z)$ and $E_3(z)$, respectively, using standard methods of differential equations [39]. The solution of equation (5.1) is,

$$E_1(z) = E_{10} \cdot e^{-(\alpha/2)z - \kappa''\,\varphi(z)} \tag{5.6}$$

where

$$\varphi(z) = \frac{1}{2\kappa''} \ln\left[1 + 2\kappa''\,|E_{10}|^2 \left(\frac{1 - e^{-\alpha z}}{\alpha}\right)\right] \tag{5.7}$$

In equation (5.7) we assumed for simplicity that $\alpha_1 \simeq \alpha_3 \simeq \alpha_4 = \alpha$. We may rewrite equation (5.6) as

$$E_1(z) = \frac{E_{10} \cdot e^{-(\alpha/2)z}}{\sqrt{1 + I_{10}/I_s(z)}} \tag{5.8}$$

where I_{10} is the pump's input intensity ($I_{10} = P_{10}/A'_{eff} = (n/240\pi)\,|E_{10}|^2$) and $I_s(z) \equiv 1/\beta[(1 - e^{-\alpha z})/\alpha] = 1/\beta L_{eff}(z)$ is defined as the waveguide saturation intensity such that I_s is the *asymptotic-limited output* intensity of a lossless waveguide

($\alpha = 0$), as may be verified from equation (5.8). Similarly, we solve equation (5.2),

$$E_3(z) = E_{30} \cdot e^{-\frac{\alpha}{2}z - 2\kappa'' \varphi(z)} \tag{5.9}$$

where $\varphi(z)$ is the same as above. Again, we may rewrite equation (5.9) as,

$$E_3(z) = \frac{E_{30} \cdot e^{-\frac{\alpha}{2}z}}{1 + I_{10}/I_s(z)}. \tag{5.10}$$

Now we use equations (5.6) and (5.9), to substitute for $E_1(z)$ and $E_3(z)$, respectively, in equation (5.3). The FWM equation (5.3) becomes,

$$\frac{\partial E_4}{\partial z} = -\frac{\alpha_4}{2}E_4 - 2\kappa'' \, |E_{10}|^2 \, e^{-\alpha z - 2\kappa'' \varphi(z)} \, E_4 + i\gamma\chi^{(3)} E_{10}^2 E_{30}^* \, e^{-\frac{3}{2}\alpha z - 4\kappa'' \varphi(z)} \tag{5.11}$$

which is of the form

$$\frac{\partial E_4}{\partial z} + f(z) \cdot E_4(z) = g(z) \tag{5.12}$$

where

$$\begin{aligned} f(z) &= \frac{\alpha_4}{2} + 2\kappa'' \, |E_{10}|^2 \, e^{-\alpha z - 2\kappa'' \varphi(z)} \\ g(z) &= i\gamma\chi^{(3)} E_{10}^2 E_{30}^* \, e^{-\frac{3}{2}\alpha z - 4\kappa'' \varphi(z)} \end{aligned}$$

The form of equation (5.12) is a standard differential equation and may be solved

using well known methods of differential equations [39]. Its solution is,

$$E_4(z) = \frac{1}{\xi(z)} \left[\int_z \xi(z)\, g(z)\, dz + C \right] \tag{5.13}$$

where

$$\begin{aligned} \xi(z) &= \exp\left(\int_z f(z)\, dz \right) \\ C &= constant \end{aligned}$$

Substituting $f(z)$ and $g(z)$ into the above formulas we obtain,

$$\xi(z) = e^{(\alpha/2)z} \left[1 + 2\kappa'' \left| E_{10} \right|^2 \left(\frac{1 - e^{-\alpha z}}{\alpha} \right) \right]$$

and

$$\int_z \xi(z)\, g(z)\, dz = c_1 \ln \left[1 + 2\kappa'' \left| E_{10} \right|^2 \left(\frac{1 - e^{-\alpha z}}{\alpha} \right) \right]$$

where

$$c_1 = i\gamma\chi^{(3)} E_{30}^* / 2\kappa''$$

Substituting in equation (5.13) and assuming the boundary condition $E_4(0) = 0$ we obtain,

$$E_4(z) = c_1 \frac{e^{-(\alpha/2)z} \ln \left[1 + 2\kappa'' \left| E_{10} \right|^2 \left(\frac{1 - e^{-\alpha z}}{\alpha} \right) \right]}{\left[1 + 2\kappa'' \left| E_{10} \right|^2 \left(\frac{1 - e^{-\alpha z}}{\alpha} \right) \right]}$$

Using the definition of the conversion efficiency ($\eta = |E_4(z)/E_3(0)|^2$) we may express η as,

$$\eta = e^{-\alpha L}\left[\left|\frac{\gamma\chi^{(3)}}{2\kappa''}\right| \cdot \frac{\ln\left[1+2\kappa''\left|E_{10}\right|^2\left(\frac{1-e^{-\alpha L}}{\alpha}\right)\right]}{\left[1+2\kappa''\left|E_{10}\right|^2\left(\frac{1-e^{-\alpha L}}{\alpha}\right)\right]}\right]^2 \tag{5.14}$$

or, in terms of input pump intensity,

$$\eta = e^{-\alpha L}\left[\left|\frac{\gamma\chi^{(3)}}{2\kappa''}\right| \cdot \frac{\ln(1+I_{10}/I_s)}{(1+I_{10}/I_s)}\right]^2 \tag{5.15}$$

Using the relationship between κ'' and κ (equation (5.5)) and between κ and the TPA coefficient β (equation (2.10)) and the fact that β is related to $Im\{\chi^{(3)}\}$ by,

$$\beta = \frac{180\,\pi^2}{\lambda\, n^2} Im\{\chi^{(3)}\}$$

assuming that TPA is the only nonlinear loss mechanism, we can rewrite $\left|\gamma\chi^{(3)}/2\kappa''\right|$ as,

$$\left|\frac{\gamma\chi^{(3)}}{2\kappa''}\right| = \left|\frac{\chi^{(3)}}{Im\{\chi^{(3)}\}}\right|$$

Hence, we arrive at the final result,

$$\eta(I_{10}) = e^{-\alpha L}\left[\left|\frac{\chi^{(3)}}{Im\{\chi^{(3)}\}}\right| \cdot \frac{\ln(1+I_{10}/I_s)}{(1+I_{10}/I_s)}\right]^2 \tag{5.16}$$

As expected, in the limit of $I_{10} \ll I_s$, the *large signal* conversion efficiency expression equation (5.16) reduces to the small-signal one, equation (2.14). However, for large input intensities, we obtain very different behavior. A plot of $\eta(I_{10})$ (solid line) is shown in Figure 5-1 (assuming $\left|\chi^{(3)}/Im\{\chi^{(3)}\}\right| \simeq 1$) along with $\eta_{ss}(I_{10})$ (dashed line) for comparison. Contrasting η_{ss} with η, we find that η_{ss}'s accuracy is rapidly lost

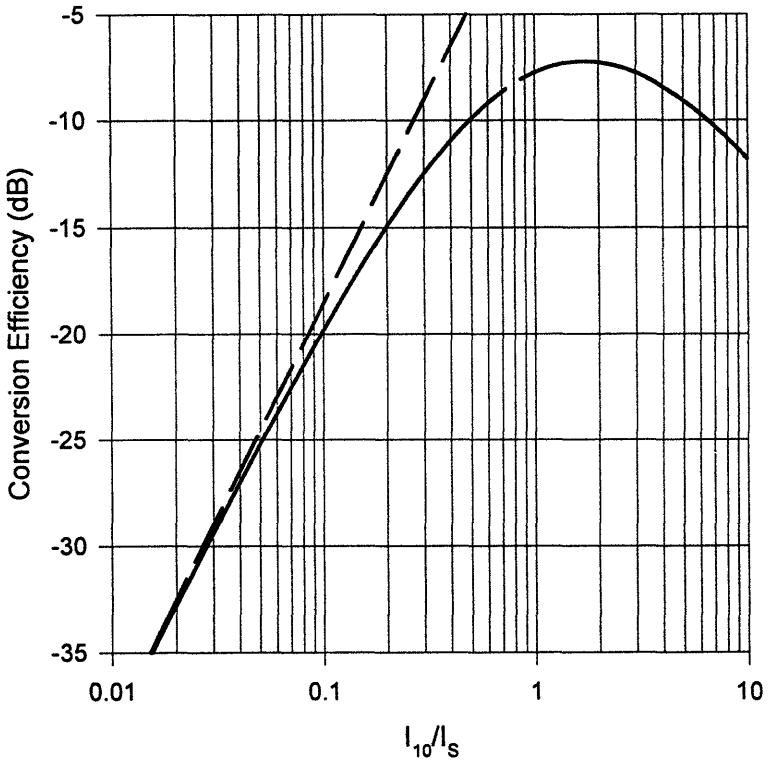

Figure 5-1: Small signal (dashed line) and large signal (solid line) conversion efficiencies as a function of normalized input pump intensity assuming $\left|\chi^{(3)}/Im\{\chi^{(3)}\}\right| \simeq 1$.

as I_{10} increases. For instance, η_{ss} overestimates the conversion efficiency by 25% for pump intensities as low as $I_{10} = 0.1I_s$, and for $I_{10} = 0.25I_s$ it is off by a factor of $\times 2$. As Figure 5-1 indicates, the large signal conversion efficiency, $\eta(I_{10})$, reaches a maximum value of,

$$\eta_{\max} = \left| \frac{\chi^{(3)}}{\mathrm{Im}\{\chi^{(3)}\}} \right|^2 \cdot e^{-\alpha L - 2} \equiv \eta_m \cdot e^{-\alpha L}$$

at an optimum input intensity of,

$$I_{10}^{opt} = (e-1)I_s = 1.72\, I_s$$

as may be verified directly from equation (5.16). First, note that the highest value $\eta_{\max}$ can assume is $\eta_m = \left|\chi^{(3)}/\mathrm{Im}\{\chi^{(3)}\}\right|^2 \cdot e^{-2}$, a geometry independent quantity. Hence, we may define a material's figure-of-merit (FOM) as,

$$FOM = \left| \frac{\chi^{(3)}}{\mathrm{Im}\{\chi^{(3)}\}} \right|^2 = 1 + \left(\frac{2\pi}{\lambda} \frac{n_2}{\beta} \right)^2$$

where n_2 is the nonlinear index of refraction (defined by $n = n_0 + n_2 I$) and we used $\mathrm{Re}\{\chi^{(3)}\} = (n^2/90\pi)\, n_2$ and $\mathrm{Im}\{\chi^{(3)}\} = (n^2\lambda/180\pi^2)\, \beta$. This FOM is similar to that for all-optical switching condition [18]. First, the FOM determines the maximum conversion efficiency allowed by the nonlinear material. Second, $\eta(I_{10})$ is almost flat around its maximum value. For example, it changes by less than 0.5 dB for $I_s \leq I_{10} \leq 3I_s$ and we can achieve 80% of $\eta_{\max}$ using a I_{10} equal to half I_{10}^{opt} only. The

conversion efficiency's flatness around I_{10}^{opt} reduces η's susceptibility to the pump's amplitude noise and, hence, reduces pump-induced SNR degradation.

To achieve $\eta_{\max}$ with low input pump intensity, I_s should be reduced through increasing the product βL_{eff}. A material with a large TPA coefficient β and a poor switching figure-of-merit may still be favorable for small signal FWM. For example, if $Im\{\chi^{(3)}\} \gg Re\{\chi^{(3)}\}$ then $\eta_{\max}$ is limited to approximately $e^{-2-\alpha L}$ $(= -(8.6+4.3\alpha L)$ dB). This leads to $\eta_{\max} \simeq -11$ dB for a 1−cm long low loss, $\alpha = 0.5$ cm^{-1}, passive waveguide. Alternatively, a material with a good switching figure-of-merit and a small $\left|\chi^{(3)}\right|$, such as many semiconductors at energies below $E_g/2$, will exhibit unfavorable small signal FWM efficiency while allowing a large $\eta_{\max}$ at very high intensities. Clearly, a material with a large, mostly real, $\chi^{(3)}$ is ideal for FWM (as well as all-optical switching). Another approach to increasing I_s $(= \beta L_{eff})$ is to increase L, however, that reduces $\eta_{\max}$ since it is proportional to $e^{-\alpha L}$. To find the optimum length L^{opt}, we differentiate equation (5.14) with respect to L and equate to zero. Unfortunately, $\partial\eta/\partial L|_{L^{opt}} = 0$ is difficult to solve analytically. Nonetheless, we can numerically compute the optimum length L^{opt} given α, β and I_{10}. Figure 5-2 shows a plot of L^{opt} normalized to L_{ss}^{opt}, the small signal optimum length. As the Figure indicates, if βI_{10} is comparable to α, then L^{opt} becomes significantly different from L_{ss}^{opt} (e.g. for $\beta I_{10}/\alpha = 1$, $L^{opt} = 0.62 \cdot L_{ss}^{opt}$). Two limiting cases are

$$L^{opt} = \left[1 - \frac{2}{3}\frac{\beta I_{10}}{\alpha}\frac{1}{\ln(3)}\right] L_{ss}^{opt} \qquad \text{for } \beta I_{10}/\alpha \ll 1 \qquad (5.17)$$

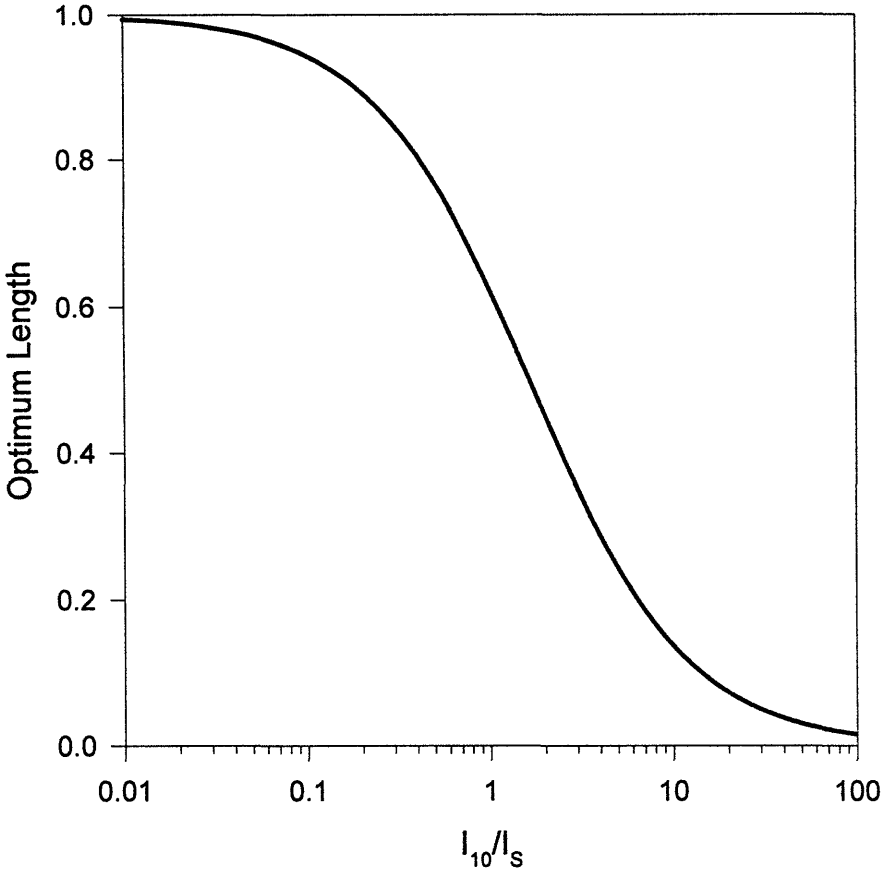

Figure 5-2: Optimum length (normalized to $\ln(3)/\alpha$) as a function of normalized input pump intensity. When I_{10} is small, the normalized optimum length equals 1. For $I_{10} \gg I_s$, L^{opt}/L^{opt}_{ss} deviates significantly from 1.

$$L^{opt} = \left[(e^1 - 1)/\beta I_{10}\right] L_{ss}^{opt} \qquad \text{for } \beta I_{10}/\alpha \gg 1 \tag{5.18}$$

Given L^{opt} (from Figure 5-2) we compute and plot (Figure 5-3) $\eta_{\max}/\eta_m$ as a function of $\beta I_{10}/\alpha$. As Figure 5-3 indicates, for $\beta I_{10}/\alpha \ll 1$, η is significantly smaller than η_m and is limited by the fact that the linear loss imposes a small L_{eff} value resulting in $I_s \gg I_{10}$. Only when $\beta I_{10}/\alpha \gg 1$ is it possible to have $\eta \simeq \eta_m$. Depending on the specific waveguide design, other restrictions (e.g. technological and phase matching constraints) may limit L, preventing η from attaining its peak value.

5.2.1 Experimental Verification

To verify the theoretical results, we performed a FWM experiment, at $\lambda = 1560$ nm, with picosecond pulses in an AR-coated, 7.5 mm long, passive InGaAsP/InP single Quantum Well (QW) ridge waveguide, with a QW bandgap of $\simeq$1490 nm waveguide. By operating far from the bandgap we minimize linear loss that increases close to the bandgap as well as changes due to accumulated photon-generated free carriers. This allows us to reach the large signal regime, $\beta I_{10}/\alpha > 1$, with modest peak powers and to have TPA as the dominant nonlinear loss mechanism.

Based on the value of $\beta = 46\, cm/GW$, we calculate $I_s = 35$ MW/cm^2. Next, $|\chi^{(3)}|$ was measured, at 1560 nm, by small signal FWM and was found to be $7.6 \cdot 10^{-14}$ cm^2/V^2 [50], [49]. Hence, $\eta_m = \left|\chi^{(3)}/\mathrm{Im}\{\chi^{(3)}\}\right|^2 \cdot e^{-2} = 0.27$ ($= -5.7$ dB) and $\eta_{\max} = \eta_m \cdot e^{-\alpha L} = 0.19$ ($= -7.2$ dB). Given α, β and $|\chi^{(3)}|$, we have all the parameters needed for equation (5.16) to predict the conversion efficiency for different input pump intensities. The measured conversion efficiency is shown in Figure 5-4 along

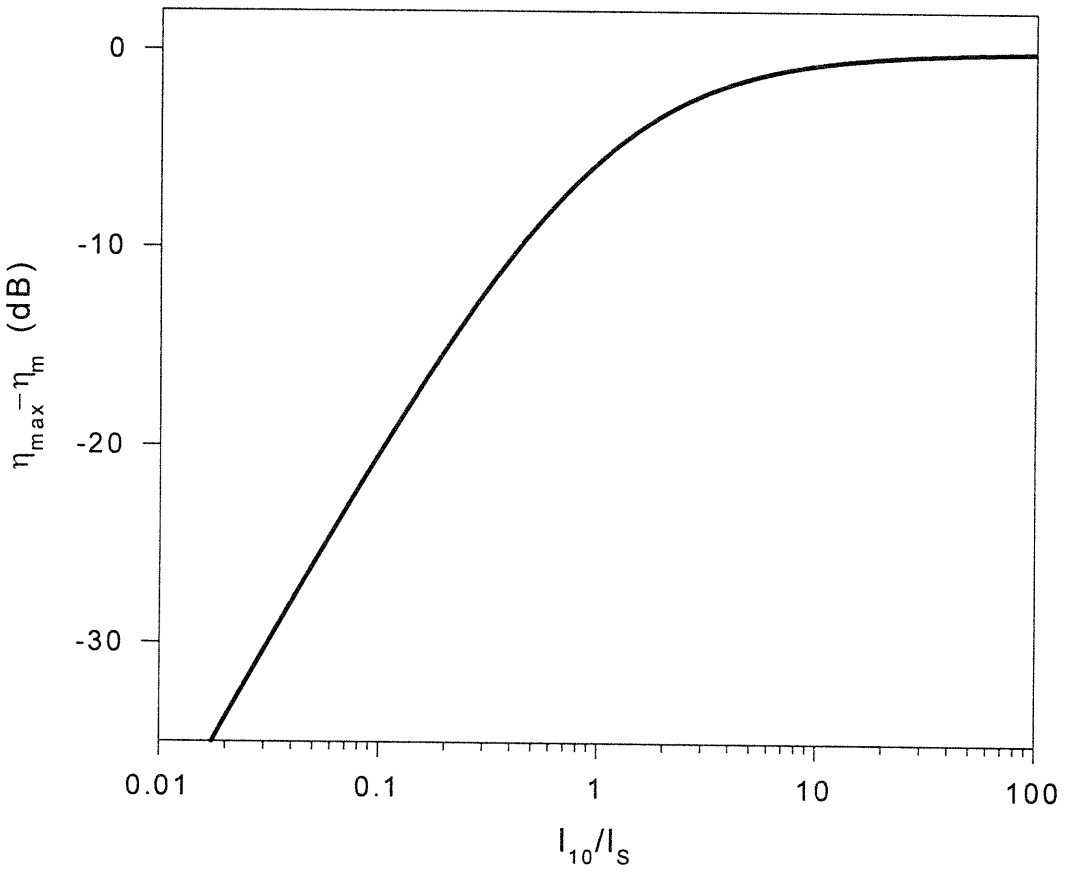

Figure 5-3: $\eta_{\max}/\eta_m$ as a function of $\beta I_{10}/\alpha$.

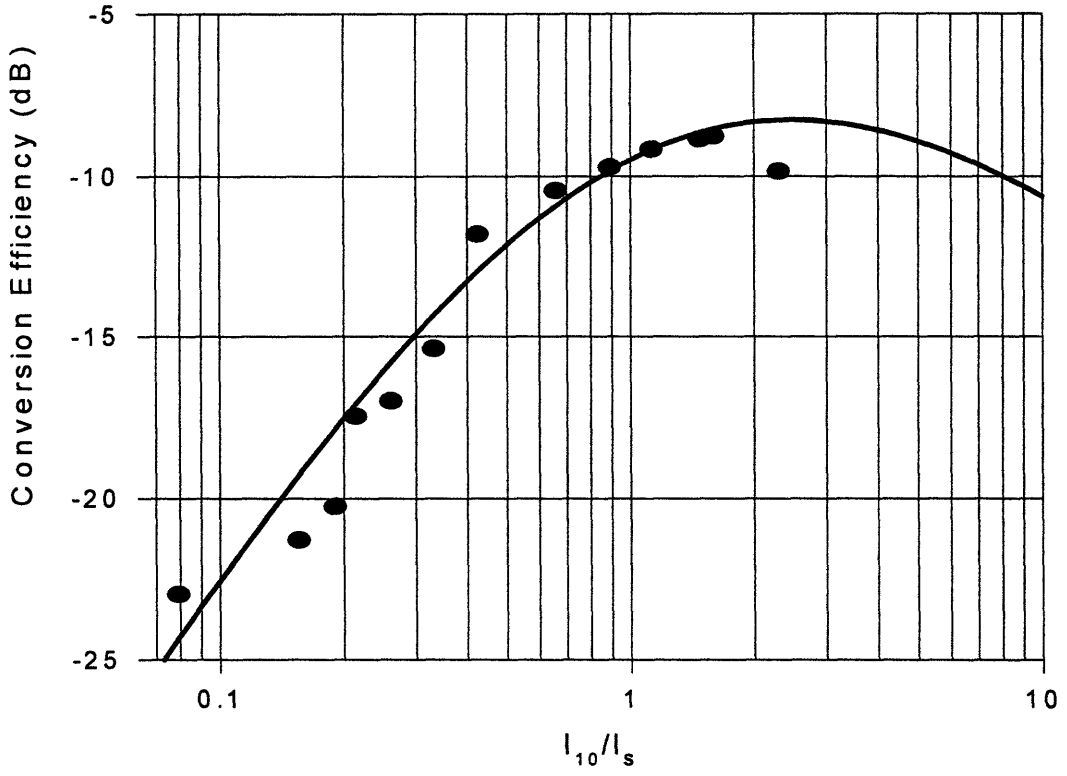

Figure 5-4: Experimentally measured conversion efficiency (solid dots) as a function of normalized input pump intensity along with theoritically predicted trace (solid line).

with the theoretical curve predicted by equation (5.16), for $sech^2(t)$ pump pulses. The experimental data in Figure 5-4 were also corrected for the mismatch between pump and signal pulsewidths. As an additional check, we measured the conversion efficiency with CW light under identical conditions. The conversion efficiencies at low intensities in Figure 5-4 match well those observed in the CW measurement.

Close agreement is observed between theory and experiment as indicated by Figure 5-4. In particular, the experimental $\eta_{\max}$ is within 1 dB of the theoretically calculated value. However, the optimum intensity is lower than that predicted in theory and the last data point deviates from the flat response anticipated theoretically. There are several explanations for this small discrepancy. The theoretical derivation of $\eta_{\max}$ and I_{10}^{opt} ignores a few second order effects which will affect the result. These effects include absorption due to accumulated photon-generated free carriers and nonlinear index changes that will alter the phase matching and distort the pulses spectrally.

5.3 Effects of Nonlinear Loss and Index Changes

In this section, we shall focus our attention on the general case where both the nonlinear loss and index changes play a role. We begin our analysis by rewriting equations (2.6)-(2.8), assuming phase matching,

$$\frac{\partial E_1}{\partial z} = -\frac{\alpha_1}{2}E_1 + i\kappa |E_1|^2 E_1 \tag{5.19}$$

$$\frac{\partial E_3}{\partial z} = -\frac{\alpha_3}{2}E_3 + 2i\kappa |E_1|^2 E_3 \tag{5.20}$$

$$\frac{\partial E_4}{\partial z} = -\frac{\alpha_4}{2} E_4 + 2\,i\,\kappa\,|E_1|^2\,E_4 + i\gamma\chi^{(3)} E_1^2 E_3^* \tag{5.21}$$

To solve for $E_4(z)$, we start by solving equations (5.19) and (5.20) for $E_1(z)$ and $E_3(z)$, respectively, using standard methods of differential equations [39]. The solution of equation (5.19) is,

$$E_1(z) = E_{10} \cdot e^{-\frac{\alpha}{2}z + \imath\,\kappa\,\varphi(z)} \tag{5.22}$$

where

$$\varphi(z) = \frac{1}{2\kappa''} \ln\left[1 + 2\kappa''\,|E_{10}|^2\left(\frac{1 - e^{-\alpha z}}{\alpha}\right)\right] \tag{5.23}$$

Similarly, we may solve equation (5.20) as,

$$E_3(z) = E_{30} \cdot e^{-(\alpha/2)z + 2\,\imath\,\kappa\,\varphi(z)} \tag{5.24}$$

where $\varphi(z)$ is the same as above. Now we use equations (5.22) and (5.24) to substitute for $E_1(z)$ and $E_3(z)$, respectively, in equation (5.21). The FWM equation (5.21) becomes,

$$\frac{\partial E_4}{\partial z} = -\frac{\alpha_4}{2} E_4 - 2\,\kappa''\,|E_{10}|^2\,e^{-\alpha z - 2\,\kappa''\,\varphi(z)}\,E_4 + i\gamma\chi^{(3)} E_{10}^2 E_{30}^*\,e^{-\frac{3}{2}\alpha z - 4\,\kappa''\,\varphi(z)} \tag{5.25}$$

and we may repeat the procedure followed in the preceding analysis with

$$\begin{aligned} f(z) &= \frac{\alpha_4}{2} + 2\,\kappa''\,|E_{10}|^2\,e^{-\alpha z - 2\,\kappa''\,\varphi(z)} \\ g(z) &= i\gamma\chi^{(3)} E_{10}^2 E_{30}^*\,e^{-\frac{3}{2}\alpha z - 4\,\kappa''\,\varphi(z)} \end{aligned}$$

$$= i\gamma\chi^{(3)}E_{10}^2E_{30}^*\, e^{-\frac{3}{2}\alpha z}\left[1+2\kappa''\left|E_{10}\right|^2\left(\frac{1-e^{-\alpha z}}{\alpha}\right)\right]^{-2}$$

The solution is,

$$E_4(z)=\frac{1}{\xi(z)}\left[\int_z \xi(z)\, g(z)\, dz + C\right] \tag{5.26}$$

where

$$\begin{aligned}\xi(z) &= \exp\left(\int_z f(z)\, dz\right)\\ C &= constant\end{aligned}$$

Substituting $f(z)$ and $g(z)$ into the above formulas we obtain,

$$\xi(z)=e^{\frac{\alpha}{2}z}\left[1+2\kappa''\left|E_{10}\right|^2\left(\frac{1-e^{-\alpha z}}{\alpha}\right)\right]^{-\imath\kappa/\kappa''}$$

and

$$\int_z \xi(z)\, g(z)\, dz = c_2\,\left[1+u(z)\right]^{-\left(1+\imath\kappa/\kappa''\right)}$$

where

$$\begin{aligned}c_2 &= \frac{-i\gamma\chi^{(3)}E_{10}^2E_{30}^*}{\left(1+i\kappa/\kappa''\right)\,2\kappa''\,\left|E_{10}\right|^2}\\ u(z) &= 2\kappa''\left|E_{10}\right|^2\left(\frac{1-e^{-\alpha z}}{\alpha}\right)\end{aligned}$$

Substituting in equation (5.26) we obtain,

$$E_4(z) = e^{-\frac{\alpha}{2}z}\ [1+u(z)]^{i\kappa/\kappa''}\left(c_2\,[1+u(z)]^{-(1+i\kappa/\kappa'')}+C\right) \tag{5.27}$$

The constant C is determined by requiring that $E_4(z)$ satisfy the boundary condition $E_4(0)=0$. Setting $z=0$ in equation (5.27), we find

$$C = -c_2$$

Hence, equation (5.27) may be rewritten as

$$E_4(z) = c_2\, e^{-\frac{\alpha}{2}z}\left([1+u(z)]^{-1} - [1+u(z)]^{i\kappa/\kappa''}\right) \tag{5.28}$$

Equation (5.28) may be simplified more using the definition of $sinh(z) = (e^z - e^{-z})/2$, to obtain

$$E_4(z) = -2\,c_2\, e^{-\frac{\alpha}{2}z}\ [1+u(z)]^{\left(-1/2+i\kappa/2\kappa''\right)}\cdot sinh\left(\left(1/2+i\kappa/2\kappa''\right)\cdot \ln\,[1+u(z)]\right) \tag{5.29}$$

Note that

$$\begin{aligned} 1+i\kappa/\kappa'' &= 1+i\,Re\{\kappa\}/\kappa'' - Im\{\kappa\}/\kappa'' \\ &= i\,Re\{\kappa\}/\kappa'' \\ &= i\,\kappa'/\kappa'' \end{aligned}$$

and

$$-\frac{1}{2}+i\frac{\kappa}{2\kappa''}=-1+i\,\kappa'/2\kappa''$$

Returning to equation (5.29) and using the fact that $sinh(a+i\,b)=sinh(a)\,cos(b)+i\,cosh(a)\,sin(b)$ we have

$$E_4(z)=-2\,i\,c_2\,e^{-\frac{\alpha}{2}z}\,[1+u(z)]^{-1+i\kappa'/2\kappa''}\,sin\left(\frac{\kappa'}{2\kappa''}\cdot\ln\,[1+u(z)]\right)$$

The quantity of interest is the conversion efficiency ($\eta=|E_4(z)/E_{30}|^2$). The final form of the conversion efficiency expression is

$$\eta=e^{-\alpha L}\left[\left|\frac{\gamma\chi^{(3)}}{2\kappa''}\right|\cdot\frac{sin\,(\rho\cdot\ln\,[1+u(z)])}{\rho\,[1+u(z)]}\right]^2 \tag{5.30}$$

where

$$\rho\equiv\frac{\kappa'}{2\kappa''}$$

Using the definition of I_1 (equation (2.9)), the relationship of κ'' and β (equation (2.10)), and the relationship of κ' and n_2 (equation (2.11)), we can express ρ as

$$\rho=\frac{2\pi}{\lambda}\frac{n_2}{\beta}$$

Moreover, $u(z)$ can be expressed as

$$u(z)\equiv I_{10}/I_s(z)$$

where we define I_{10} and $I_s(z) \equiv 1/\beta L_{eff}(z)$ as the input pump intensity and the waveguide saturation intensity. For an ultrafast nonlinearity,

$$Im\{\chi^{(3)}\} = \frac{n^2 \lambda}{180\,\pi^2}\beta$$

and we can express equation (5.30) as

$$\eta = e^{-\alpha L}\left[\left|\frac{\chi^{(3)}}{Im\{\chi^{(3)}\}}\right| \cdot \frac{sin\left(\rho \cdot \ln\left[1 + I_{10}/I_s(z)\right]\right)}{\rho\left[1 + I_{10}/I_s(z)\right]}\right]^2 \tag{5.31}$$

This is the final form of the conversion efficiency expression and the main result of all the preceding analysis. As a check, observe that when nonlinear loss dominates equation (5.31) reduces to our earlier result, equation (5.16). As expected, in the limit of $I_{10} \ll I_s$, the *large signal* conversion efficiency expression equation (5.31) reduces to the small-signal one, equation (2.14). Before we examine equation (5.31) let us consider the case where nonlinear index changes dominate ($\kappa' \gg \kappa''$).

5.3.1 Effects of Nonlinear Index Changes

In the section on nonlinear loss effects we examined the limiting case where nonlinear loss dominates. In this section we examine the other limiting case where nonlinear index changes dominate. In practice, we may classify FWM in fiber in this category. Therefore, it is important to understand these effects. In the limit, $\ln(1+\Delta x) \longrightarrow \Delta x$

and expression (5.31) becomes

$$\eta = e^{-\alpha L}\left[\left|\frac{\gamma\chi^{(3)}}{\kappa'}\right| \cdot sin\left(\kappa'|E_{10}|^2\, L_{eff}(z)\right)\right]^2 \tag{5.32}$$

Using the relationship between κ' and κ and between κ and the nonlinear index of refraction n_2 (equation (2.11)) and the fact that n_2 is related to $Re\{\chi^{(3)}\}$ by,

$$n_2 = \frac{90\,\pi^2}{n^2} Re\{\chi^{(3)}\}$$

we can rewrite $\left|\gamma\chi^{(3)}/\kappa'\right|$ as,

$$\left|\frac{\gamma\chi^{(3)}}{\kappa'}\right| = \left|\frac{\chi^{(3)}}{Re\{\chi^{(3)}\}}\right|$$

Hence, we arrive at the final result,

$$\eta = e^{-\alpha L}\left[\left|\frac{\chi^{(3)}}{Re\{\chi^{(3)}\}}\right| \cdot sin\left(I_{10}/I_{\pi}(z)\right)\right]^2 \tag{5.33}$$

where we define

$$I_{\pi}(z) \equiv \frac{1}{((2\pi/\lambda)\; n_2 \cdot L_{eff}(z))} \tag{5.34}$$

Note that

$$\frac{I_{10}}{I_{\pi}} = \frac{2\pi}{\lambda}\, n_2 I_{10} \cdot L_{eff} \equiv \varphi_{nl}$$

where φ_{nl} is the nonlinear phase shift induced by the pump field. To understand nonlinear index changes we examine equation (5.33) closely. A plot of $\eta(I_{10})$, based on

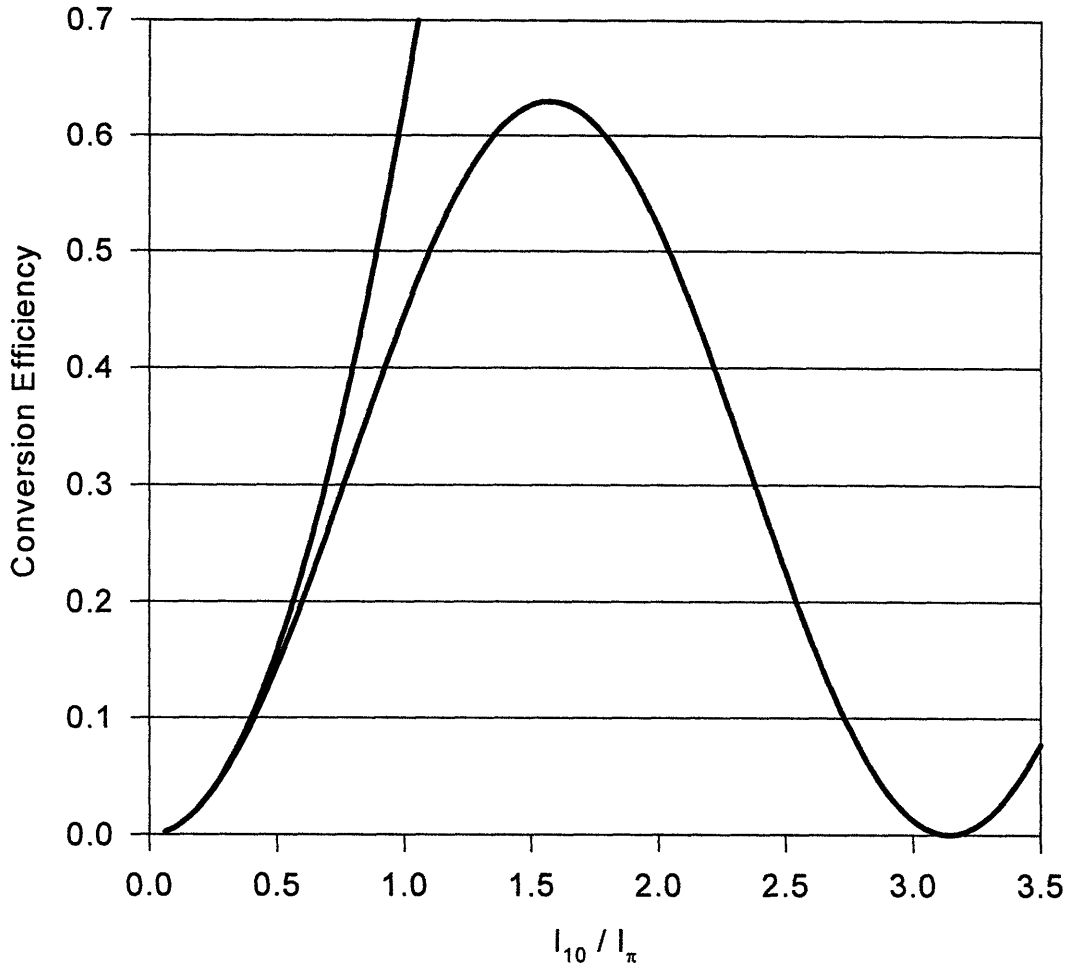

Figure 5-5: Small signal and large signal conversion efficiencies as a function of normalized input pump intensity assuming $\left|\chi^{(3)}/Re\{\chi^{(3)}\}\right| \simeq 1$, $\alpha = 0.46\,cm^{-1}$, and $L = 1\,cm$. The large signal conversion efficiency's dependence on intensity resembles that of phase matching.

equation (5.33), is shown in Figure 5-5 (assuming $\left|\chi^{(3)}/Re\{\chi^{(3)}\}\right| \simeq 1$, $\alpha = 0.46\,\mathrm{cm}^{-1}$, and $L = 1\,cm$) along with $\eta_{ss}(I_{10})$ for comparison. Again, contrasting η_{ss} with η, we find that η_{ss}'s accuracy is rapidly lost as I_{10} increases. For instance, η_{ss} overestimates the conversion efficiency by 10% for pump intensities as low as $I_{10} = 0.5I_{\pi}$ and for $I_{10} = 1.4I_{\pi}$, it is off by a factor of $\times 2$. Also note that while the small signal formula predicts a strictly increasing conversion efficiency, the large signal expression predicts an oscillatory behavior. In fact, the oscillations with intensity are caused by the fact that the strong pump produced phase shifts drive the FWM process in- and out-of-phase. The same mechanism was encountered in phase matching. In deriving equation (5.33) we assumed $\Delta k = 0$. If that is not the case, then we must account for both ΔkL-type phase shifts as well as pump induced phase shifts in order to phase match the FWM process. As Figure 5-5 indicates, the large signal conversion efficiency, $\eta(I_{10})$, reaches a maximum value of,

$$\eta_{\max} = \left|\frac{\chi^{(3)}}{Re\{\chi^{(3)}\}}\right|^2 \cdot e^{-\alpha L} \equiv \eta_m \cdot e^{-\alpha L}$$

at an optimum input intensity of,

$$\begin{aligned} I_{10}^{opt} &= (n\pi + \pi/2)\, I_{\pi} \\ n &= 0, 1, 2 \ldots etc. \end{aligned}$$

as may be verified directly from equation (5.33). First, note that the highest value

$\eta_{\max}$ can assume is $\eta_m = \left|\chi^{(3)}/Re\{\chi^{(3)}\}\right|^2$, again a geometry independent quantity. We may define, as before, a material's figure-of-merit (FOM) as, in the case where nonlinear index changes dominate,

$$FOM = \left|\frac{\chi^{(3)}}{\mathrm{Re}\{\chi^{(3)}\}}\right|^2 = 1 + \left(\frac{\lambda}{2\pi}\frac{\beta}{n_2}\right)^{-2}$$

The FOM determines the maximum conversion efficiency allowed by the nonlinear material.

To achieve $\eta_{\max}$ with low input pump intensity, I_π should be reduced through increasing the product $n_2 L_{eff}$. A material with a large nonlinear index of refraction coefficient n_2 is favorable. A material with a large, mostly real, $\chi^{(3)}$ is ideal for small and large signal FWM (as well as all-optical switching). Another approach to increasing I_π $(= n_2 L_{eff})$ is to increase L, however, that reduces η since it is proportional to $e^{-\alpha L}$. To find the optimum length L^{opt}, we differentiate equation (5.14) with respect to L and equate to zero. Unfortunately, $\partial\eta/\partial L|_{L^{opt}} = 0$ is difficult to solve analytically. Nonetheless, we can numerically compute the optimum length L^{opt} given α, n_2 and I_{10}. Equation $\partial\eta/\partial L|_{L^{opt}} = 0$ results in an equation of the form $\tan(c - x) = 2x$, where $c = (2\pi/\alpha\lambda)\, n_2\, I_{10}$ and $x = c\, e^{-\alpha L_{opt}}$, which is simple to solve numerically. Figure 5-6 shows a plot of L^{opt} normalized to L_{ss}^{opt}, the small signal optimum length. As the Figure indicates, if $(2\pi/\lambda)\, n_2 I_{10}$ is comparable to α, then L^{opt} becomes significantly different from L_{ss}^{opt} (e.g. for $(2\pi/\lambda)\, n_2 I_{10}/\alpha = 1$, $L^{opt} = 0.62 \cdot L_{ss}^{opt}$). Given L^{opt} (from Figure 5-6) we compute and plot (Figure 5-7) $\eta_{\max}/\eta_m$ as a function of $(2\pi/\lambda)\, n_2 I_{10}/\alpha$. As Figure 5-7 indicates, for $(2\pi/\lambda)\, n_2 I_{10}/\alpha \ll 1$, η is

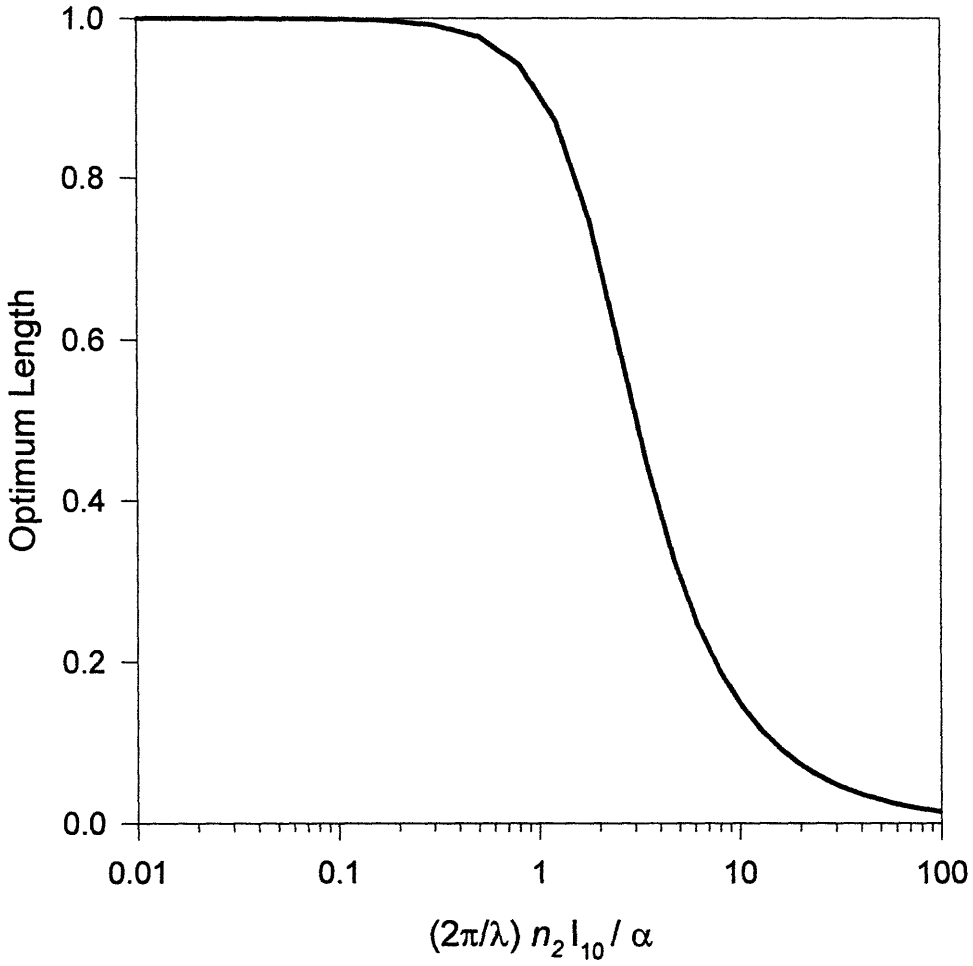

Figure 5-6: Optimum length (normalized to $\ln(3)/\alpha$) as a function of normalized input pump intensity. When I_{10} is small, the normalized optimum length equals 1. For $I_{10} \gg I_\pi$, L^{opt}/L_{ss}^{opt} deviates significantly from 1.

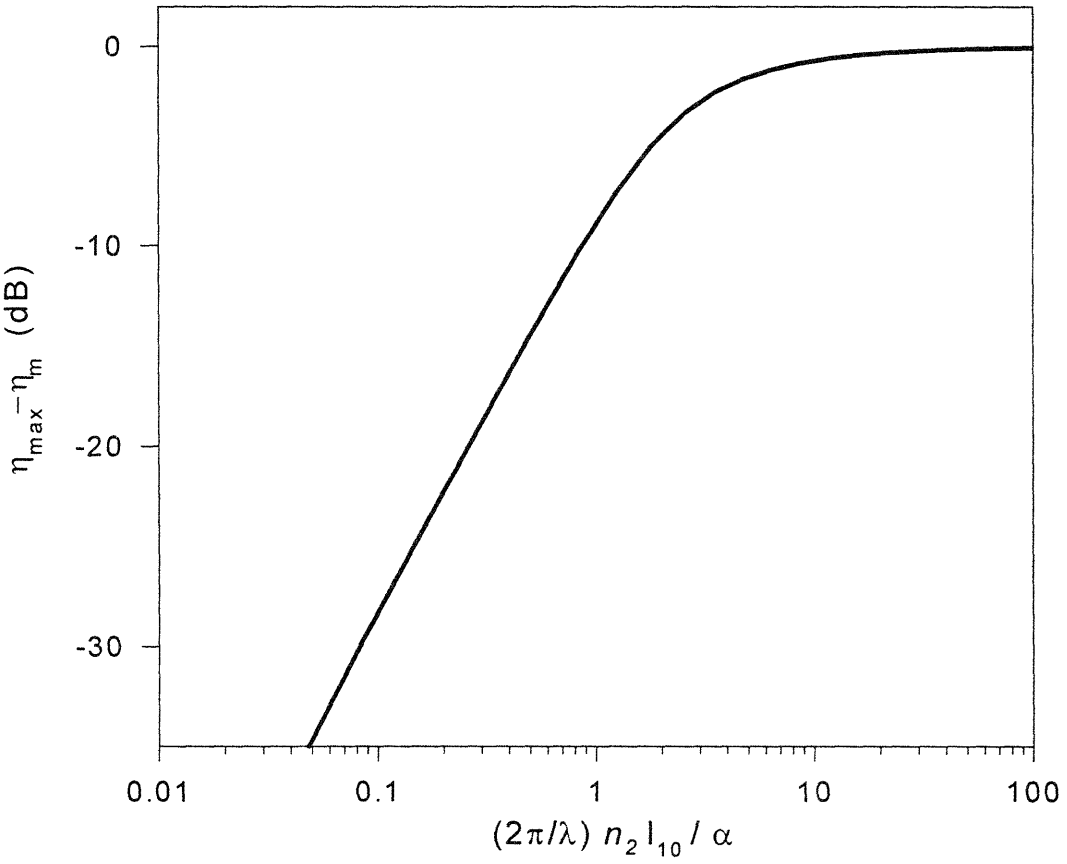

Figure 5-7: $\eta_{\max}/\eta_m$ as a function of $(2\pi/\lambda)\, n_2 I_{10}/\alpha$.

significantly smaller than η_m and is limited by the fact that the linear loss imposes a small L_{eff} value resulting in $I_\pi \gg I_{10}$. Only when $(2\pi/\lambda)\, n_2 I_{10}/\alpha \gg 1$ is it possible to have $\eta \simeq \eta_m$.

5.3.2 Effects of Nonlinear Loss and Index Changes

In the general case, both nonlinear loss and index changes affect the FWM conversion efficiency. Having examined the two limiting cases in the previous sections, we may now study the general case by focusing on equation (5.31), rewritten below for convenience,

$$\eta = e^{-\alpha L}\left[\left|\frac{\chi^{(3)}}{Im\{\chi^{(3)}\}}\right| \cdot \frac{sin\left(\rho \cdot \ln\left[1 + I_{10}/I_s(z)\right]\right)}{\rho\left[1 + I_{10}/I_s(z)\right]}\right]^2 \tag{5.35}$$

A plot of $\eta(I_{10})$, based on equation (5.31), is shown in Figures 5-8 – 5-11 (assuming $\alpha = 0.46\,\mathrm{cm}^{-1}$, and $L = 1\,\mathrm{cm}$) along with $\eta_{ss}(I_{10})$ for comparison for values of ρ equal to $\rho = 0$, $\rho = 1, \rho = 2$, and $\rho = 5$. Note that as ρ increases several things happen. First, η's roll-off following its peak steepens as it approaches the case of nonlinear index changes only (there, $\eta \propto sin(x)$). Second, note the emergence of the oscillatory behavior as ρ increases. By differentiating η and equating to zero, we obtain the maximum value of the conversion efficiency,

$$\eta_{\max} = \left|\frac{\chi^{(3)}}{Im\{\chi^{(3)}\}}\right|^2 \cdot \frac{e^{-\alpha L - 2\,tan^{-1}(\rho)/\rho}}{1+\rho^2} \equiv \eta_m \cdot e^{-\alpha L}$$

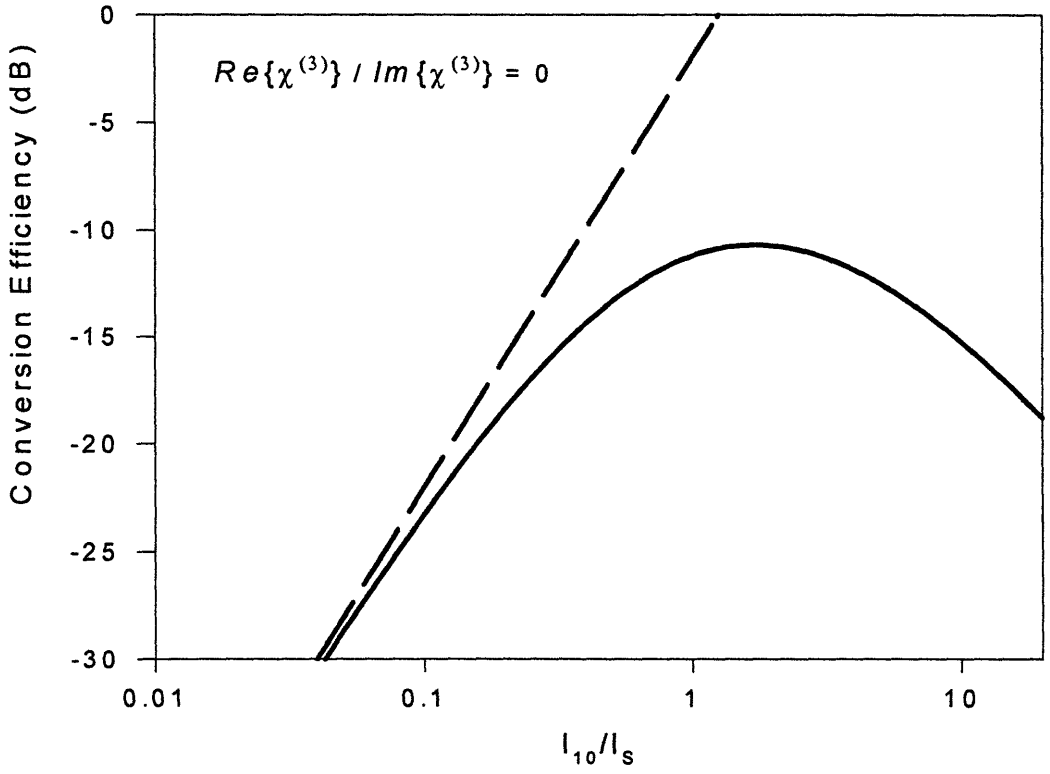

Figure 5-8: Conversion efficiency as a function of normalized input pump intensity for the case where $\rho = 0$.

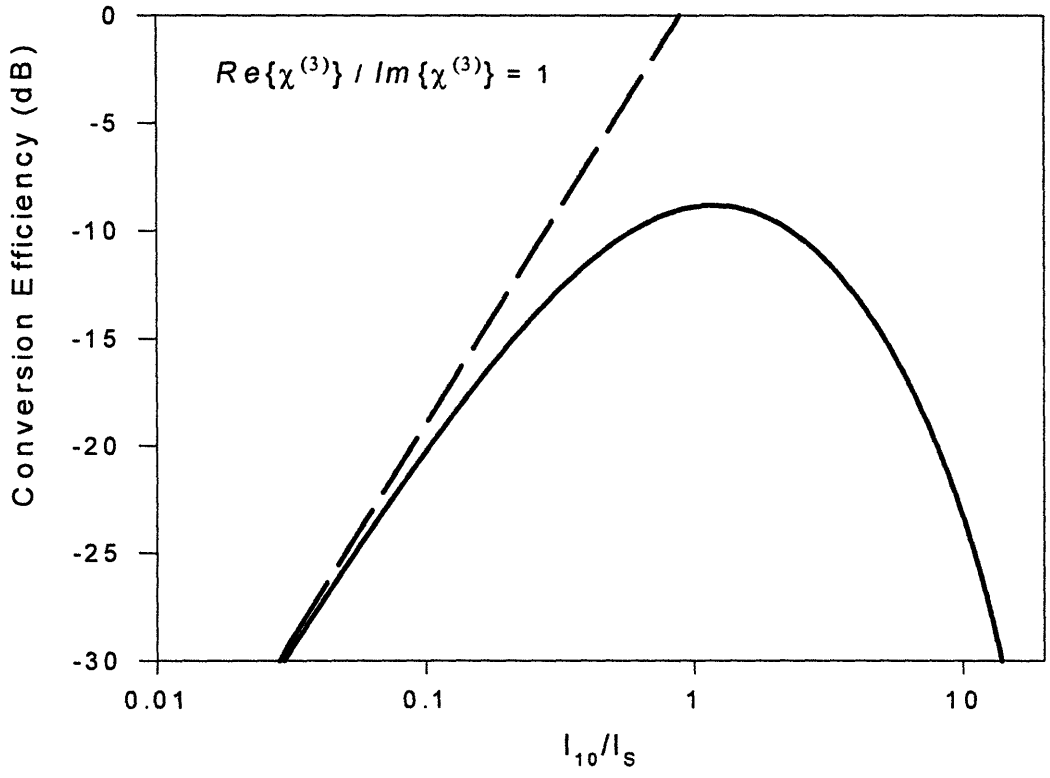

Figure 5-9: Conversion efficiency as a function of normalized input pump intensity for the case where $\rho = 1$.

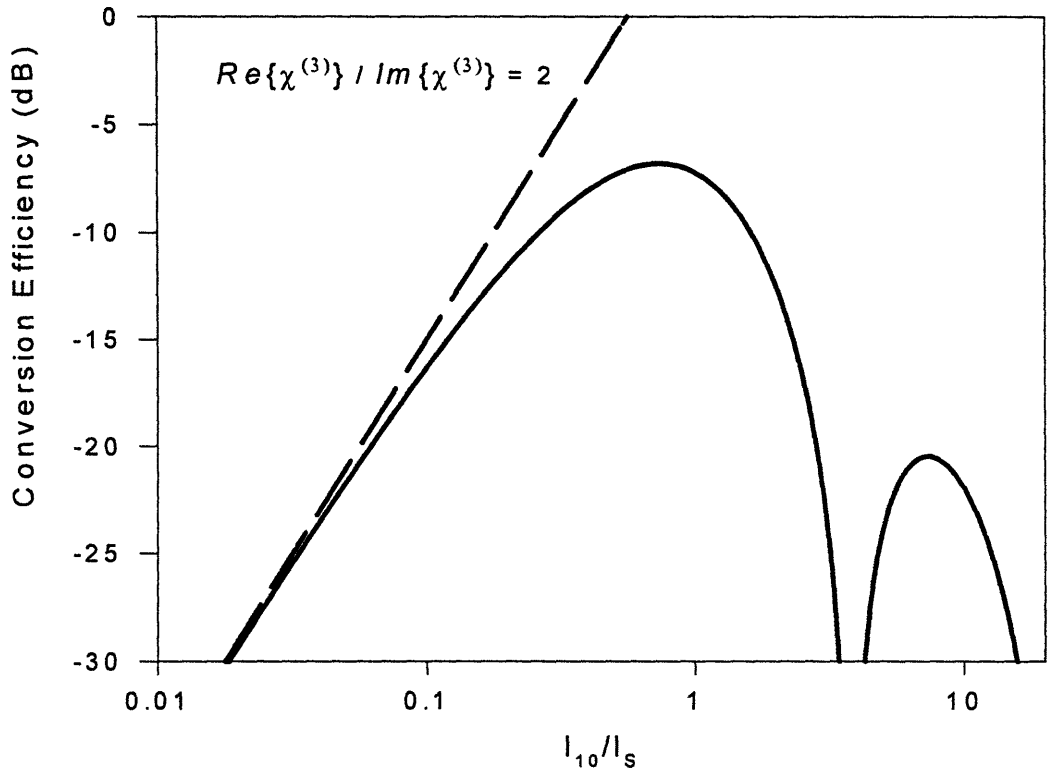

Figure 5-10: Conversion efficiency as a function of normalized input pump intensity for the case where $\rho = 2$.

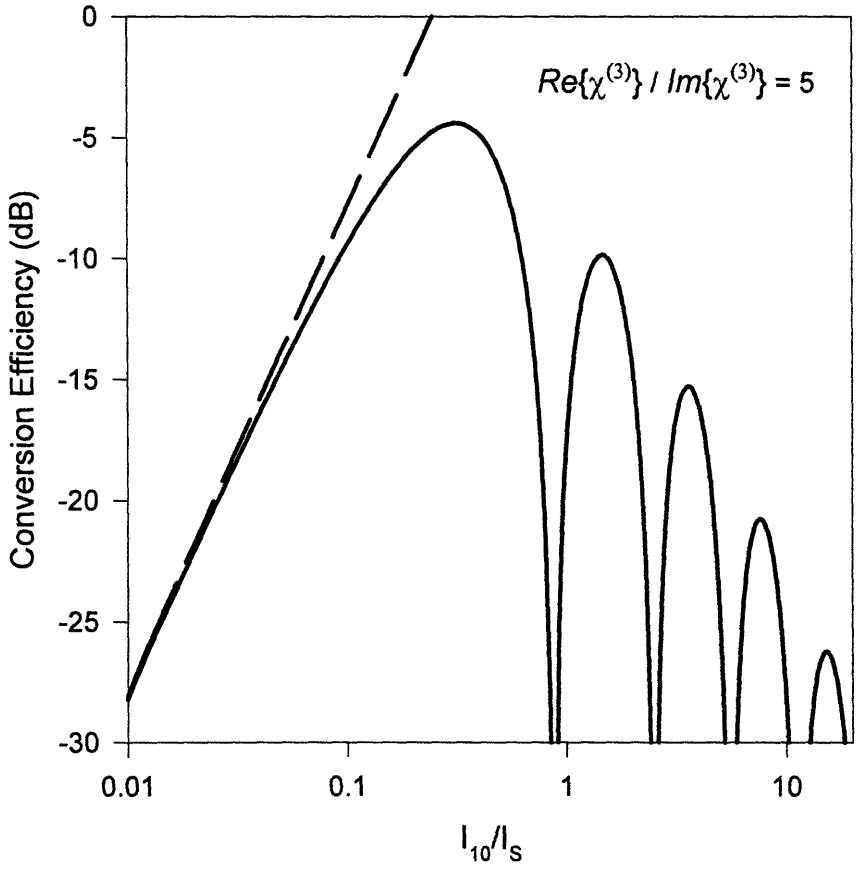

Figure 5-11: Conversion efficiency as a function of normalized input pump intensity for the case where $\rho = 5$.

at an optimum input intensity of,

$$I_{10}^{opt} = (e^{-\tan^{-1}(\rho)/\rho} - 1)I_s$$

as may be verified directly from equation (5.35). First, note that the highest value $\eta_{\max}$ can assume is $\eta_m = e^{-2\tan^{-1}(\rho)/\rho} \cdot \left|\chi^{(3)}/Im\{\chi^{(3)}\}\right|^2 / (1+\rho^2)$, again a geometry independent quantity. The expressions for $\eta_{\max}$ and I_{10}^{opt} reduce to the corresponding expressions in the special case of pure nonlinear loss or pure nonlinear index changes, as expected.

To find the optimum length L^{opt}, we differentiate equation 5.35 with respect to L and equate to zero. Again, $\partial\eta/\partial L|_{L^{opt}} = 0$ is difficult to solve analytically. Nonetheless, we can numerically compute the optimum length L^{opt} given α, β, n_2 and I_{10}. Actually, finding L^{opt} reduces to numerically solving the following equation for L,

$$tan(\rho \ln(1 + \Phi - \Phi e^{-\alpha L})) = \frac{2\rho\Phi e^{-\alpha L}}{1 + \Phi + \Phi e^{-\alpha L}}$$

where

$$\Phi \equiv \frac{\beta I_{10}}{\alpha}$$

Figure 5-12 shows a plot of L^{opt} normalized to L_{ss}^{opt}, the small signal optimum length, for $\rho = 0, 1, 2$ and 5, respectively. In the case of $\rho = 0$, L^{opt} is identical to that of dominant nonlinear loss and the case of large ρ corresponds to dominant nonlinear index of refraction. Note that the $x-$axis here is the same as in Figure 5-2 but different than that of Figure 5-6. Given L^{opt} (from Figure 5-12) we compute and

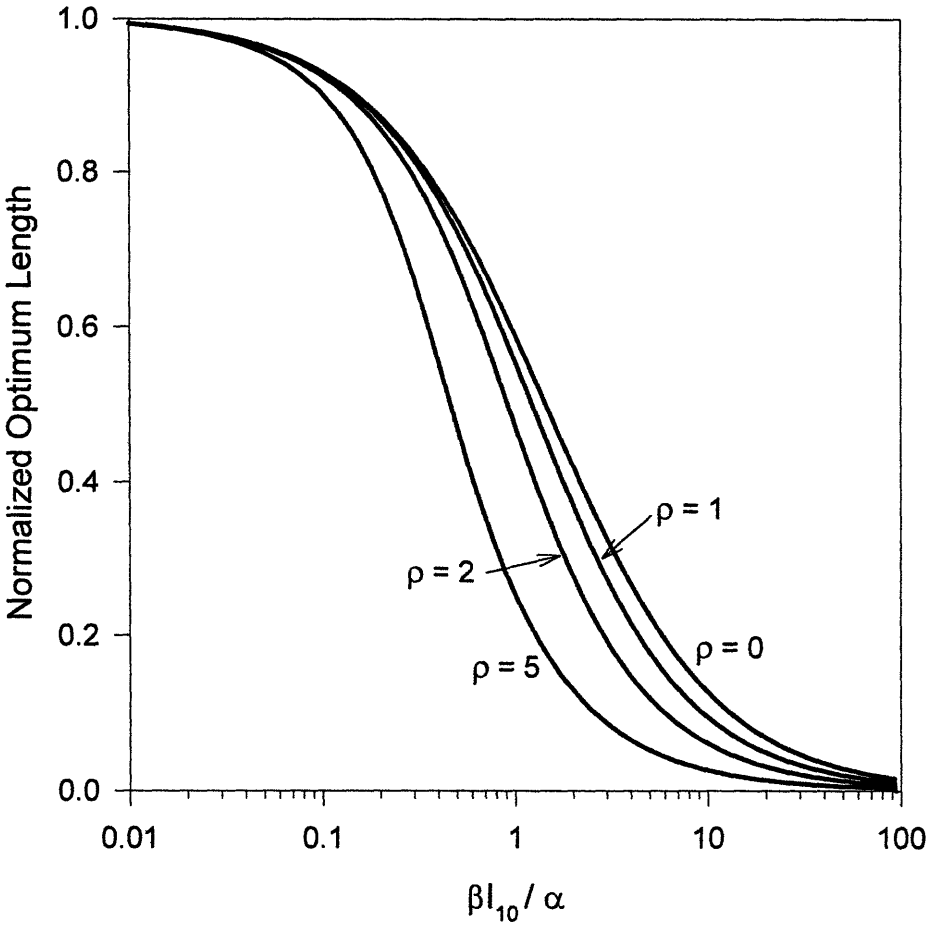

Figure 5-12: Optimum length (normalized to $\ln(3)/\alpha$) as a function of normalized input pump intensity for different values of ρ. The case of $\rho = 0$ corresponds to that of dominant nonlinear loss. The case where $\rho \longrightarrow \infty$ corresponds to that of dominant nonlinear index of refraction.

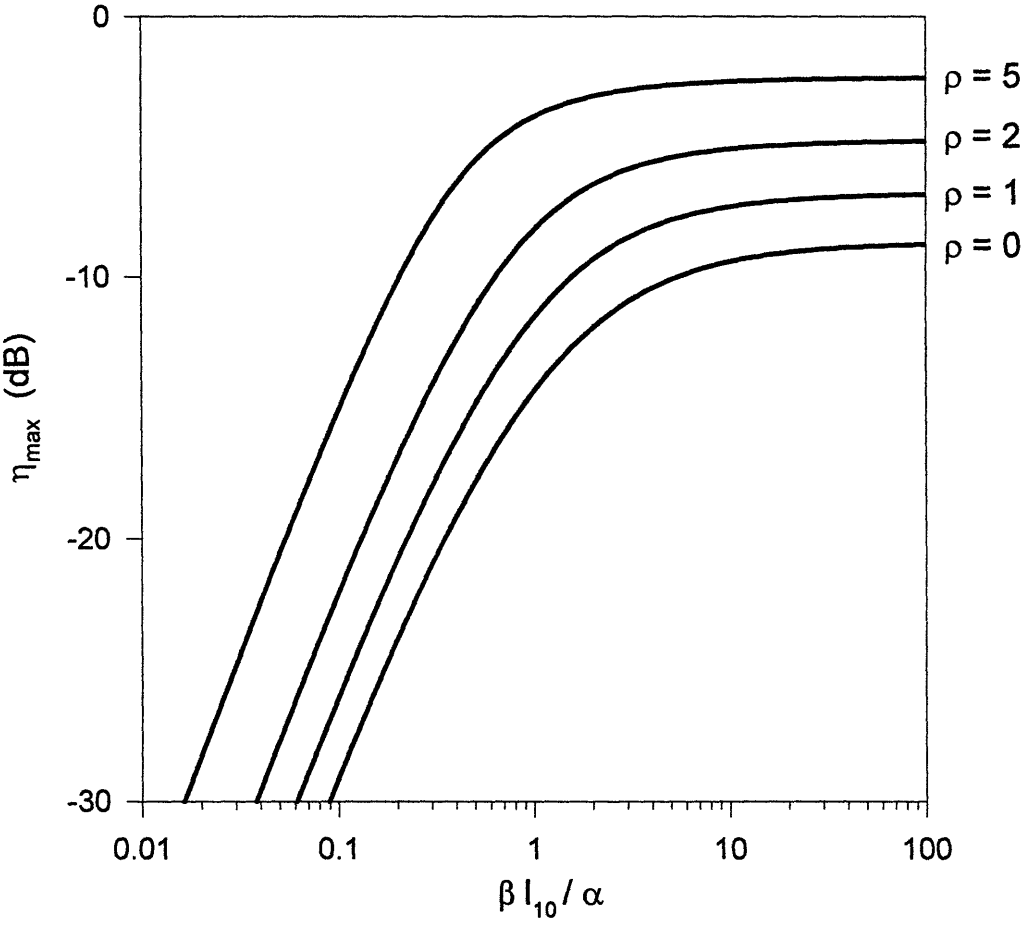

Figure 5-13: $\eta_{\max}$ as a function of $\beta I_{10}/\alpha$ for different values of ρ–Assuming $Re\{\chi^{(3)}\}$, and $Im\{\chi^{(3)}\}$ are ultrafast, hence, directly proportional to n_2 and β, respectively. Note that $\eta_{\max}$ is proportional to $|\chi^{(3)}/Im\{\chi^{(3)}\}|^2 = 1 + \rho^2$, hence increases with ρ (assuming $Im\{\chi^{(3)}\}$ is fixed).

plot (Figure 5-13) $\eta_{\max}$ as a function of $\beta I_{10}/\alpha$, assuming $Re\{\chi^{(3)}\}$, and $Im\{\chi^{(3)}\}$ are ultrafast, hence, directly proportional to n_2 and β, respectively. As Figure 5-13 indicates, $\eta_{\max}$ is proportional to $|\chi^{(3)}/Im\{\chi^{(3)}\}|^2 = 1 + \rho^2$, hence increases with ρ (given a fixed $Im\{\chi^{(3)}\}$).

Chapter 6

Ultrashort Pulse FWM

Previous research in FWM temporal effects has concentrated on the OPC [10] or time-reversal aspect of FWM for image distortion correction and chirp and dispersion compensation [11]. Short pulse compression using FWM is another area that received some attention. Theoretical efforts predict the ability to perform a wide range of signal processing functions including logic gating and temporal correlation [52]-[53]. High peak power pulses are expected to be utilized more and more to achieve high conversion efficiencies and improve the output SNR through the suppression of Amplified Spontaneous Emission (ASE) [54] (for the case of semiconductor amplifiers).

Short pulse FWM analysis using the preceding large signal results (see Chapter 5) brings into focus many considerations. As an example, consider the case where nonlinear loss dominates. Short pulses with their high peak intensities will typically approach the $\beta I_{10}/\alpha \gg 1$ limit leading to high conversion efficiencies ($\eta \rightarrow \eta_m$). The optimum length in this case, normalized to L_{ss}^{opt}, satisfies the relation $L^{opt} I_{10} =$

$1.72/\beta$ (see equation (5.18)) and we have a fixed length-intensity product $L^{opt}I_{10}$. Suppose, for the purposes of a rough estimate, that $\beta = 46$ cm/GW, $L_{ss}^{opt} = 1$ cm, and $A_{eff} = 3 \cdot 10^{-8}$ cm^2, then $L^{opt} = 224\ \mu m$ for a 100 W peak power pulse, and for a 1 kW peak power pulse, $L^{opt} = 22\ \mu m$ only. If the length-intensity product exceeds $1.72/\beta$ appreciably, then a number of unfavorable effects take place; such as conversion efficiency degradation and spectral distortion.

Short pulse FWM, in the small signal regime, produces an output signal that is shorter in duration than both pump and signal pulses as a consequence of the multiplication operation, $E_4(t) \propto |E_1(t)|^2 E_3(t)$ [55]. Figure 6-1 shows an example of a gaussian pump and signal pulses along with FWM generated pulse. The FWM pulse is shorter than the pump and signal pulse. FWM can therefore be used as a pulse compression scheme as was demonstrated experimentally with the compression of femtosecond pulses by $\times 1.8$ [12]. In this small signal regime, the FWM pulse scales with $|E_1(t)|^2$ but does not change its shape. In contrast, in the large signal regime, η does *not* scale linearly with $|E_1(t)|^2$. When I_{10} is comparable to I_s, $\eta(I_{10})/I_{10}^2$ is smaller at the peak of the pump pulse than at the wings. This leads to pulse broadening. Figure 6-2 shows the FWM pulse shape for different values of $\beta I_{10}/\alpha$. As $\beta I_{10}/\alpha$ increases, the pulse becomes broader and changes its shape (it becomes more square).

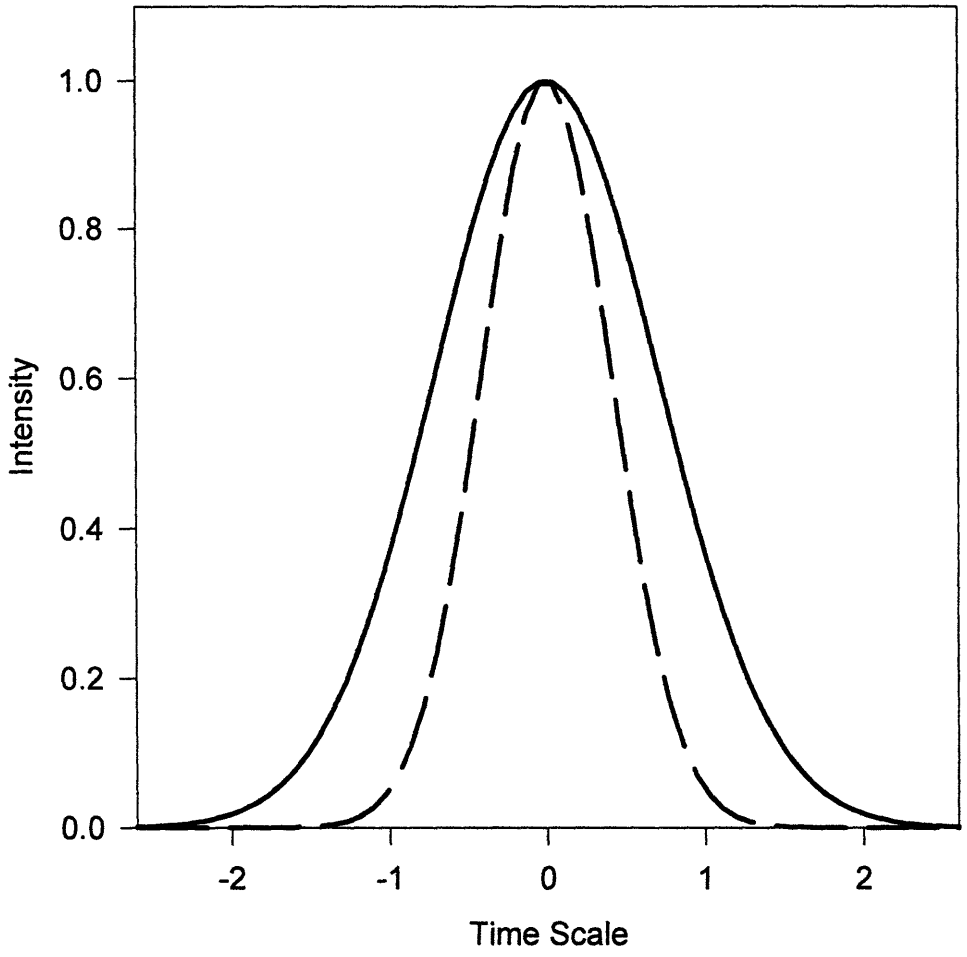

Figure 6-1: Input gaussian pump and signal pulses (solid line) and FWM generated pulse (dashed line). The FWM pulse is shorter than both the pump and siganl pulses.

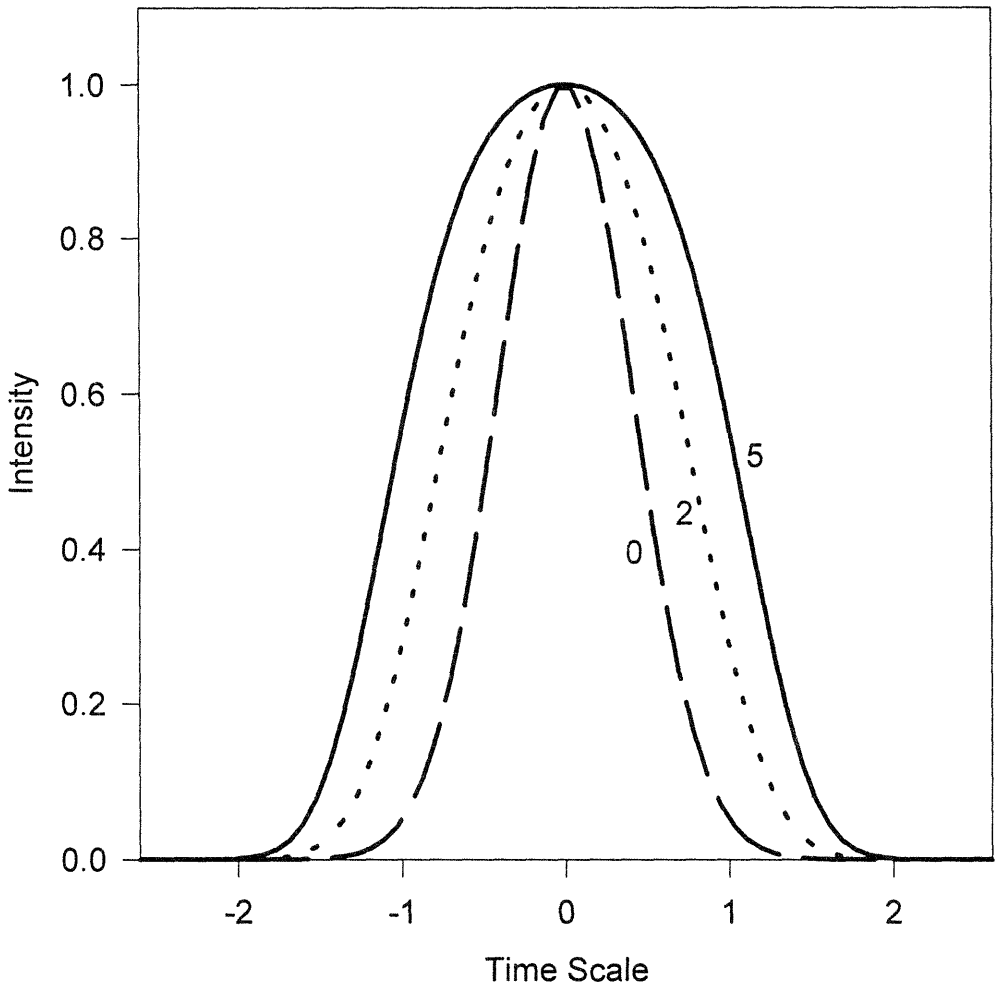

Figure 6-2: FWM pulse shape for $\beta I_{10}/\alpha$ equal to 0 (dashed line), 2 (dotted line), and 5 (solid line). As $\beta I_{10}/\alpha$ increases, the FWM pulse broadens.

Chapter 7

Summary

This thesis is concerned with FWM as a wavelength conversion technique in low-loss passive InGaAsP/InP single quantum well waveguides at $\lambda = 1.5\mu m$. Fundamental parameters such as the third order nonlinearity (real and imaginary parts), linear loss, and GVD were characterized. The nonlinearity was shown to be ultrafast and mostly real. A conversion efficiency of -11 dB was demonstrated with picosecond pulses. The issue of wavelength conversion in the presence of nonlinear loss and index changes was examined. It was shown that the nonlinear loss and index changes place fundamental limits on the maximum conversion efficiency and lead to pulse distortions. Closed form solutions for the conversion efficiency in the presence of nonlinear effects were derived. The optimum pump power and device length were calculated.

There are several issues that remain unexplored. First, the resonant enhancement of the nonlinearity was achieved using a single QW device. A multiple QW waveguide should provide significantly greater nonlinearity enhancement and make passive waveguides more attractive as wavelength shifters. Second, the anisotropic nature of

the nonlinearity may potentially be removed by incorporating strain in the QW. If that is achieved, passive waveguides will provide polarization insensitive wavelength conversion. Third, methodical experimentation is needed to clarify the relationship between the time-domain and frequency-domain techniques for nonlinearity characterization. Fourth, many of the analytical results derived in Chapter 5 still need experimental verification. FWM in fiber with high peak power pulses may provide direct evidence for the effect of nonlinear index changes on FWM conversion efficiency. The issue of ultrashort pulse FWM remains unexplored, for the most part, analytically or experimentally.

Bibliography

[1] M. Saruwatari, "All-optical Signal Processing in Ultrahigh-Speed Optical Transmission," IEEE Comm. Mag., **32** , 98, (1994).

[2] H. A. Haus, Waves and Fields in Optoelectronics (Prentice-Hall, Englewoods Cliffs, 1984).

[3] Y. R. Shen, The Principles of Nonlinear Optics (Wiley, New York, 1984), p. 505.

[4] A. Yariv, Optical Electronics (Saunders College Publishing, Philadelphia, 1991), p. 608.

[5] G. Agrawal, Nonlinear Fiber Optics, (Academic Press, London, 1989), p. 289.

[6] R. Boyd, Nonlinear Optics, (Academic Press, London, 1989).

[7] K. L. Hall, G. Lenz, A. M. Darwish and E. P. Ippen, Optics Comm. **111**, 589 (1994).

[8] R. Ludwig, G. Raybon, "All-optical demultiplexing using ultrafast four-wave-mixing in a semiconductor laser amplifier at 20 Gbit/s," ECOC '93 19th European Conf. On Optical Comm., **3**, 57 (1993).

[9] S. Kawanishi and O. Kamatani, "All-optical time division multiplexing using four-wave-mixing," Electron. Lett. **30**, 1697, (1994).

[10] See for example M. Gower and D. Proch, Optical Phase Conjugation, (Springer-Verlag, New York, 1994).

[11] R. M. Jopson, A. H. Gnauck, and R. M. Derosier, "Compensation of chromatic dispersion by spectral inversion," Electron. Lett. **29**, 576, (1993).

[12] J. G. Fujimoto and E. P. Ippen, "Transient Four Wave Mixing and Optical Pulse Compression in the Femtosecond Regime," Optics Lett. **8**, 446, (1983).

[13] H. Le, W. Goodhue, and K. Rauschenbach, Optics Lett. **15,** 1126, (1990).

[14] A. Uskov, J. Mork, J. Mark, M. C. Tatham and G. Sherlock, "Terahertz four-wave mixing in semiconductor optical amplifiers: experiment and theory," Appl. Phys. Lett. **65,** 944 (1994).

[15] R. Schnabel, W. Piper, R. Ludwig and H. G. Weber, "Multiterahertz frequency conversion of picosecond pulse train using nonlinear gain dynamics in a 1.5 μm MQW semiconductor laser amplifier," Electron. Lett. **29**, 821 (1993).

[16] H. Q. Le and DiCecca, "Ultrafast, room-temperature, resonance-enhanced third order optical susceptibility tensor of an AlGaAs/GaAs quantum well," Opt. Lett., 4, p. 901, (1991).

[17] H. Q. Le and DiCecca, "Ultrafast, multi THz-detuning, third order frequency conversion in semiconductor quantum well waveguides," IEEE Photon. Tech., 4, p. 878, (1992).

[18] V. Mizrahi, K. DeLong and G. Stegeman, Optics Lett. **14**, 1140 (1989).

[19] E. W. Van Stryland, H. Vanherzeele, M. A. Woodall, M. J. Soileau, A. L. Smirl, S. S. Guha and T. F. Boggess, Opt. Eng. **24**, 613 (1985).

[20] K. W. DeLong and G. I. Stegeman, Appl. Phys. Lett. **57**, 2063 (1990).

[21] T. Durhuus, R. J. Pedersen, B. Mikkelsen, K. E. Stubkjaer, M. Oberg, and S. Nillson, IEEE Photonics Tech. Lett. **5**, 86, (1993).

[22] J. M. Wiesenfeld, B. Glance, J. S. Perino, and A. H. Gnauck, IEEE Photonics Tech. Lett. **5**, 1300, (1993).

[23] B. Mikkelsen, T. Durhuus, R. J. Pedersen, C. Braagaard, and K. E. Stubkjaer, Electron. Lett. **30**, 260, (1994).

[24] M. Schilling, K. Daub, W. Idler, D. Baums, U. Koerner, E. Lach, G. Laube, and K. Wunstel, Electron. Lett. **30**, 2128, (1994).

[25] E. A. Swanson and J. D. Moores, IEEE Photonics Tech. Lett. **6**, 1341 (1994).

[26] K. Inoue, T. Hasegawa, K. Oda and H. Toba, Electron. Lett. **29**, 1708 (1993).

[27] J. Zhou, N. Park, K. Vahala, M. Newkirk and B. Miller, "Broadband wavelength conversion with amplification using four-wave mixing in semiconductor travelling-wave amplifier," Electron. Lett. **30**, 859 (1994).

[28] G. Agrawal, Nonlinear Fiber Optics (Academic Press, New York, 1989).

[29] K. L. Hall, G. Lenz, E. P. Ippen, J. Lightwave Tech. **10**, 616, 1992.

[30] K. L. Hall, A. M. Darwish, E. P. Ippen, U. Koren, and G. Raybon, "Femtosecond index nonlinearities in InGaAsP optical amplifiers," Appl. Phys. Lett. **62**, 1320 (1993).

[31] D. Hanna, M. Yuratich, and D. Cotter, Nonlinear Optics of Free Atoms and Molecules (springer-Verlag, Berlin, 1979), p. 21.

[32] R. J. Pressley, Handbook of Lasers with Selected Data on Optical Technology, (The Chemical Rubber Co., Cleveland, 1971).

[33] H. C. Casey, Jr., D. D. Sell, and M. B. Panish, Appl. Phys. Lett. **24**, 63, 1974.

[34] J. P. Donnelly, H. Q. Le, E. A. Swanson, S. H. Groves, A. M. Darwish and E. P. Ippen, IEEE LEOS '94, Conf. Proc. v. 2, no. 10.2, 330, Boston, 1994.

[35] J. P. Donnelly, H. Q. Le, E. A. Swanson, S. H. Groves, A. M. Darwish and E. P. Ippen, IEEE Photo. Tech. Lett. **8**, 623, 1996.

[36] H. K. Tsang, R. Penty, I. White, R. Grant, W. Sibbet, J. Soole, H. LeBlanc, N. Anderadakis, R. Bhat, and M. Koza, J. Appl. Phys. **70**, 3992, 1991.

[37] M. J. LaGasse, Femtosecond Optical Nonlinearities in AlGaAs, Doctoral Thesis, MIT, 1989.

[38] M. J. LaGasse, K. K. Anderson, C. A. Wang, H. A. Haus, and J. G. Fujimoto, "Femtosecond measurements of the nonresonant nonlinear index in AlGaAs," Appl. Phys. Lett. **56**, 417, 1990.

[39] See for example A. Nelson, K. Folley and M. Coral, Differential Equations, (D. C. Heath and Company, Boston, 1964), p. 39.

[40] P. S. Zory, Jr., Quantum Well Lasers, (Academic Press, London, 1993), p. 17.

[41] M. Seto, A Shahar, R. J. Deri, W.T. Tomlinson and A. Yi-Yan, Appl. Phys. Lett. **56**, 990 (1990); D.F. Clark and M. S. Iqbal, Optics Lett. **15**, 1291 (1990).

[42] A. Villeneuve, M. Sundheimer, N. Finlayson, and G. Stegeman, Appl. Phys. Lett. **56**, 1865 (1990).

[43] M. N. Islam, Ultra-fast Fiber Switching Devices and Systems (Cambridge Univ. Press, Cambridge, 1992).

[44] A. Mecozzi, Opt. Lett. **19**, 892, (1994).

[45] D. J. Hagen, E. W. Stryland, M. J. Soileau, and Y. Y. Wu, "Self-protecting semiconductor optical limiters," Opt. Lett. **13**, 315, 1988.

[46] E. W. Stryland, Y. Y. Wu, D. J. Hagan, M. J. Soileau, and K. Mansour, "Optical limiting with semiconductors," J. Opt. Soc. Am. B **5**, 1980, 1988.

[47] C. R. Pidgeon, B. S. Wherrett, A. M. Johnson, J. Dempsey, and A. Miller, "Two-photon absorption in zinc-blende semiconductors," Phys. Rev. Lett. **42**, 1785, 1979.

[48] M. J .Weber, CRC Handbook of Laser Science and Technology, (CRC Press, Boca Raton, Florida, 1986), p. 229.

[49] A. M. Darwish, E. P. Ippen, H. Q. Le, J. P. Donnelly, S. H. Groves, E. A. Swanson, "Short Pulse Wavelength Shifting by Four Wave Mixing in Passive InGaAsP/InP Waveguides," Appl. Phys. Lett. **68**, April 8, 1996.

[50] A. M. Darwish, G. Lenz, E. P. Ippen, H. Q. Le, J. P. Donnelly, S. H. Groves and E. A. Swanson, CLEO/QELS 95, QThJ2, Baltimore, 1995.

[51] A. Mecozzi, A. D'Ottavi, F. Romeo, P. Spano, R. Dall'Ara, G. Guekos and Eckner, Appl. Phys. Lett. **66**, 1184, (1995).

[52] T. R. O'Meara, and A. Yariv, "Time-domain signal processing via four-wave mixing in nonlinear delay lines," Opt. Engineering **21**, 273 (1982).

[53] J. H. Marburger, "Optical pulse integration and chirp reversal in degenerate four-wave mixing," Appl. Phys. Lett. **32**, 372 (1978).

[54] A. D'Ottavi, E. Iannone, A. Mecozzi, S. Scotti, P. Spano, R. Dall'Ara, J. Eckner, and G. Guekos, "Efficiency and Noise Performance of Wavelength Converters Based on FWM in Semiconductor Optical Amplifiers," IEEE Photon. Tech. Lett. **7**, 357, (1995).

[55] M. Gower, D. Proch, Optical Phase Conjugation (Springer-Verlag, Berlin, 1994).